CAIT-UTC-004

Forensic Testing of Prestress Concrete Girders after Forty Years of Service

FINAL REPORT
September 2013

Submitted by:

Paul Barr
Associate Professor
Utah State University
4110 Old Main Hill
Logan, UT 84332

Marv Halling
Professor
Utah State University
4110 Old Main Hill
Logan, UT 84332

Arek Higgs
Utah State University
4110 Old Main Hill
Logan, UT 84332

Submitted to:
Utah Department of Transportation
Russ Scovil

In cooperation with
Rutgers, The State University of New Jersey
And
Utah Department of Transportation
And
U.S. Department of Transportation
Federal Highway Administration

Disclaimer Statement

The contents of this report reflect the views of the authors, who are responsible for the facts and the accuracy of the information presented herein. This document is disseminated under the sponsorship of the Department of Transportation, University Transportation Centers Program, in the interest of information exchange. The U.S. Government assumes no liability for the contents or use thereof.

The Center for Advanced Infrastructure and Transportation (CAIT) is a Tier I UTC Consortium led by Rutgers, The State University. Members of the consortium are the University of Delaware, Utah State University, Columbia University, New Jersey Institute of Technology, Princeton University, University of Texas at El Paso, University of Virginia and Virginia Polytechnic Institute. The Center is funded by the U.S. Department of Transportation.

TECHNICAL REPORT STANDARD TITLE PAGE

1. Report No.	2. Government Accession No.	3. Recipient's Catalog No.	
CAIT-UTC-004			
4. Title and Subtitle **Forensic Testing of Prestress Concrete Girders after Forty Years of Service**		5. Report Date September 2013	
		6. Performing Organization Code CAIT/Utah State University	
7. Author(s) Paul Barr, Marv Halling, and Arek Higgs		8. Performing Organization Report No. CAIT-UTC-004	
9. Performing Organization Name and Address Utah State University 4110 Old Main Hill Logan, UT 84332		10. Work Unit No.	
		11. Contract or Grant No. DTRT12-G-UTC16	
12. Sponsoring Agency Name and Address Center for Advanced Infrastructure and Transportation Rutgers, The State University of New Jersey 100 Brett Road Piscataway, NJ 08854		13. Type of Report and Period Covered Final Report 06/01/12 to 09/06/13	
		14. Sponsoring Agency Code	

15. Supplementary Notes
United States Department of Transportation/Research and Innovative Technology Administration
1200 New Jersey Avenue, SE
Washington, DC 20590-0001

16. Abstract
This report describes an investigation to quantify the behavior of precast, prestressed concrete bridge girders made with high-strength concrete. As part of the investigation, four bridge girders that were made with 77.2 MPs (11.2 ksi) concrete were salvaged from a decommissioned bridge in Orem, Utah. Each girder was subjected to a cracking test to determine the residual prestress force after approximately seven years of service life. Once the prestress losses were quantified, a flexural capacity test was performed on one girder and shear capacity tests were performed at various distances from the support on the remaining three girders. The measured losses and capacities were compared to estimated values calculated according to procedures in the AASHTO LFRD Specifications. It was concluded that, in general, the AASHTO LRFD procedures were accurate despite the current limitation of restricting the concrete compressive strength to 68.9 MPs (10.0 ksi). In addition to the physical tests, a nonlinear finite element analysis (FEA) was conducted using ANSYS that was found to replicate the experimental behavior, failure and mechanism magnitude.

17. Key Words	18. Distribution Statement
Prestress concrete, shear, flexure, capacity, forensic	No restrictions

19. Security Classification (of this report)	20. Security Classification (of this page)	21. No. of Pages	22. Price
Unclassified	Unclassified	127	

Form DOT F 1700.7 (8-69)

Table of Contents

Table of Equations

Table of Figures

1. Introduction

This research is focused on the shear and flexure strength capacity of Type-I AASHTO high strength self-consolidating prestressed concrete bridge girders. Four girders were salvaged from the 400 South I-15 bridge in Orem, Utah. These girders were tested to failure with a point load at different locations to induce flexure, flexure-shear, and shear failures. The results from the tests were compared to AASHTO LRFD Specifications (2012) and an ANSYS Finite Element model.

2. Introduction to Preliterate Review

2.1. Analysis of Flexural Strength of Prestressed Concrete Flanged Sections (Eray, et. al, 2005)

This research focuses on the differences of two different bending analyses for various prestressed girder cross section using the AASHTO Standard Specifications and AASHTO LRFD Specifications. Strain compatibility was used for each methodology in order to determine the strain in the prestressed steel, which can be found using the geometry of the girder along with the neutral axis location. This study investigated the accuracy of the two methods as compared to experimental and theoretical data for I and T cross sections.

For concrete I and T sections, the neutral axis is determined based on the shape of the cross section. The top flange depth was decreased from 381 mm (15 in.) to 102 mm (4 in.), by removing the concrete on the under part of the over hangs so as to keep the total depth of the girder will remain constant. The deeper the top flange, the closer to the top flange the neutral axis will be. This study used a conceptual girder with dimensions of 2.5m (100 in.) tall with a 2 m (78 in.) wide top flange and a 0.305 m (12 in.) thick web. The compressive strength of the concrete was 55 MPa (8000 psi) and the prestressed strands had a yield value of 1654 MPa (240 ksi) and ultimate strength of 1862 MPa (270 ksi). The results were not obtained based on experimental data, but rather a strain compatibility analysis was computed and compared to AASHTO LRFD and Standard values were compared to.

Top flange depth vs. neutral axis location, strand stress and moment were plotted for ultimate capacity. The AASHTO Standard procedure was comparable to the calculations from strain compatibility with a minimum depth of the neutral axis at 254 mm (10 in.) from the top of

the girder with a top flange depth of 165 mm (6.5 in.). The location of the neutral axis did not change even with an increasing flange depth. The LRFD procedure was not as close to the predicted values using the strain compatibility analysis. The LRFD procedure reached the same minimum neutral axis depth, but at a flange thickness of 254 mm (10 in.).

The maximum moment capacity using the strain compatibility, Standard and LRFD methods was 35 MN-m (26,500 kip-ft.) when the top flange thicknesses corresponding to that of the neutral axis locations for all three analyses.

This research concluded that a modified LRFD approach was necessary for accuracy. By increasing the influence the top flange from the original LRFD procedure to replicate the behavior of the strain compatibility analysis. The proposed modified method had similar values as the AASHTO Standard procedure for maximum moment and neutral axis location for various values of top flange thickness.

2.2. Comparative Study on Flexural Response of Full and Partial Depth Fiber-Reinforced High-Strength Concrete (Padmarajaiah, 2000)

High-strength concrete is known for its extremely high compressibility, but one inherent characteristic is it is more brittle than normal-strength concrete. Fiber has been shown to increase the tensile capacity of concrete making high-strength concrete more ductile and therefore more advantageous.

For this research, a total of 15 square beams with dimensions of 100 mm (3.9 in.) width and depth and 500 mm (19.7 in.) long. The beams were supported 50 mm (2 in.) in from each end for an effective span length of 400 mm (15.7 in.). There was two point loads symmetrically located at 67 mm (2.6 in.) from the center of the beam. There were 5 mechanical strain gauges

on the side of the beam, from bottom to top, 50 mm (2 in.) on each side of the center of the beams. There was also a dial gauge at the center of the beams to record mid span deflection. They were constructed using four different percentages of Trough shaped steel fiber reinforcing, 0.0, 0.5, 1.0 and 1.5. The fiber was added to the beams in two ways, the full height and the tension portion of the beam. The improved tensile stress capacity increases the toughness and flexural strength of the beams.

Compression tests conducted with all three fiber percentages have the same maximum compressive capacity of 58 MPa (8400 psi.). The concrete specimens all obtained the peak strength at a strain of 0.003. Failure strain values increased with higher fiber percentages such as the following, 0.008 with 1.5% fiber, 0.006 with 1% fiber, 0.005 with 0.5% fiber and 0.004 with no fiber. The fiber may not increase the compressive strength of concrete; however, it facilitates a more ductile failure.

Strain compatibility analysis along with the correlating stress distribution was used to calculate the maximum moment for each beam. The different amounts fiber reinforcing was accounted for in each analysis in the tension part of the beam. The tensile stress distribution starts at the neutral axis and increases linearly with depth until the yield strength of the steel fibers is reached, then it remains at the yield strength for the remaining depth of the beam. The beams with the highest fiber content had more capacity, because they had the greatest area of steel in the tension area. The compression block was modeled with a parabolic stress distribution with a maximum stress just above the center of the block; which matched the stress strain curve from the compression tests.

The result of introducing fiber reinforcing to concrete beams varies on the amount. The beams flexural load capacity with an amount of 0.5% fiber compared to no fiber was 12.5 kN

(2810 lbs.). The beam with 0.5% fiber had a mid-span deflection of 1.5 mm (0.05 in.), where the beam with no fiber had a deflection value of 0.75 mm (0.03 in.), the addition of fiber increased the ductility by 67%. The beams with 1.0% fiber attained a maximum flexure load of 18 kN (4057 lbs.) and a center deflection of 1.75 mm (0.07 in.). At a value of 1.5% the ultimate flexural capacity of the beams was 22.5 kN (5058 lbs.), nearly double that of the beams with no fiber, and a center deflection of 2 mm (0.08 in.).

The placement of the fiber was only critical in the tension region. Test results of half depth to full depth reinforcing were compared and found to have the same results for the same percentages of fiber. This coincides with the cylinder compression tests in that the maximum compressive stress was found not to increase, however the tensile capacity of the concrete was increased. These beams were a tension govern failure, therefore the increased tension capacity increased the moment capacity of the beams.

2.3. Flexural strength predictions of steel fiber reinforced high strength concrete in fully/partially prestressed beam specimens (S.K. Padmarajaiah, Ananth Ramaswamy)

Eight beams were tested with differing prestress forces and amounts of fiber in the concrete mix. They were box beams with a depth of 240 mm, width of 105 mm, and length of 2200 mm. Shear reinforcing was placed within 750 mm of each end to ensure a flexural failure. The amount of fiber varied from 0% to 1.5% of the concrete mix. Fiber was placed in the bottom of a third of the beams and throughout the whole beam in another third. The remaining third had no fiber reinforcing. Every beam had the same steel reinforcing.

The beams were made on site and tested 29-30 days after casting. The use of a 500 kN load frame was used to test the beams. Sensors were placed in and around the beam to measure

strain, deflection and curvature. Load increased by 4.5 kN until hairline cracks were visible in the most extreme tension face. The cracks were marked and loads recorded. The beams were then unloaded and retested to failure.

Each beam was analyzed with the Whitney Stress Block with some modifications to account for the fiber in two thirds of the beams. However, fig. 3 shows a strain analysis of fully/partially prestressed members without fiber. Figure 3 shows how the strain in the prestressing strands is the addition of three parts: effective strain, concrete strain at level of prestressing, and strain due to loading. The total strain is used to calculate the maximum moment a beam is able to hold.

Load vs. deflection and moment vs. curvature diagrams were plotted for each beam. Those graphs showed that the fiber did increase the capacity and stiffness of the beams. The analysis predicted the maximum load capabilities of the beams very closely, usually within a couple of percents. The deflections predicted were in contrast to that and varied in accuracy a great deal.

The energy absorption increased with the amount of fiber in the beam. In the cases for the fully prestressed beams it was nearly double the amount of energy than beams with no fiber. Therefore, depending on the application of the concrete member there could be a great deal of strength acquired with a fiber reinforced concrete mix at a small cost.

2.4. Structural Tests of 27 yr. Old Prestressed Concrete Bridge Beams

A bridge in East Hartford, Connecticut replaced in 1984 had some deterioration and was made up of 13 prestressed box beams. The beams were AASHTO-PCI type BI-36 with an effective span of 16.456 m (54 ft.) long with 22 strands of 11 mm (7/16 in.) diameter in the

bottom of the beam. The box beams have dimensions 686 mm x 914 mm (27 in. x 36 in.) and a hollow center. The beams were placed side by side and the road asphalt was placed on top of the beams. The edge beams were larger and constituted the sidewalk, they were not tested in this study.

The beams had a wide range of deterioration, mostly from bridge salting during the winter months. The two beams closest to the edge beam had the most damage done to them, being as the water would run off the road to the curb then off the bridge. There were also some stains on the underside of the bridge from sodium deposits. The study mentions that the sodium damage was mainly due to the fact that there was no water proof membrane between the asphalt and the beams.

The material properties of the beams were found after testing. Concrete core samples tested showed a compressive strength of 49 MPa. (7100 psi.). The stress strain curve of the core samples show very little yielding before rupture, indicating a very brittle concrete. This is not uncommon as concrete strength increases and becomes more brittle with age. Tensile tests were done to determine the modulus of elasticity and yielding strength of the prestressing strands. The strands have a modulus of 28300 MPa. (4.1×10^6 psi.) and a yield strength of 1724 kPa (250 ksi.).

The beams were simply supported with loads applied at third points along the length. Strain gauges were applied to the concrete and some strands. To apply the gauges to the strands, the concrete was carefully removed from a 450 mm (18 in.) section on the bottom of the beam. The concrete strain gauges were placed on the top and down the side of the beam.

Two of the beams were tested, beam 4 and beam 7. Beam 7 was in the center of the bridge and beam 4 was in the center of a lane. They both had similar results with maximum

loads of 222.8 kN (50.1 kips) and 212.6 kN (47.8 kips) for beams 4 and 7 respectively. There was no flexural cracking until 158 kN (35.5 kips) and 129 kN (29 kips) for beams 4 and 7 respectively, which is well above the service load of 69.4 kN (15.6 kips) and about the same as the factored load of 164.5 kN (34.7 kips). This cracking load corresponds with a residual prestressing force of 671.6 kN (151 kips), which was verified theoretically as well.

Both beams were proven to be strong and ductile even though one had minor deterioration, they performed similarly. The predictions made, using strain compatibility, proved to be accurate in both the maximum load and deflection. Strain compatibility was able to predict the strand stresses measured from the gauges on them. Therefore strain compatibility is a good tool used to accurately model prestressed concrete beams.

2.5. Testing of Two 50 yr. Old Prestressed Concrete Bridge Beams

The two girders tested for this research had a span length of 13.7 m (45 ft.) long and were designed using a post-tensioned, concrete I cross section. The girders had a small section of deck that acted compositely. Prior to testing, the girders were inspected and found to have some longitudinal cracks and other damage as a result of the transportation. The post-tensioned rods had a diameter of 29 mm (1-1/8 in.). There are four bars that run the length of the girder, two of which harped in the web and the final two were straight in the bottom flange.

Compression tests were done on cylinder samples of the girders. The concrete compressive strength was measured to be 67 MPa (9.8 ksi), and the splitting tensile strength was 5.5 MPa (800 psi). The reinforcing steel in the girders was also tested. The post-tensioned bars had a yield strength of 689 MPa (100 ksi) and a ultimate strength of 993 MPa (144 ksi) with a modulus of elasticity of 196501 MPa (28,500 ksi). The mild reinforcing steel was not tested.

The ends of the girders were damaged to the point that the supports for the test had to be adjusted so that the effective span length was decreased to 12.8 m (42 ft.). The girders were supported with two elastomeric pads. A spreader beam was used to distribute the applied point load of a hydraulic ram to two point loads. This loading scheme created a constant moment region spanning 1.52 m (5 ft.) on each side of the center of the girder.

Strain gauges were attached to the side of the girder at mid span. These gauges were used to determine the compression block and neutral axis. An extra strain gauge was attached when the girder initially cracked. Initial testing cracked the girders, the cracks were marked and the load was released. The additional strain gauge was placed over the crack and the load was reapplied to determine the tensile force in the post-tensioned bars.

The average moment capacity of the girders was 1830 kN-m (1350 k-ft.). The initial calculation for moment capacity was 17%-21% higher than the experimental results. This was due to the fact that these calculations used assumed material values and didn't account for the deck concrete detaching during the test. The corrected value of moment was 1762 kN-m (1300 k-ft.).

2.6. Ultimate Flexural Strength of Prestressed and Conventionally Reinforced Concrete Beams (J. R. Janney, et. al, 1956)

In this study there was 19 concrete beams tested to failure. The beams have a width of 152 mm (6 in.) and a depth of 305 mm (12 in.), with an effective depth of 211 mm (8.3 in) and a length of 3.05 m (10 ft.). The beams were separated in to five groups of different types of reinforcement. All of the reinforcement is straight and the strands are 9.5 mm (3/8 in.) diameter with a total cross sectional area of 51.6 mm^2 (0.08 in^2). The strands have a yield strength of 1.62

GPa (235 ksi) and had an initial prestress value of 823.4 MPa (120 ksi). All the concrete was five bag mix with an average compressive strength of 37.9 MPa (5.5 ksi).

The five groups and their qualities are as follows: Group 1, prestressed stands; Group 2, bonded post-tension strands; Group 3, unbounded post-tension strands; Group 4, unbounded post-tension strands with conventional reinforcement; and Group 5, conventional reinforcement. Each group with the seven wire strands had three different reinforcement percents such as 0.322, 0.644, and 0.965. The group with only conventional reinforcing had percentages of reinforcing of 1.20, 1.87, 2.65, 3.61 and 4.75.

The beams were simply supported 152 mm (6 in.) in from the ends making an effective span length of 2.74 m (9 ft.) long. The load was applied in two locations at third distances. Strain gauges were placed on the reinforcement and the concrete at the middle, and 610 mm (2 ft.), 914 mm (3 ft.), and 1.22 m (4 ft.) off the center line of the beam. These gauges were used to find the stain at different stages of the tests. The strain readings are correlated with the stress-strain plot to show what stress the strands are at.

2.7. Investigation of Damaged 12-year Old Prestressed Box Beams (Clay Naito, Ph.D., P.E.; 2008)

This research was focused on a three span bridge built in 1989 and demolished in 2000. The bridge was inspected early in 2000 and cracks on the concrete box beam were found by the piers and abutments. The bridge had three spans and carried three lanes of highway traffic for both directions. The span lengths for spans 1, 2 and 3 were 18.9 m (62 ft.), 21.7 m (71.3 ft.) and 14.9 m (49 ft.) respectively. The roadway was straight, but the abutments and piers were skewed at an angle of $4^0$13’24.7” off a line perpendicular to the roadway. The foundations of the piers and abutments were supported by H piles driven to bedrock.

The bridge beams were fixed at each end with a diaphragm and the road deck, which was a continuous cast in place slab for all three spans. The beams were made of concrete and had prestressed seven wire strands and mild shear reinforcing. The square beams were 1.2 m (4 ft.) tall and wide with the associated span length. The bottom flange was 139.7 mm (5.5 in.) thick and the top flange was 76.2 mm (3 in.) thick with webs at 127 mm (5 in.) wide. All inside edges had a 76.2 mm (3 in.) chamfer and the bottom outside edges had a 19.1 mm (0.75 in.) chamfer. The ends of the beams were solid concrete to a point 610 mm (24 in.) to 721 mm (28.4 in.) in from the ends. The depth of this solid part of the beam depended on where on the bridge it was being placed due to the skew of the bridge. The 228.6 mm (9 in.) thick concrete roadway was connected to the beams with shear studs to attain composite action between them. The prestressing strands were located in the bottom and up the sides of the webs. All strands were made of grade 270 low relaxation strands with a diameter of 13 mm (0.5 in.). The strands were debonded for 635 mm (25 in.) on each side of the beam to prevent prestress transfer cracking.

The damage to the beams consisted of flexure-shear, flexure and shear cracks. Most of the damage was concentrated around the piers, mainly pier 2, with minimal damage by the abutments. All cracks were located were the hollow section of the beams starts. The westbound bridge was monitored with transducers, strain gauges and thermocouples. The cracks were found to open and close under live loads, such as traffic and a 4-axle 326 kN (73280 lb.) truck used for a standard test. The standard truck used is the maximum legal load defined by PennDOT. Traffic loads were compared to the standard test and were found to have 1.4 times the strain, which could be explained by the effect of multiple vehicles driving over the bridge at the same time. The temperature difference between the top of the deck and bottom of the beams

would cause the crack to open. When the top of the deck would heat up the bottom flange cracks would open.

A beam from span 1 was selected for a materials and quality testing. The beam had concrete cores removed for testing and the strands were located by chipping the concrete off the beam. The concrete cylinders were tested and a compressive strength of 59.5 MPa (8630 psi) was found; which was 33% higher than the specified 28 day strength. The dimensions of the beam were compared to the specified drawings with few major differences. The debonded length of the strands varied from the specified length of 635 mm (25 in.) to 1.0 m (40 in), almost double the specified length. The shear studs used to connect the deck to the beams were spaced different in the solid areas of the beam, but along the hollow length of the beam they were as specified.

A beam from span 3 was used for testing. The beam was simply supported with a point load 3.56 m (11.75 ft.) from the end of the beam. The point load was placed near the end of the beam to induce a stress combination of shear and flexure on the beam. The beam was tested twice; the damaged end was first followed by the undamaged end. The support on the damaged end was moved to a location of 4.04 m (13.25 ft.) to support the beam past the initial test, therefore the second test had a shorter effective length. The restrain conditions during testing were not the same in situ conditions. The beam was monitored with displacement transducers and strain gauges. Two displacement transducers were placed on the side of the beam under the point load, the average of the two were used as the vertical displacement. Strain gauges were placed on the bottom flange to determine the decompression load. There were gauges placed on the ends of the strands, at the end of the beam nearest the applied load, to measure strand slip.

Each end of the beam performed similarly for each test. Test #1 and test #2 were 7% and 9% respectively higher than the calculated flexural strength of 4.84 MN-m (3.57 Kip-ft.) using AASHTO 2006 standards. Each test failed in flexure with strand rupture.

The decompression load was determined by cracking the section and placing a strain gauge next to the crack. The load is then reapplied, the strain gauge should increase until cracking at which point the strain will remain constant. This was repeated three times and averaged to determine the prestressing value.

The cracking moment was determined from the undamaged end test. This moment was larger than the moment from the demands on the beam; therefore the in situ stresses were not large enough to cause cracking. It was determined that errors in design, detailing and production caused the cracks. The location where the beam changes from solid to hollow was a large discontinuity. This discontinuity combined with longer debonded lengths of the prestressed strands caused increased localized tensile stress. Production of the beams could have been an influence, during production some reinforcing contaminated by form oil, and other discrepancies that led to the rejection of over 40 beams before the necessary 36 beams were accepted.

3. Bridge Description

The 400 South Bridge on I-15 in Orem, Utah was decommissioned during the fall of 2011. The replacement of this bridge was part of UDOT's south I-15 core project. Originally, when the highway section was built in 1960 there were two bridges, one for the north bound and one for the south bound lanes of traffic. Subsequently, in 2004 this section of I-15 was expanded to accommodate additional lanes; the space between the two bridges was used for the addition. The entire bridge is comprised of three independent spans as seen in Figure 3.1. The girders that were tested for this research were salvaged from span1.

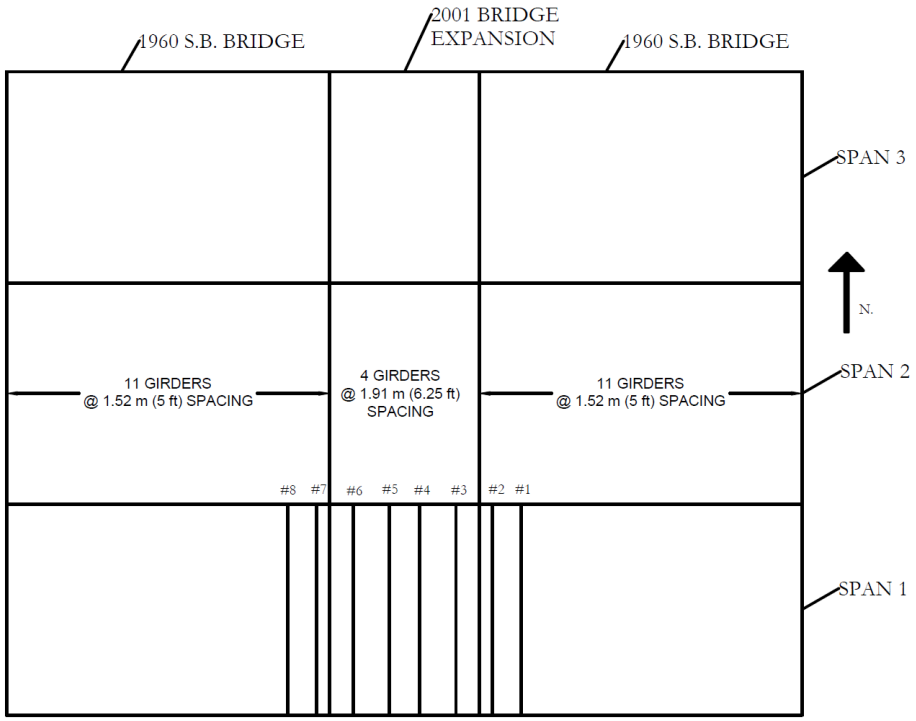

Fig. 3.1 Plan view of the Bridges

The salvaged girders were simply supported on a pier and an abutment. The 1960 bridge pier consisted of a rectangular concrete beam that spanned the width of the roadway and supported the bridge girders. The I-shaped girders were supported at each pier with three concrete columns. The columns were connected to one continuous concrete footing with twenty

two 9.1 m (30 ft.) concrete piles with a diameter of 305 mm (12 in.) staggered along the length of the footing for a deep foundation. The entire pier was made of reinforced concrete with moment resisting connections as shown in Figure 3.2.

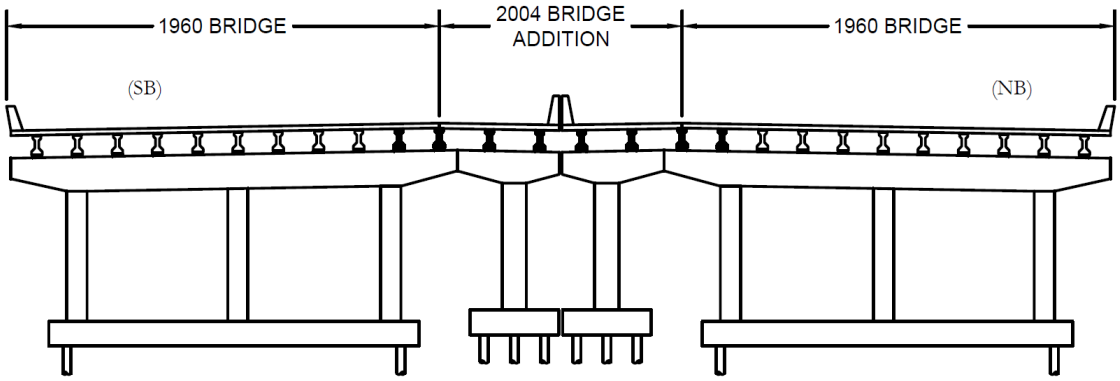

Fig. 3.2 Section view of the bridges at a pier

The 2004 addition to the bridge was of a similar design. The bridge was a three span bridge with two piers and two abutments. The piers had rectangular concrete beams supporting the girders, similar to the original bridge design. These beams were attached to the original pier beams. There was only one concrete column supporting the girders that had its own footing with six piles of the same dimensions as the original piles that made the deep foundation. The north bound and south bound bridges were not connected to each other. A cross section of the bridge at a pier, shown in Figure 3.2, shows the girder support system and the foundation. The shaded I-girders were salvaged for this research.

3.1. Bridge Dimensions

The original bridges were constructed with three spans. Each span was 16.9 m (55.5 ft.) wide and supported three 3.657 m (12 ft.) wide lanes of traffic. Spans 1 and 3 had a length of 11.1 m (36.3 ft.) and Span 2 had a length of 11.6 m (38 ft.), (Figure 3.1). The original girders

(1,2,7,8) were spaced at 1.5 m. (5 ft.) apart for all spans. The concrete deck was 178 mm. (7 in.) thick with a 51 mm (2 in.) asphalt overlay.

The bridge widening was accomplished by providing one additional lane for each the Northbound and Southbound traffic with the median between the two original bridges. The decks of the bridges were cut off at the middle of the inside edge beams. Those edge girders supported half the old and new decks. The new portion was 4.5 m. (15 ft.) wide on each bridge. The new girders (3,4,5,6) were placed at a spacing of 1.9 m (6.3 ft.). The edge girders (4 and 5) were 737 mm. (29 in.) from the center of the bridge. The new deck is 203 mm. (8 in.) thick with a 76 mm. (3 in.) of total asphalt on top. Both the new and the old girders have the same span length. A cross sectional view of the complete bridge is seen in Figure 3.2.

3.2. Girder Dimensions

Both the new and the older girders were fabricated using the same AASHTO Type I cross-sections as see in Figure 3.3. The girders had a total bottom flange width of 406 mm (16 in.) and total height of 711 mm (28 in.). The bottom flange was 127 mm (5 in.) tall then angles in at a one-to-one slope for another 127 mm (5 in.) of vertical distance before reaching the web. The web is 152 mm (6 in.) thick and 279 mm (11 in.) tall. Then the beam widens at a one-to-one slope for 76 mm (3 in.) of vertical distance to a total top flange width of 305 mm (12 in.). The top flange is 102 mm (4 in.) tall. The total concrete cross sectional area is 0.2 m^2 (279 $in.^2$).

3.3. Girder Reinforcing

Both sets of girders were designed with mild steel reinforcing and either prestressed strands or post-tensioned bars. Mild reinforcement was primarily used as shear reinforcing. Six longitudinal bars were used to hold the shear bars in place during casting. Tensile tests were

performed on the reinforcing to determine their material properties. The configuration of the prestressing steel can be seen more clearly in Figure 3.3.

The girders were prestressed using a seven wire, 13 mm (1/2 in.) diameter strand. There are 11 straight strands in the bottom flange and 2 in the top flange with an overall centroid of prestressing at 181 mm (7.1 in.), as seen in Figure 3.3, from the bottom for the mid span and end cross sections. The strands run straight through the beam. The strands are made of high strength, low relaxation steel with a yielding point of 1586 MPa (230 ksi) and an ultimate strength of 1862 MPa (270 ksi) with a modulus of elasticity of 19.65 GPa (28500 ksi). The plans indicated that after losses the prestressing strands would have an effective prestressing force of 1424 kN (320 kip) which is an equivalent stress of 1132 MPa (164 ksi)

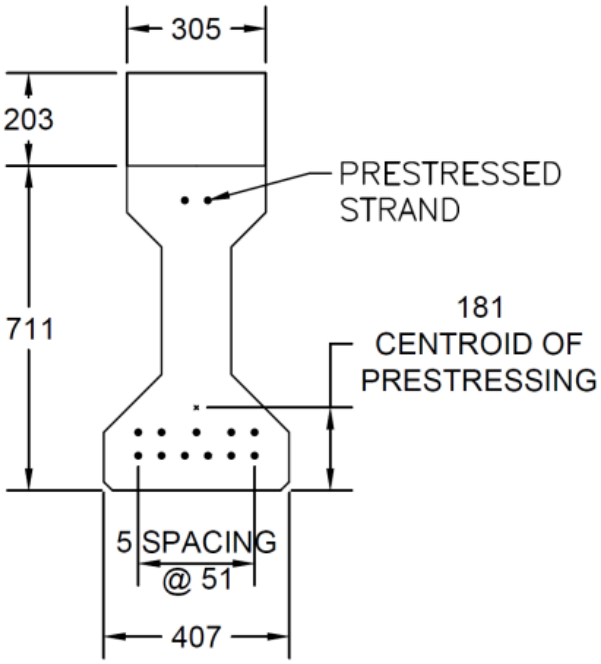

Fig. 3.3 Prestressing steel configuration

The shear reinforcing was provided using #13 (#5) rebar at three different spacing's seen in Figure 3.4, which shows the shear spacing and a cross section of the mild reinforcing. The first stirrup was at 51 mm (2 in.) from the end of the girder with the subsequent spacing at 152

mm (6 in.) on center 1.371 m (4.5 ft.) from the end of the girder. The next spacing was 305 mm (12 in.) on center for the following 2.133 m (7 ft.). The third spacing was 457 mm (18 in.) on center for the next 1.829 m (6 ft.) leaving a 191 mm (7-1/2 in.) gap from the center of the girder to the last shear bars. The shear reinforcing is symmetrical about the center of the beam. Shear reinforcing was shorter than developmental length; therefore, in order to ensure the shear bars would not pull out of the concrete they were bent 90^{o} at the each end. These bends also enable the bars to attain their yield strength. The bars extend out of the beam by 102 mm (4 in.) into the deck concrete in order to develop composite behavior with the deck.

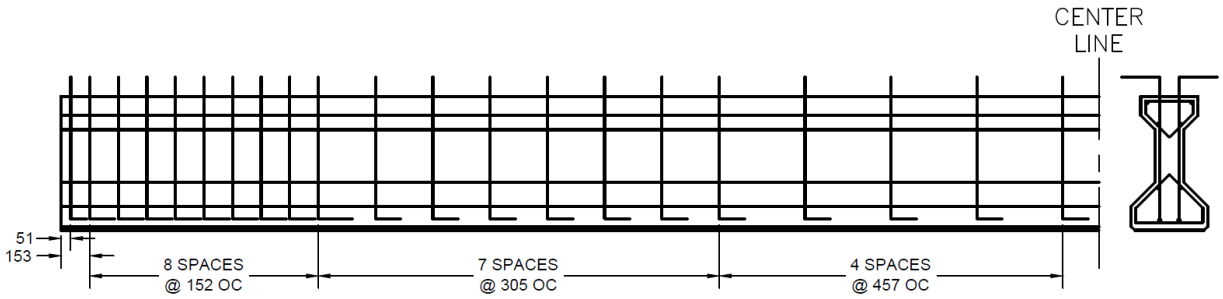

Fig. 3.4 Mild reinforcing of girder

The girder concrete was specified to have a compressive strength of 27 MPa (4 ksi) at transfer and 34.5 MPa (5 ksi) at 28 days. Concrete cylinders cored from the deck and girder concrete with a diameter of 95 mm (3.75 in.) and a length of 191 mm (7.5 in.) were tested to determine the maximum compressive stress, f'_c. Four cylinders from the deck and three from the girder were tested using a Fourney 5000 concrete compression machine. The average of each group was used. The deck and girders were found to have an average maximum compressive stress of 58.6 MPa (8.5 ksi) and 77.9 MPa (11.3 ksi), respectively.

At the time the bridge was decommissioned, the girders were found to be in relatively good condition. The newer girders were in excellent shape, after being in service for only 8

years. There was still some missing concrete, mainly near the end of the girders, which was patched with concrete and existing reinforcement was used to ensure composite action.

4. Experimentation

All testing for this research was performed at the Structural Materials And Systems Health Lab (SMASH Lab). The SMASH Lab is located at 1500 Canyon Rd. Logan, UT., and is a part of Utah State University Campus. The lab is equipped with a strong floor, reaction frame, hydraulic rams, and a Vishay 5000 data acquisition system. Figure 3.1 shows the reaction frame with two girders under it being prepped for testing. The strong floor is 0.914 m (3 ft.) thick made with reinforced concrete with conduits spaced every 0.914 m (3 ft.) to allow for various positioning of the reaction frame. The steel reaction frame has two columns, which were bolted to the strong floor, and a spreader beam connected to the columns. The spreader beam holds the hydraulic rams in place for testing. A 222 kN (500 kip) hydraulic ram was used to apply the static load. The Vishay is a data acquisition system that is capable of monitoring various sensors such as the load cells and strain gauges that were used in this test.

Fig. 4.1 Reaction frame with two girders ready to test.

There were four girders tested for this study. The girders were numbered 3, 4, 5, 6 and were fabricated in 2004. Four additional girders (1, 2, 7, 8) from the older portion of the bridge were also removed but were tested as part of a different study. The numbering was assigned according to the order that they were removed from the bridge. Each girder was tested to determine the prestress force with a cracking test and subsequently the capacity for either pure moment, predominately shear or a flexure-shear failure. In order to accomplish this, a mid-span, 1d, 2d, and 4d tests were completed, where d is the total depth of the girders including the deck as seen in Figure #. Table 1 lists which girder was used for which test.

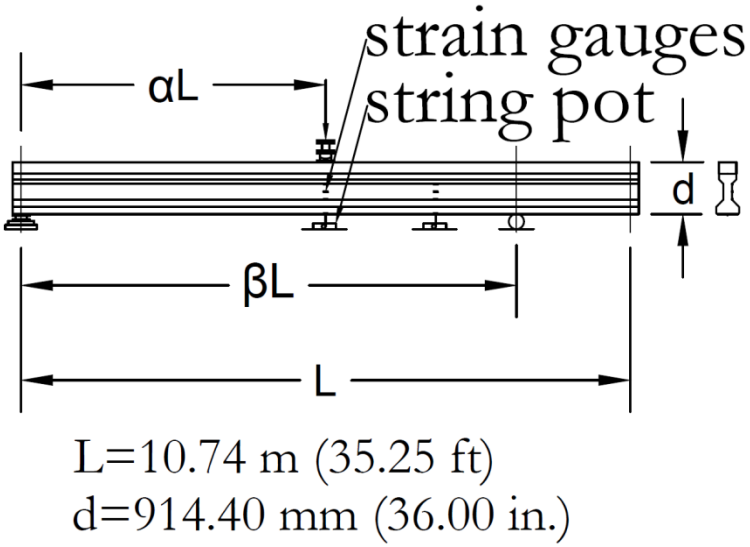

Fig. 4.2 Diagram of test set up

Table 4.1 Dimensions for each experiment

Girder # Test Type	α	β
G3-1d(a)	0.914 m (3.00 ft.)	10.74 m (35.25 ft.)
G3-1d(b)	0.914 m (3.00 ft.)	9.22 m (30.25 ft.)
G4-4d(a)	3.66m (12.00 ft.)	10.74 m (35.25 ft.)
G4-2d(b)	1.83m (6.00 ft.)	6.63 m (21.75 ft.)
G5 (Mid Span)	5.37 m (17.63 ft.)	10.74 m (35.25 ft.)
G6-2d(a)	1.83m (6.00 ft.)	10.74 m (35.25 ft.)
G6-4d(b)	3.66m (12.00 ft.)	8.50 m (28.00 ft.)

Strain gauges were attached to the girder at four different elevations at the location of the load and a third distance. There was one on the underside of the bottom flange and three on the web. The gauges on the web were placed at the bottom, middle and top of the web with elevations from the bottom of the girder equal to 256 mm (10.0 in.), 393 mm (15.5 in.) and 530 mm (21.0 in.) respectively. Figure 3.# shows the strain gauges on the side and bottom of the girder. The strain gauges were oriented with the length of the girder.

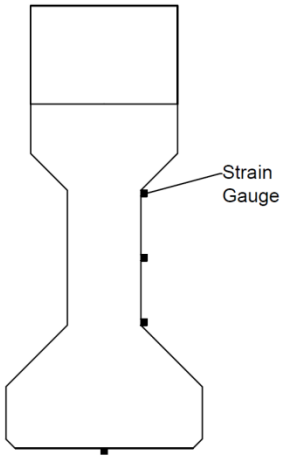

Fig. 4.3 Strain gauge placement

The deck depth varied slightly, about 12.7 mm (0.50 in.), from girder to girder. This difference was attributed to the sloping road way and irregularities in the construction of cast in place concrete. The difference was cut off the girders that were taller in order to have uniform cross sections for all girders to compare results.

4.1. Moment Cracking Test

The girders were positioned under the reaction frame such that the load could be applied at the mid span for the cracking test. Two steel plates were used as bearing plates on the strong

floor with an elastomeric pad positioned between the plates and the girder. The elastomeric pad was used to allow rotation at the ends while still supporting the girder and to replicate the in-service bridge girder supports.

A steel plate was placed on top of the girder at the mid span under the load. The plate was a 305 mm (12 in.) square plate that supported a spherical bearing. The bearing was greased to ensure a pure vertical load was applied during testing. A load cell was placed between the ram and the plate to record the applied load throughout the test.

Cracking tests were performed in order to determine the effective prestress force. The cracking test was performed by applying a load at the mid span of the girders until a visible transverse crack appeared along the bottom of the girder. The magnitude of the load was recorded and the crack location was identified with a marker, seen in Figure 3.4. After the crack was marked the load was removed. The crack would close tight after the load was removed.

Fig. 4.4 Strain gauge attached over crack on bottom of Girder

A strain gauge was then attached on the bottom of the girder across the crack, as shown in Figure 4.4. After words, the load was then reapplied. The reapplied load was increased by 25% in order to ensure the crack reopened. However, magnitude of the load did not exceed that which would result in permanent damage to the girders.

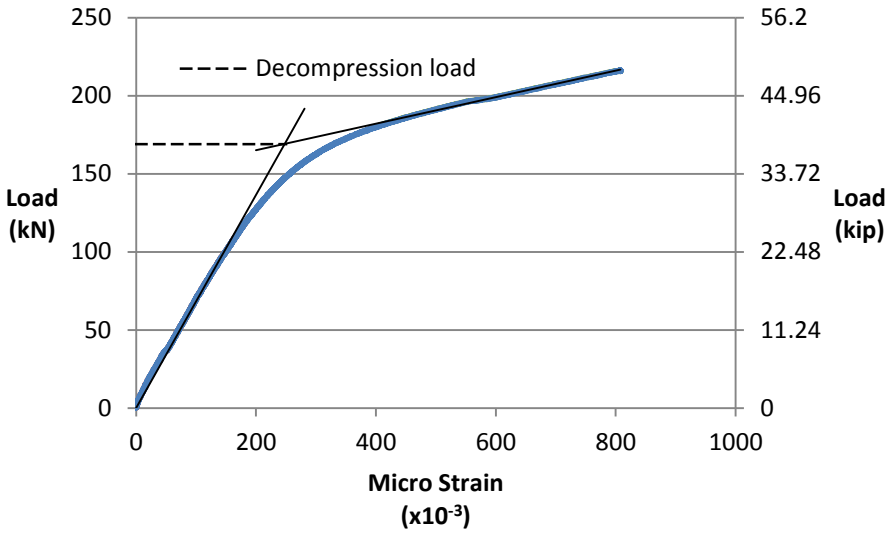

Fig. 4.5 Girder #3 cracking moment test data

After testing, a load vs. strain plot was created to determine the magnitude of the applied load where the crack opened. A typical plot can be seen in Figure 4.5 which is for the cracking test of Girder 3. The nonlinear behavior is illustrated as the strain increasing dramatically when the crack opens which can be seen in the cracking moment test of Girder #3. There are two different slopes which can be interpreted as the pre cracking stiffness, the steeper slope, and the post cracking stiffness. Two cracking tests were performed on each of the four girders. If there were any discrepancies between the decompression load of the two tests, a third test was performed to confirm the results.

The decompression or cracking load was acquired using the intersection of a straight line fit of the pre and post girder stiffness as shown in Figure 4.5. The load that corresponded to the intersection of the two lines was defined as the decompression load. The decompression load is the magnitude of the external load that causes zero stress at the bottom of the girder. Equation 4.1 can be used to calculate the stress at the bottom of a prestressed concrete girder subjected to an external load.

$$\boldsymbol{\sigma = -\frac{P}{A} - \frac{Pe_pC}{I_g} + \frac{M_{sw}C}{I_g} + \frac{M_{app}C}{I}}$$

Eq. 4.1

Where: σ = Stress at the bottom of the girder

P = Effective prestressing force

e_p = Eccentricity of the prestressing force from the centroid of the girder

C = Distance from the girder neutral axis to the bottom of the girder

M_{sw} = Moment at crack location due to girder self-weight

M_{app} = Moment caused by decompression load at crack

A = Total cross sectional area of girder and deck concrete

I_g = Moment of inertia of girder cross section

I = Composite moment of inertia

The stress, σ, is zero at the decompression load and the Equation 4.1 is used to solve for the effective prestressing force P. Equation 4.1can be manipulated to solve for P directly and is provided in Equation 4.2. It should be noted that P is the total effective prestressing force and not the force for each strand.

$$\boldsymbol{P = \frac{\left(\frac{M_{xt}C + M_{sw}C}{I_g}\right)}{\left(\frac{1}{A} + \frac{e_{pg}C}{I}\right)}}$$

Eq. 4.2

$$\boldsymbol{\sigma_{ps} = \frac{P}{A_{ps}}}$$

Eq. 4.3

Where: σ_{ps} = Effective stress of prestressing strands

A_{ps} = Total area of prestressing strands

After calculating the total effective prestressing force for each girder the effective prestress was calculated using Equation 4.3. The same can be done for individual strands if *P* is divided by the number of strands. The stress is calculated the same way but with individual strand area; however, the stress will be the same value.

Table 4.2 Prestressing values for each girder from cracking tests

2004 Girder #	Calculated *P* (kN/kip)	Calculated σ_s (MPa/ksi)	Initial Value (kN/kip)	% Losses
3	1303/293	1036/150	1425/320	8.43
4	1259/283	1001/145	1425/320	11.6
5	1281/288	1018/148	1425/320	10.0
6	1236/278	983/143	1425/320	13.1
Ave.	1268/287	1010/147	1425/320	10.3

The calculated effective prestressing values are fairly consistent for each of the tested girders. The values of the effective prestress is compared to the initial values for each girder in Table 4.2, the initial values were taken the bridge plans (see Appendix A4).

4.2. Capacity Testing

After all the cracking moment tests were completed, the girders were evaluated to determine which ones would be used for which test. This was done to avoid having the load on a location where there was significant damage. A list of which girder was used for which test(s) is found in Table 4.1.

4.2.1. Flexure Capacity Test

Girder 5 was used for the mid span flexural test shown in Figure 4.6 where the locations of the strain gauges on the web can be seen. An additional gauge was attached on the bottom of the girder at the location of the load as shown in Figure 4.3. An extra set of gauges of the same configuration were also attached at a third distance from the end of the girder. Strain gauges

were only placed on one side of the girder. String pots were attached to both sides of the girder at the same locations as the strain gauges and at one end directly at the center of the support. The string pots the end of the girder measured the compression of the elastomeric pad during testing. This distance was subtracted from the other deflection readings in order to obtain actual girder deflection.

Fig. 4.6 mid-span test set up in lab

The girders were monotonically loaded through failure. All data was at a rate of 10 Hz. Prior to testing, all sensors were initially zeroed and the string pots and load cell were calibrated prior to experimentation. The load cell was tested by applying a small load with the ram and reading the output load from the Vishay to ensure it was not calibrated wrong. The string pots were tested by simply lifting the strings a predetermined amount and making sure the Vishay output was an equivalent amount of deflection. All these checks were completed before each test to reduce the number of errors in data collection. The strain gauges couldn't be checked, but they could be shunt calibrated. Strain gauges read a resistance difference as they expand or

compress, but the wire from the gauge to the Vishay has resistance which can reduce the accuracy of the reading. Shunt calibration is a way to subtract out the wire resistance.

Fig. 4.7 Cracking prior to failure of mid-span test

Girder 5 was loaded to complete failure, which resulted due to a rupture of the compression block. During the flexure loading process the concrete at the bottom flange would initially start to crack, with cracks first appearing directly under the load. Additional cracks appeared that were more angled appeared and propagated.

The cracks became visible at the bottom flange at an applied load of 311 kN (70 kips) and would continue to widen up until failure. The cracks propagated out 1.5 m (5 ft.) on each side of the load location as seen in Figure 4.7 and were spaced 127 mm (5 in.) apart.

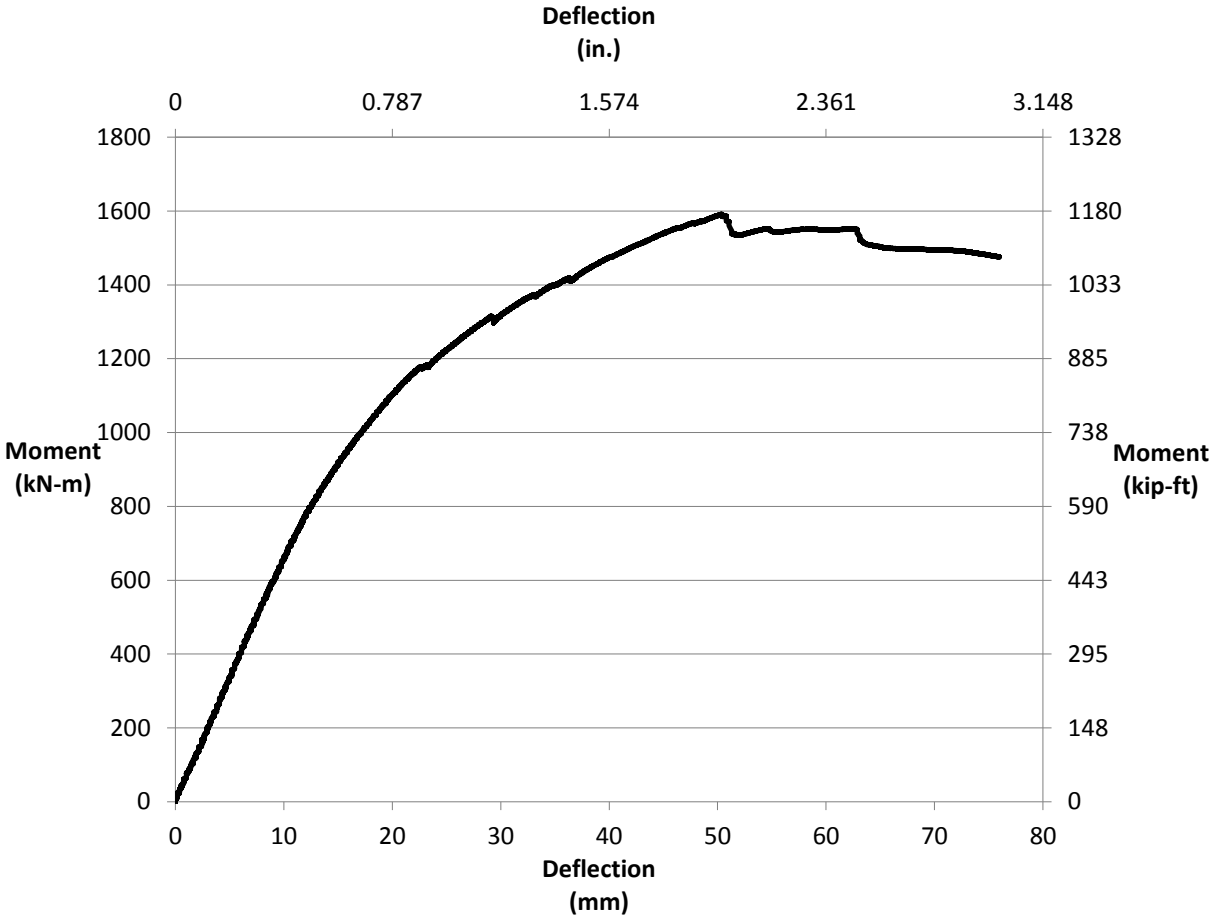

Fig. 4.8 Moment vs. Deflection of mid-span test

The maximum load was achieved at a magnitude of 592 kN (133 kips), which corresponds to a moment of 1590 kN-m (1174 kip-ft.) as seen in Figure 4.8. When the girder was at the maximum load then the concrete in the compression block started to fail and the load decreased by 22.2 kN (5 kips) and the deflection increased. The load never recovered after the top portion of the deck concrete failed in compression. The load was maintained until the girder had an ultimate failure of concrete crushing. The remaining deck concrete and top flange of the girder were strained to the point of crushing as the load was maintained on the girder.

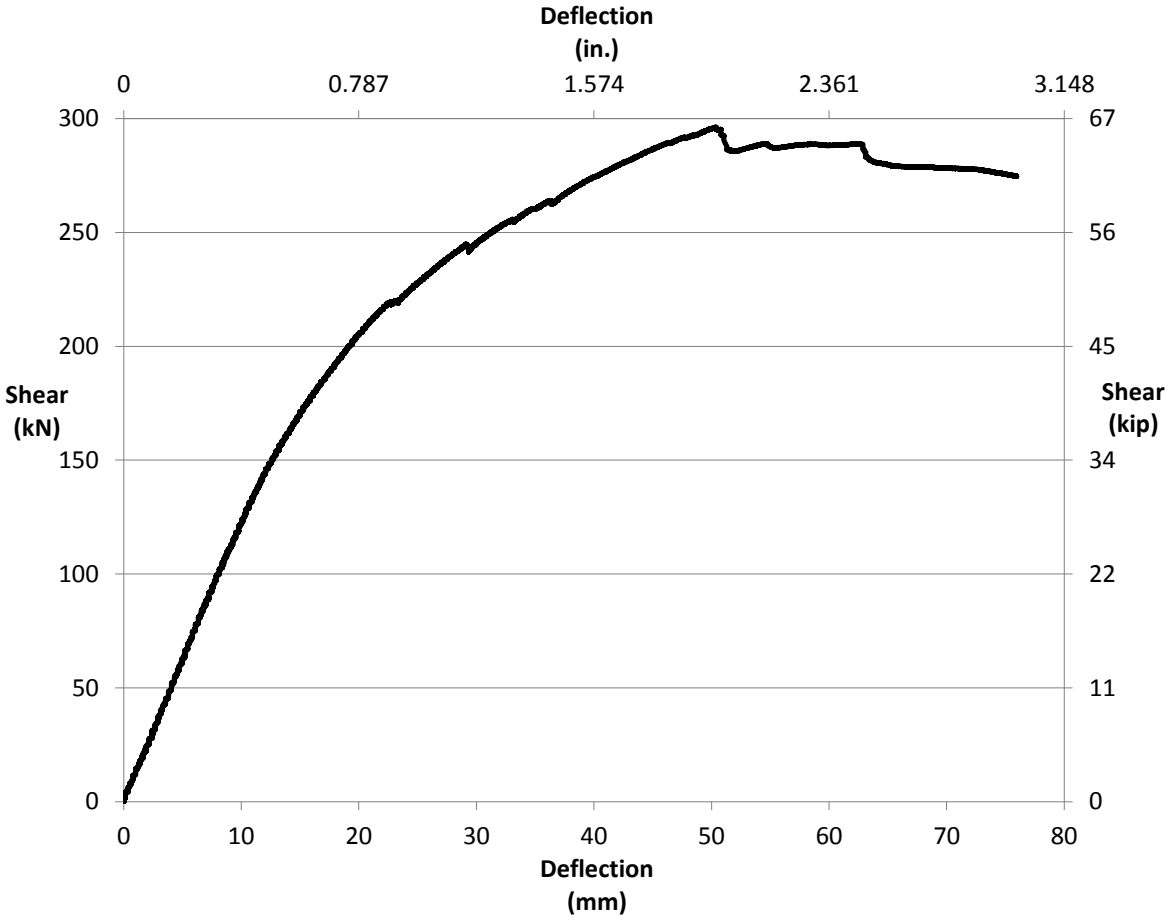

Fig. 4.9, Shear vs. Deflection plot for Mid-Span flexure test

Figure 4.9 above shows the shear that developed in the girder during testing. The shear was equal on both sides of the girder because the point load was located at the mid-span of the girder. The maximum shear force in the girder during the test was 296 kN (66 kip), which is the least of all the test.

Fig. 4.10, The complete failure of the girder

Figure 4.10 shows the final concrete failure of girder 5. The mild reinforcing can be seen to have buckled under the compressive stress. This buckling caused the concrete to fail in a compressive manner.

The strain gauges directly under the load suffered damage due to cracking. Once a crack would propagate through a strain gauge it would break it. Data was still recovered from the gauges directly under the applied load; however the strain distribution is not linear as expected. The skew in the data is attributed to the non-linear behavior of the girder directly under an applied load, but the strain is still consistent for this test. However the second set of gauges at a third distance on the girder did not have much cracking occur around them until the applied moment was high. A plot of different load increments and the corresponding strain readings is shown below in Figure 4.11 and Figure 4.12 for the mid-span gauges and third span gauges respectively is shown below.

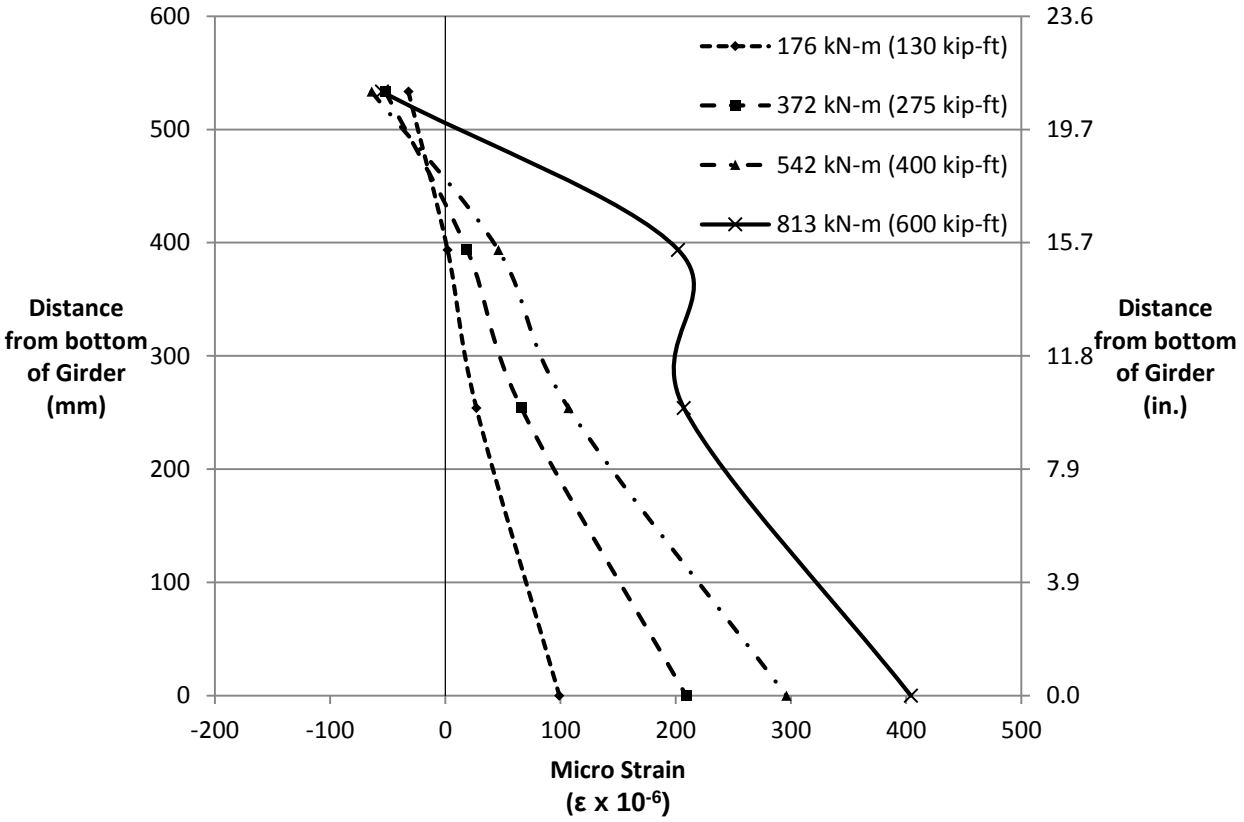

Fig. 4.11 Strain distribution along girder height during testing at mid-span

Plane sections remain plane for lower applied moments and then become non-linear when cracking occurs. Cracking occurred earliest under the applied load at the mid-span for this test and therefore Figure 4.12 is the second set of gauges at the same height on the girder and it shows a more linear plot. However for the mid-span the cross section has a neutral axis in approximately the same location and then it begins to rise as more moment is applied.

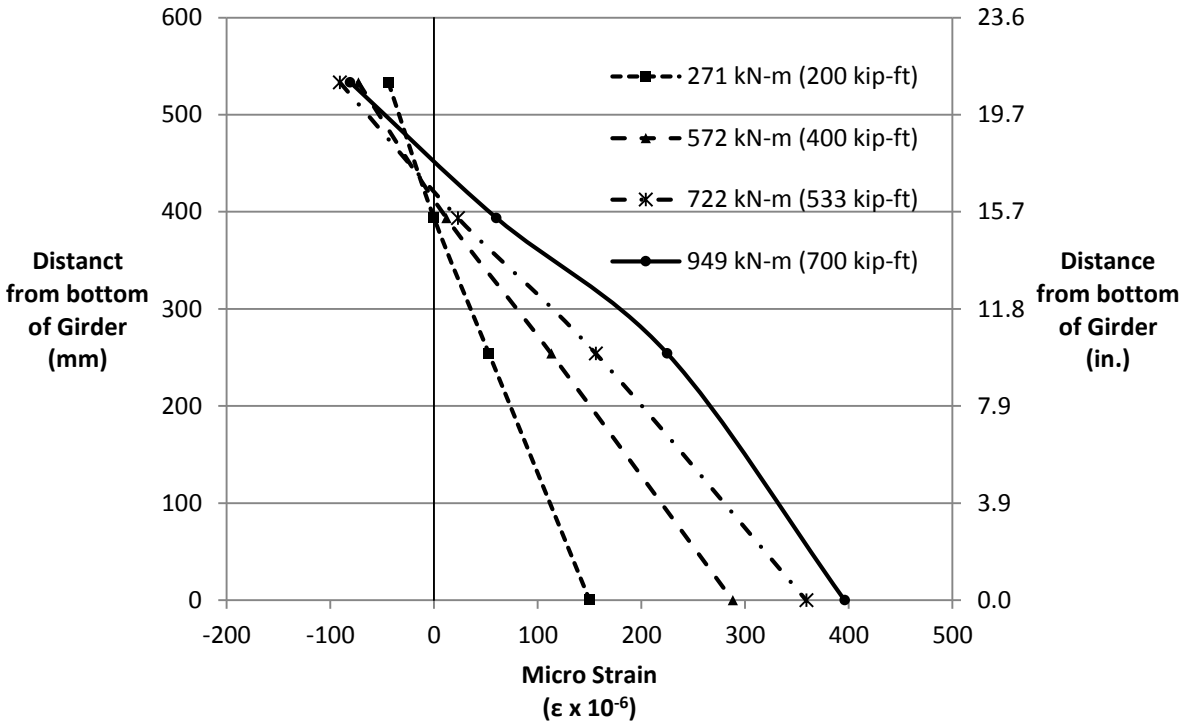

Fig. 4.12, Strain distribution along height of the girder during testing at a third span

The plot clearly shows that plane sections remained plane through the linearly elastic region of the loading and when cracking occurs the neutral axis rises up the cross section and the strain distribution is becomes non-linear. The moments shown on the graph were the applied moments at the location of the gauges from the point load. Figure 4.12 shows the same theme as Figure 4.11 in that the neutral axis is about the same location and then begins to rise with more applied moment.

4.2.2. 1-d Test

The next series of tests performed on the three remaining girders was based on the dimension *d*, which is the depth from the top of the deck concrete to the bottom of the girder. The 1-*d* test was performed with the load applied at a distance *d*, 0.914 m (36 in.), from the center of the support. This test was designed to determine the capacity of the girder with the

load primarily applied in shear. Girder #3 was used for both of the 1-*d* tests. There were two 1-*d* tests performed on Girder #3, one on each end. The set up for the shear test is shown below in Figure 4.13 and was the same as the mid-span flexural test.

Fig. 4.13 Test set up for G3-1d(b)

The load was monotonically applied through failure. Figure 4.14 shows the measured Shear vs. Deflection Plot for G3-1d(a). This plot clearly shows an initial elastic region up through a shear of approximately 1500 kN (337 kip). At this point cracking initiated. The cracking slightly reduced the stiffness of the girder; however, in this case it didn't decrease it by much mainly because the cracks were not very large. This secondary stiffness was observed through failure.

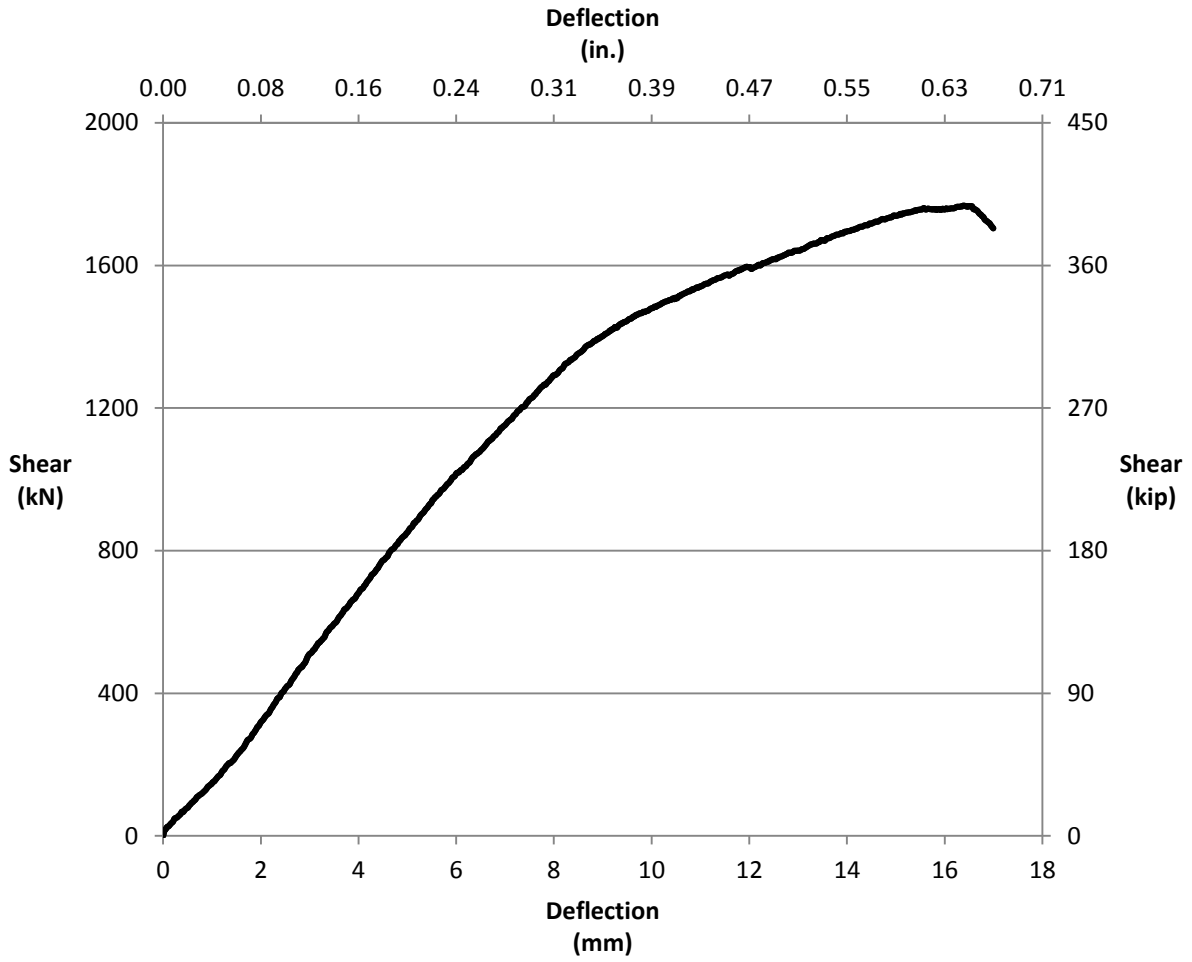

Fig. 4.14, G3-1d(a) shear vs. deflection

The maximum recorded load for G3-1d(a) was 1935 kN (435 kip) resulting in a maximum shear value of 1769 kN (398 kip), which can been seen in Figure 4.14 above.

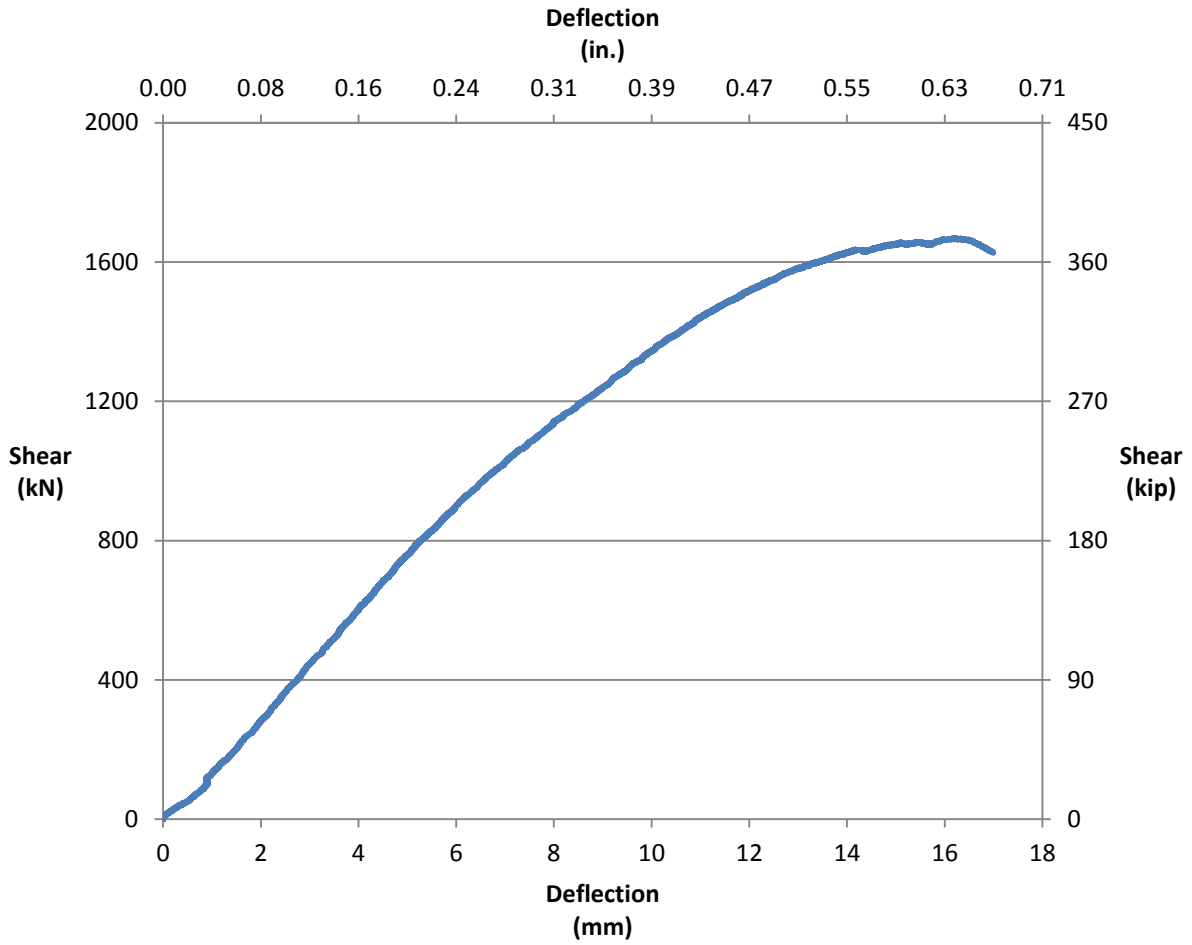

Fig. 4.15, G3-1d(b) shear vs. deflection

The maximum load for the G3-1d(b) test was 1843 kN (414 kip) correlates to a shear capacity of 1670 kN (375 kip),which can be seen in the plot above. An average of the two shear capacities is 1720 kN (386 kip) with G3-1d(b) was 5.54% less than G3-1d(a).

Both 1d test failures occurred with a very fast, brittle cracking that propagated along the shear cracks leading from the support to the load. The failure cracking pattern indicated a direct shear failure as seen in Figure 4.16.

Fig. 4.16 Failure crack of G3-1d(a)

However, on closer inspection of the girder it was observed that the prestressing strands had deboned from the concrete and is seen in Figure 4.17. Only the strands at the bottom of the girder were pulled in. The two strands in the top flange had not moved.

Fig. 4.17 Prestressing steel pulled into the girder at failure

The strands were pulled into the girder 2.5 mm (0.10 in.). The strands would have had a tensile force applied to them in order to be pulled into the girder. Section 5.3.2 describes a strut and tie model that explains how a large tensile force could develop in the prestressing steel. The strands being pulled in could have also been due to the fact that the concrete was crushing

around them and therefore the bond was broken. Either way the strands were resisting a large tensile force.

The figures below are the plots of Moment vs. Deflection for G3-1d(a and b). The moments were plotted to remain consistent with the other tests in this section.

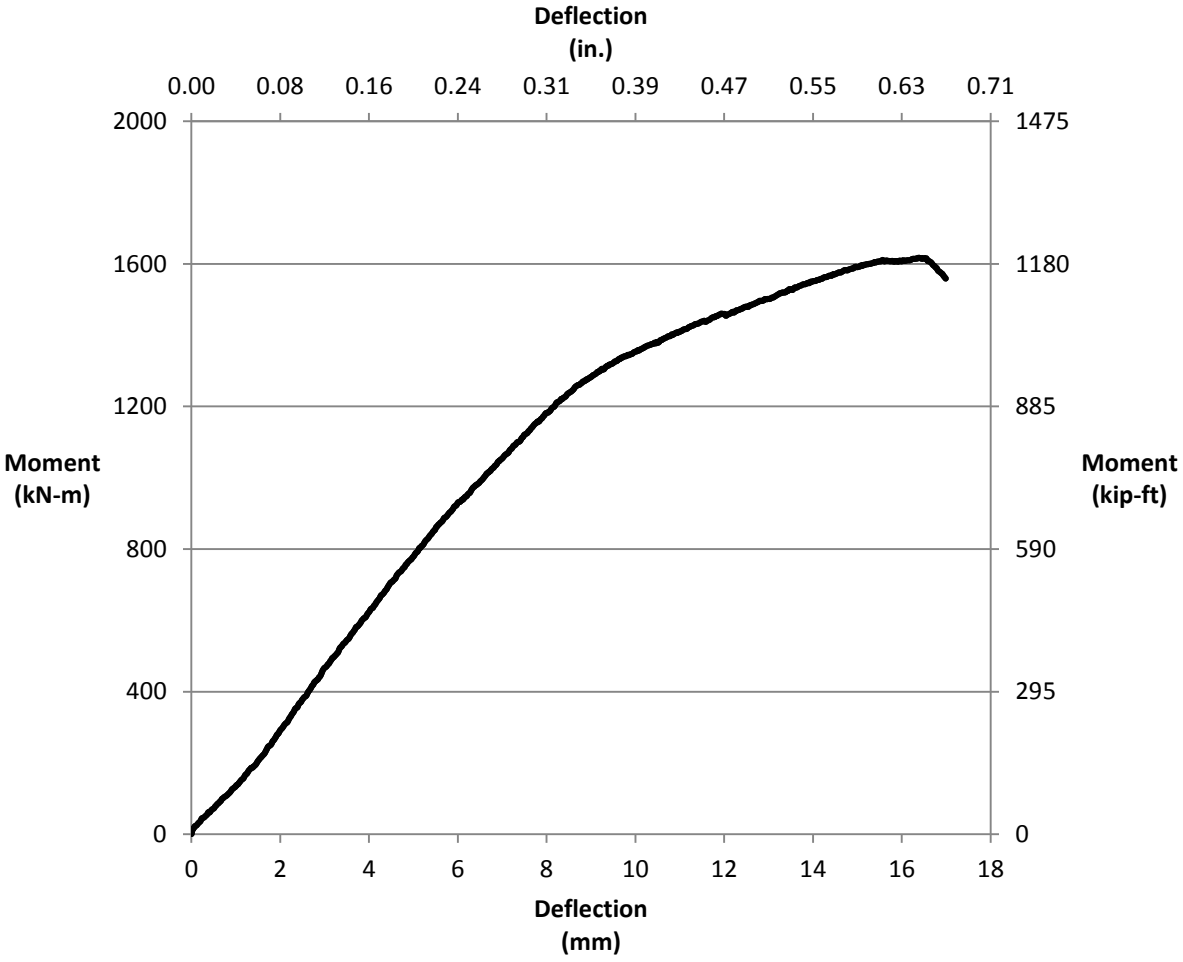

Fig. 4.18, G3-1d(a) moment vs. deflection plot

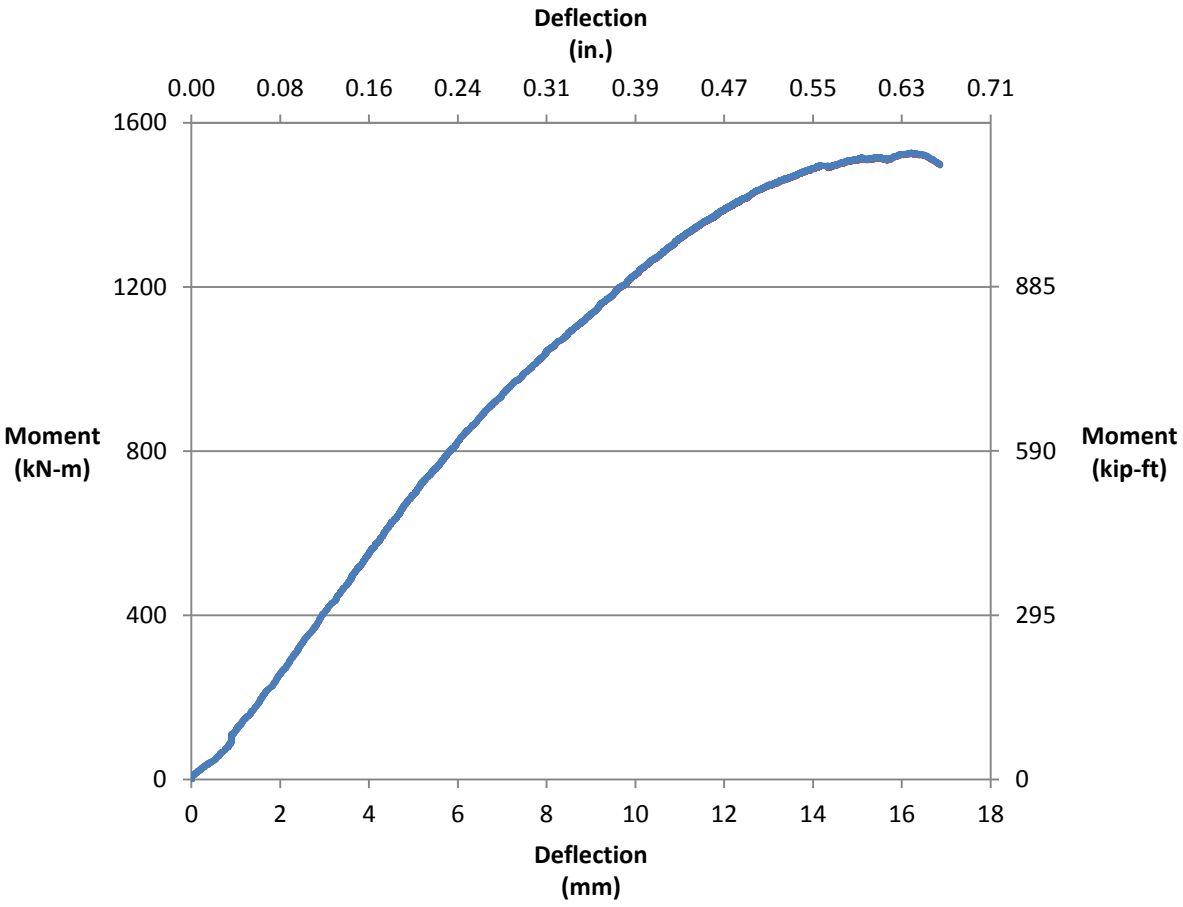

Fig. 4.19, G3-1d(b) Moment vs. Deflection

The moment capacities associated with the maximum loads of the G3-1d(a) and the G3-1d(b) tests were 1620 kN-m (1190 kip-ft.) and 1526 kN-m (1126 kip-ft.), respectively. An average of the two is 1573 kN-m (1158 kip-ft.), which is 1.36% less than the maximum moment capacity for the mid-span flexure test. The 1d tests have the possibility of failing under the combined shear and flexure stresses. Section 4.4 has the calculations for determining a direct shear failure or a combination of flexure and shear.

4.2.3. 2-d & 4-d Tests

Girders #4 & #6 were used for the remaining two tests which consisted of 2-*d* and 4-*d* tests. The focus of these two tests was to quantify the capacity subjected to flexural-shear

loading. Similarly as the 1-*d* tests, the loading locations for the 2-*d* and 4-*d* were 1.83 m (6 ft.) and 3.66 m (12 ft.) from the center line of the support, respectively.

Two tests were performed for each load position performed on Girder 6. The 2-*d* test was first on one end and then subsequently the 4-*d* test was performed on the opposite end. The testing of Girder 4 was performed in the opposite order. The order and alternative loading of the tests was selected to minimize the effects of one test on another.

Each of the tests had a failure similar to the mid-span flexural test, which was a concrete compression failure in the deck coupled with flexural cracking at the bottom of the girder. Figures 4.20 & 4.21 are the cracking scheme of G4-2d(b) and G6-4d(b) test. Figure 4.20 shows the concrete compression block during failure and the mild reinforcing in the deck can be seen as buckling in compression and lifting the cracked concrete up. Figure 4.21 is after the concrete has completely crushed and fell off the girder and the yielded mild reinforcing can be more easily seen.

Fig. 4.20 G4-2d(b) just prior to failure

Fig. 4.21 G6-4d(b) just after concrete crushing

The maximum externally applied load for the 2-*d* test was higher than that of the 4-*d* test, which was expected due to the closer proximity of the supports. However the moment of the two

girders are comparable because both failed in the same manner with the concrete crushing. Figures 4.22, 4.23, 4.24 & 4.25 are the moment vs. deflection plots of both of the 2-*d* and 4-*d* tests performed on Girders 4 and 6. The plots are moment vs. deflection and because of the different span lengths (L_e) of the girders at the time of testing the second test on each girder had a higher applied load because the load was closer to the supports, which increases the load for the same applied moment.

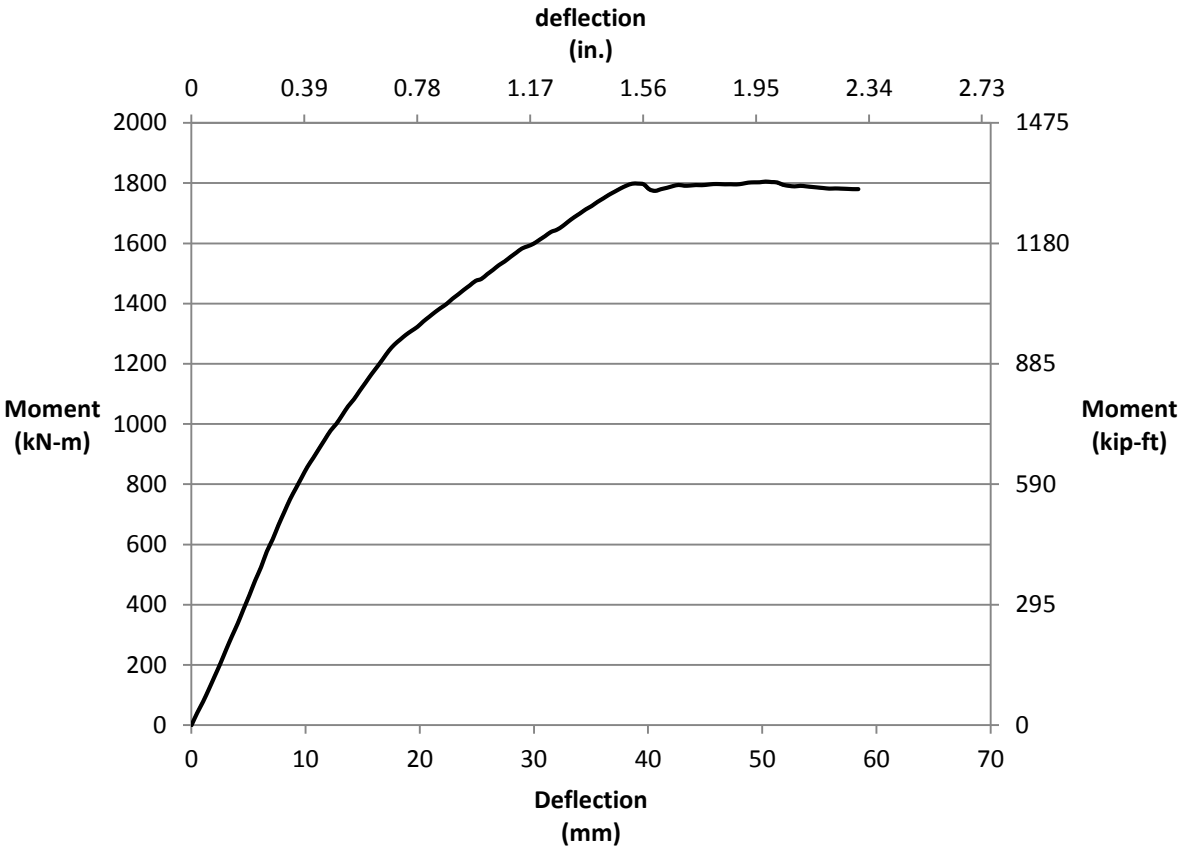

Fig. 4.22, G6-2d(a) moment vs. deflection

Figure 4.22 shows a maximum moment value of 1805 kN-m (1331 kip-ft.) and also has the same type of shape of the mid span flexure test that was recorded for girder 5 in section 3.2.1. There is a noticeable stiffness change at about 1200 kN-m (885 kip-ft.) which relates to the cracked section. This stiffness change is seen below in Figure 4.21, the second 2d test on girder 4, at about the same moment.

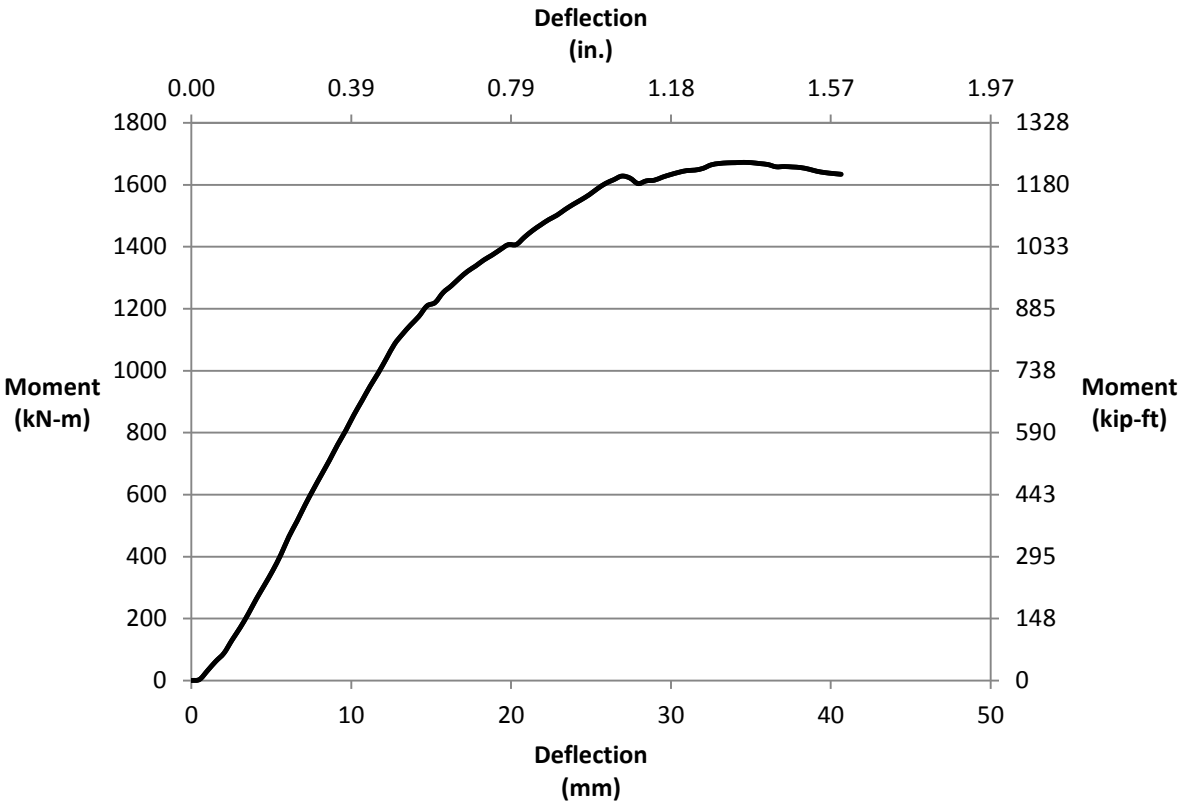

Fig. 4.23, G4-2d(b) moment vs. deflection

The maximum moment that was achieved in Figure 4.23 was 1673 kN-m (1233 kip-ft.), which is 7.36% less than the first 2d test. They both have the same general shape of a flexure failure. This test had a cracking stiffness change just before reaching 1200 kN-m (885 kip-ft.) which correlates with a lower maximum moment capacity. The average moment capacity for both 2d tests is 1739kN-m (1282 kip-ft.).

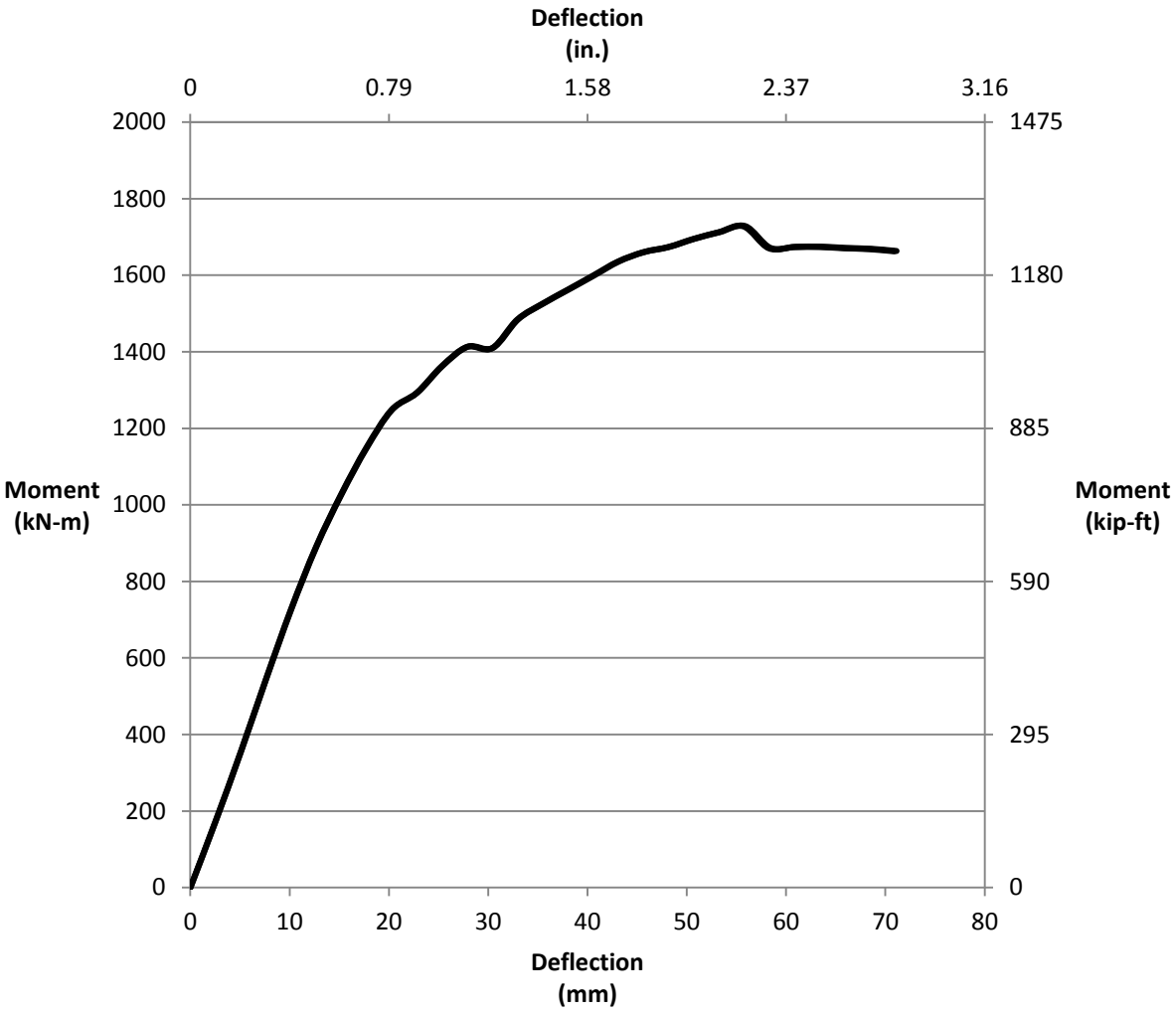

Fig. 4.24, G4-4d(a) moment vs. deflection

The data for G4-4d(a) in Figure 4.24 has the exact same shape as the previous 2d tests. There is a change in stiffness at about 1200 kN-m (885 kip-ft.). This test had a maximum moment capacity of 1731 kN-m (1276 kip-ft.).

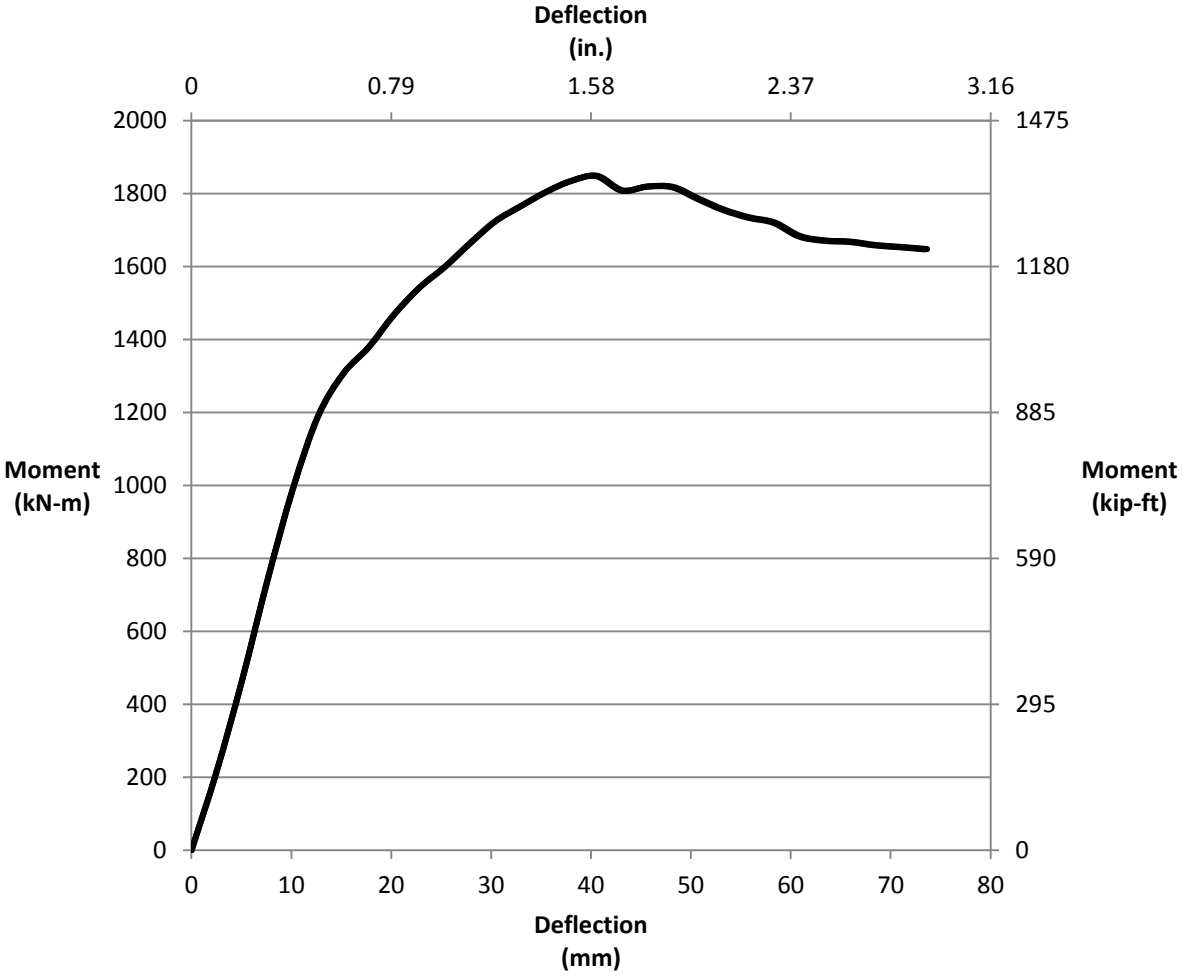

Fig. 4.25, G6-4d(b) moment vs. deflection

The final 4d test above in Figure 4.25 has the same stiffness change at the same applied moment. The maximum moment capacity is higher than all the other tests at 1849 kN-m (1363 kip-ft.), which is not much more than the capacity of the G6-2d(a). The average moment capacity for both 4d tests is 1790kN-m (1320 kip-ft.).

The following figures are the shear vs. deflection plots of each 2d and 4d test. The shear values will be used in section 4.4.1 to determine if the failures were a combination of flexure and

shear. Figures 4.26 and 4.27 are the 2d shear vs. deflection plots and Figures 4.28 and 4.29 are the 4d shear vs. deflection plots.

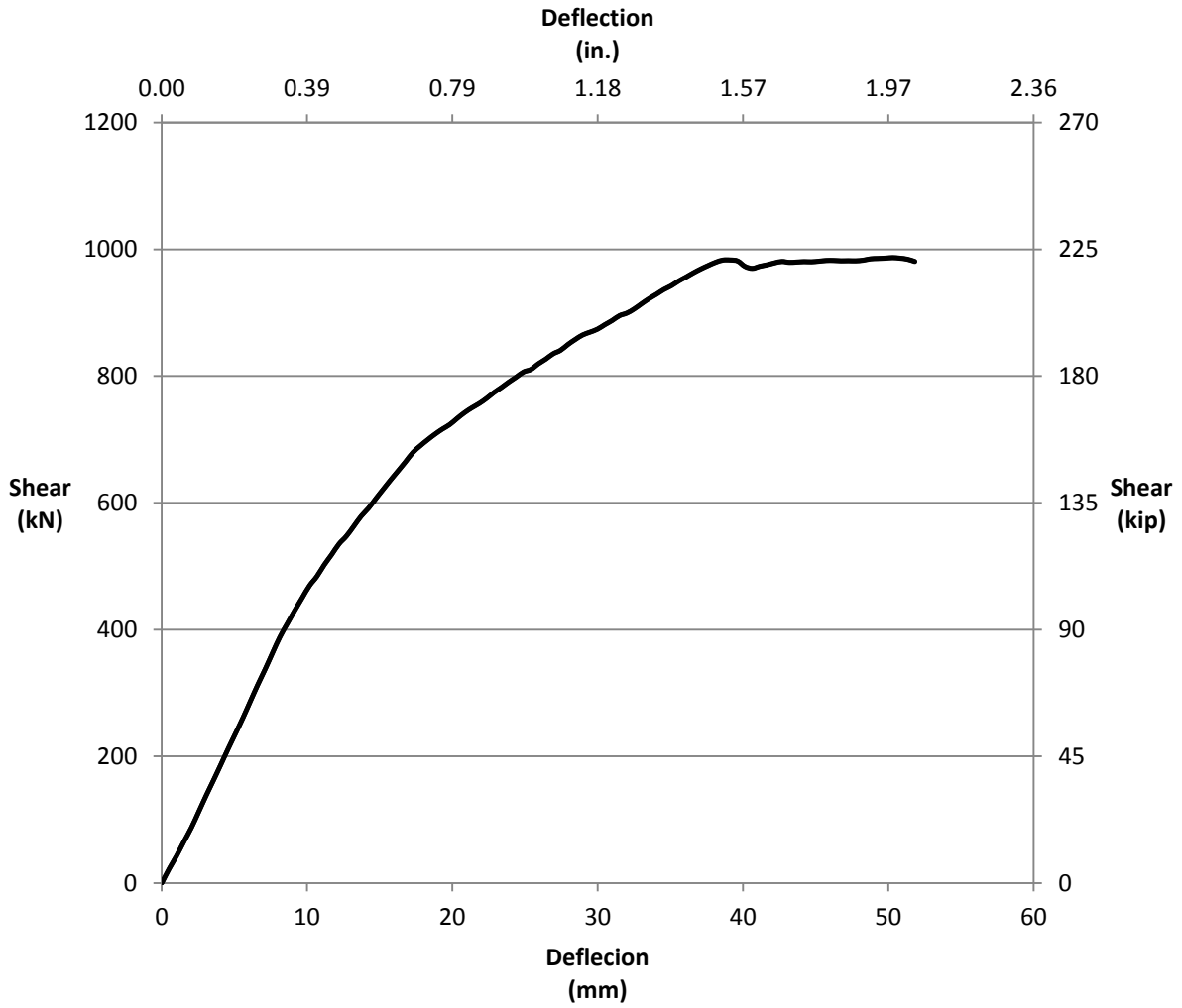

Fig. 4.26, G6-2d(a) shear vs. deflection plot

From Figure 4.26 the maximum shear was 987 kN (222 kip) which is higher than the maximum shear value for the G4-2d(b) test by 7.8% as compared to the G4-2d(b) test. This is showing that even though the G4-2d(b) test was the second test on that girder the capacity of the girder was consistent and therefore they were comparable.

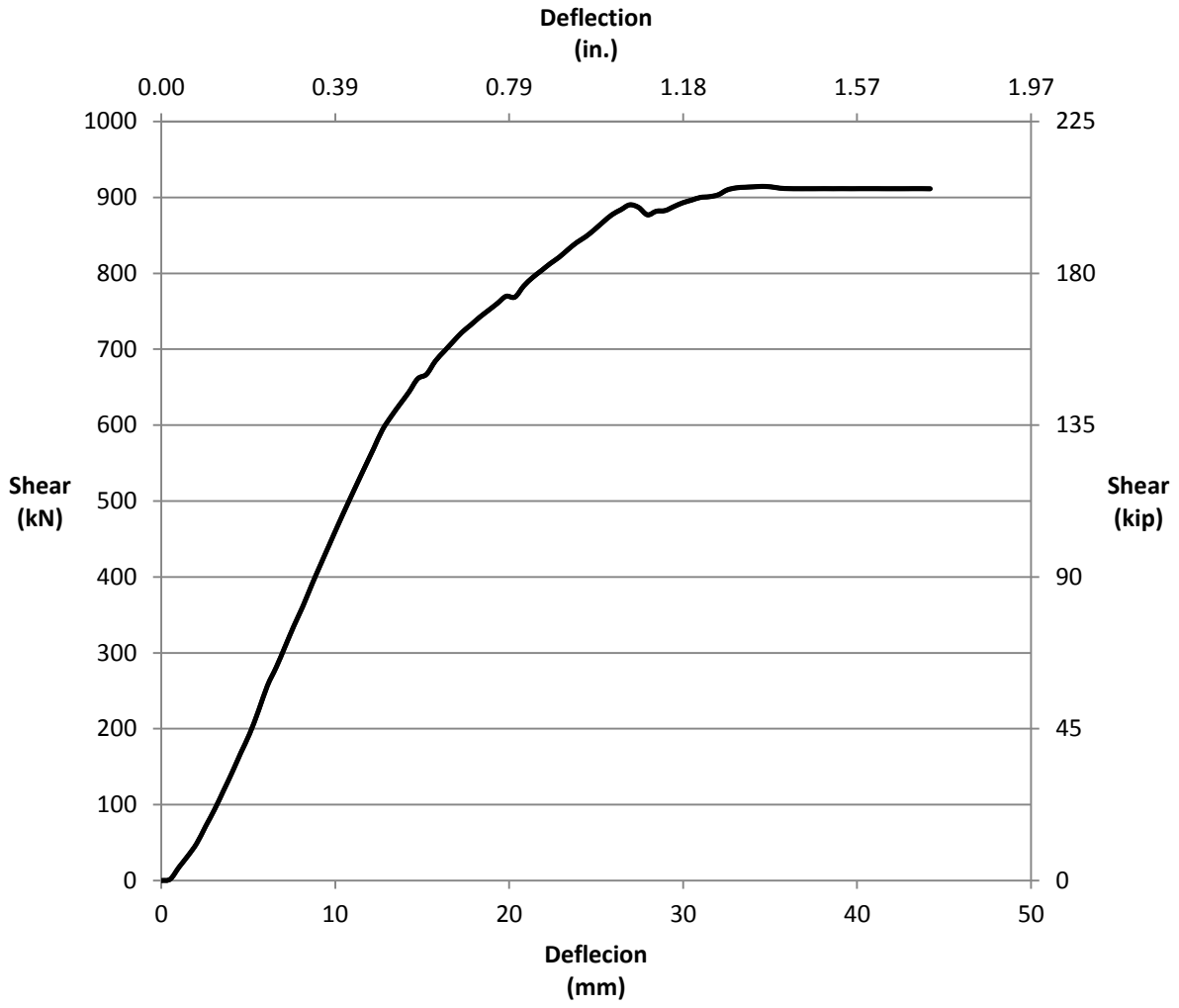

Fig. 4.27, G4-2d(b) shear vs. deflection plot

The maximum shear from the above data is 915 kN (206 kip). These values for both the 2d tests have an average of 951 kN (214 kip) and G4-2d(b) is 7.2% less than G6-2d(a) .

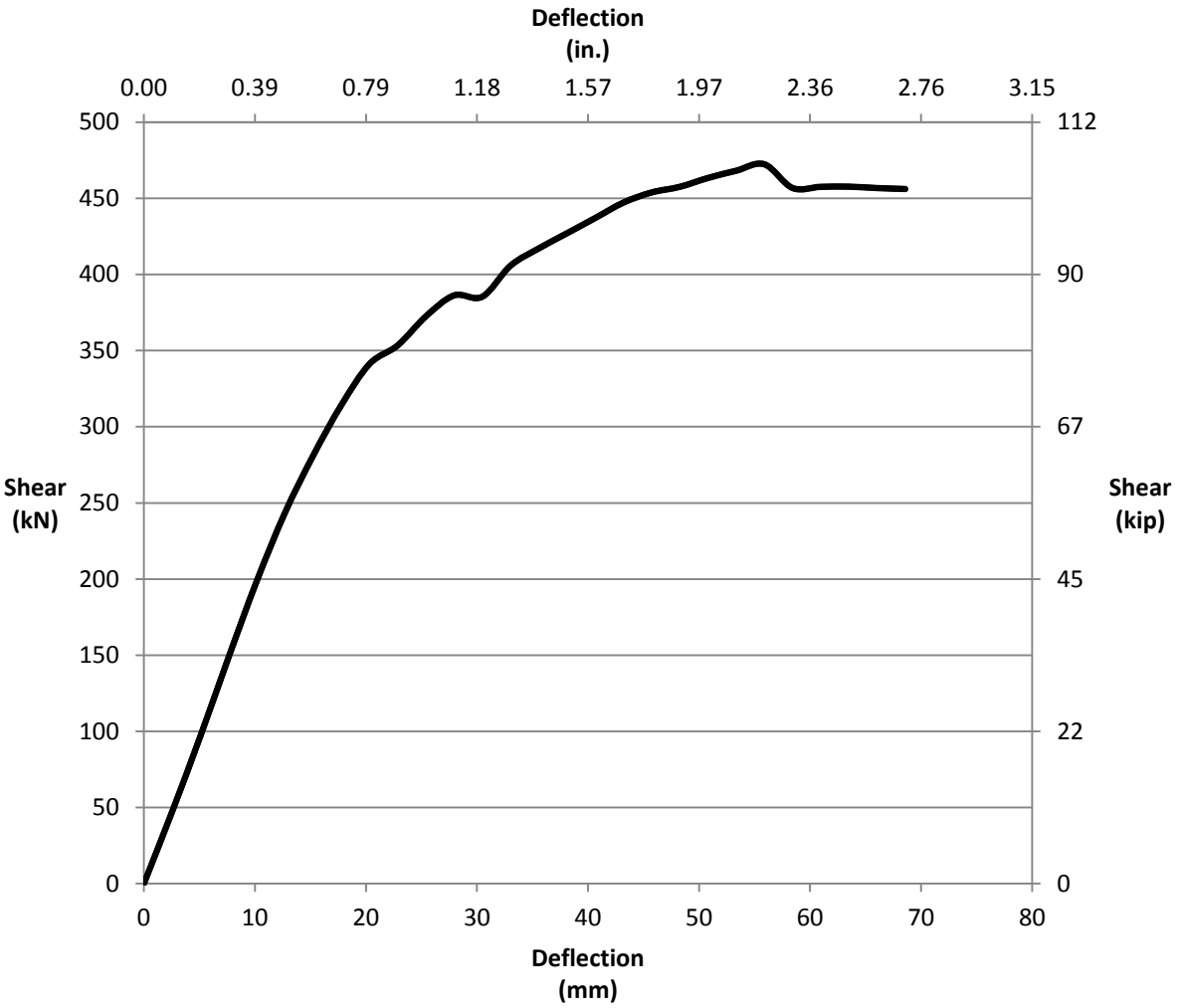

Fig. 4.28, G4-4d(a) shear vs. deflection plot

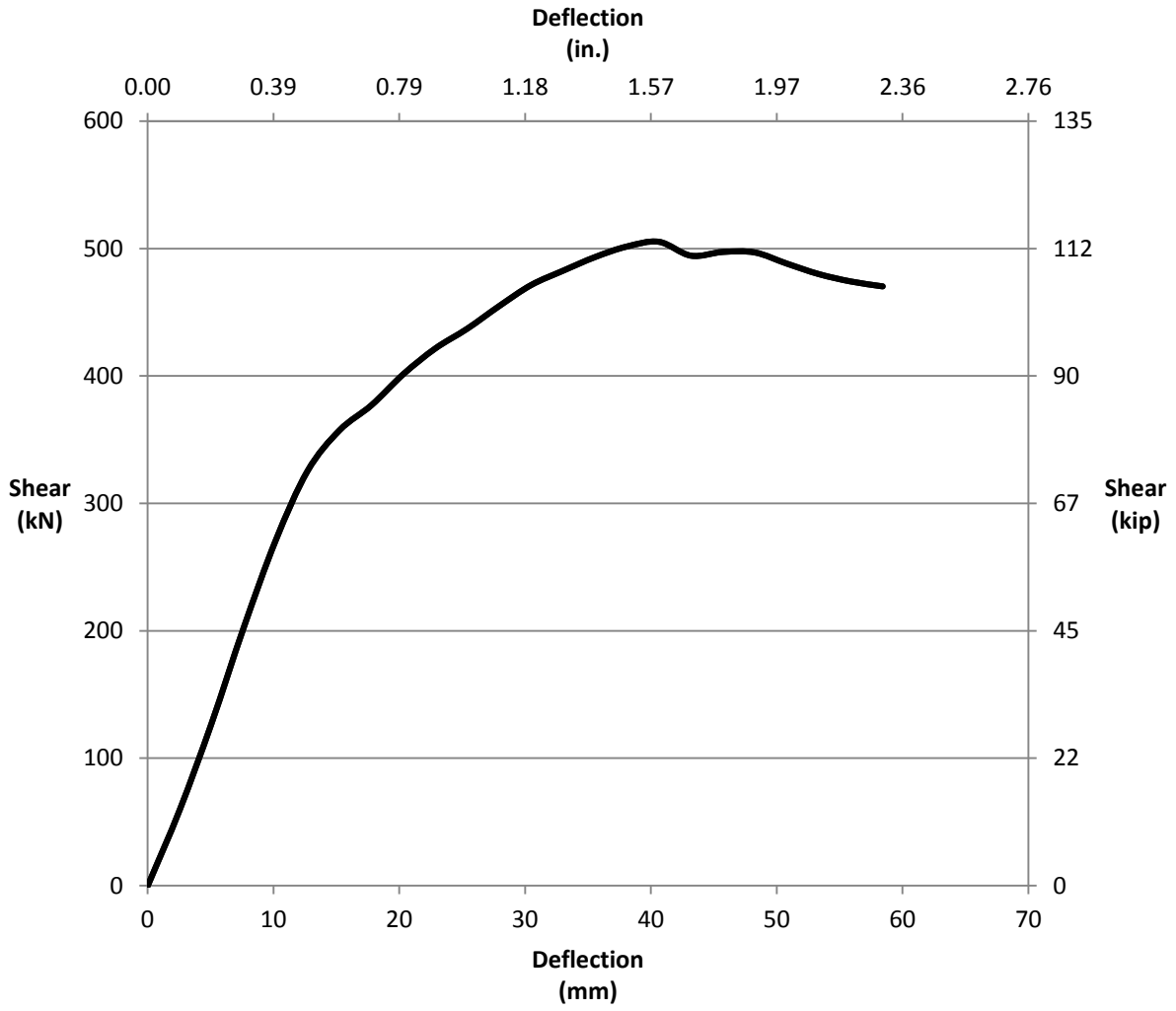

Fig. 4.29, G6-4d(b) shear vs. deflection plot

Figure 4.29 shows a maximum value of shear for the G4-4d(a) test to be 505 kN (113 kip). The maximum value of shear from Figure 4.27 was 472 kN (106 kip), which yields an average shear value for both 4d tests of 489 kN (110 kip). Just as G4-2d(b) had a lower value for shear and moment than girder G6, so it is for the 4d test. G4-4d(a) is 6.2% lower than the G6-4d(b) test. Girders G6 is about 7% stronger than G4 which is seen in the both the 2d and 4d test data.

The strain gauges that were placed on the girders during the testing are plotted below. Figure 4.28 is the strain readings for G4-2d(b) and Figure 4.29 is the readings for G6-4d(b). These strain readings are from directly under the load on the girder and can be seen in Figure 4.19.

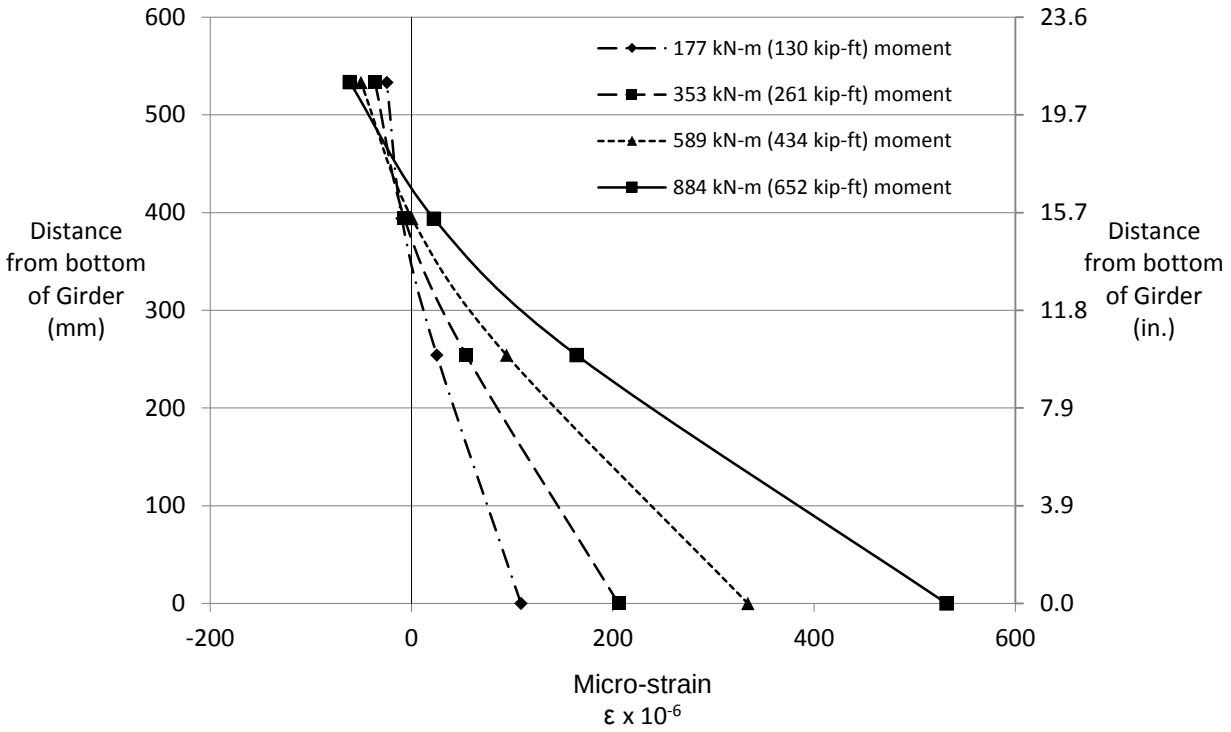

Fig. 4.30 Strain readings for G4-2d(b)

The neutral axis in Figure 2.30 starts to move up at an applied moment of 884 kN-m (652 kip-ft.), which is about when some cracking started to form. The neutral axis continues to move up the girder; however because of increased cracking in the girder some strain gauges were lost when a crack went through them. If a crack propagated through a strain gauge it would be torn in half and rendered useless. The strain gauges start to show the nonlinear trend of a plastic hinge with higher applied moments and the data is difficult to interpret. The same trend is seen in Figure 4.31 for G6-4d with the same placement of gauges.

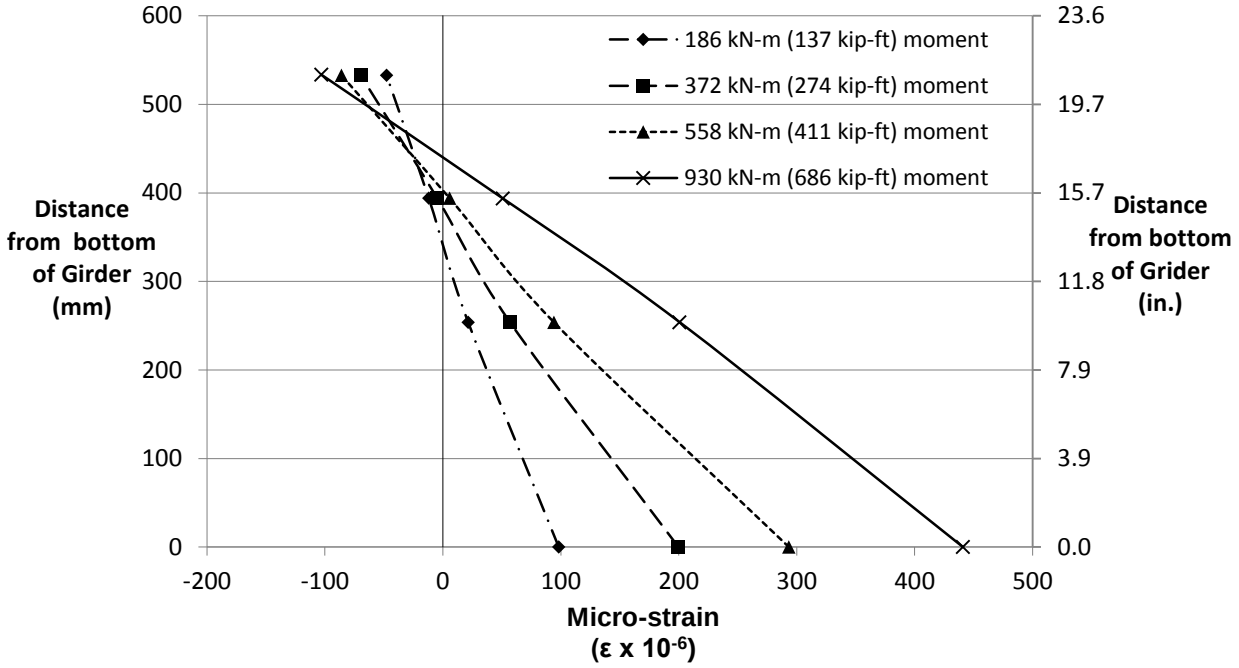

Fig. 4.31 Strain readings for G6-4d(b)

The gauge readings for each test indicate that the neutral axis was in the same location for small moments then it jumps up as the girder cracks. When the strain is plotted at higher moment values it is clear that the strain becomes none linear, which was expected for the cracked sections. The neutral axis also continues to climb up the girder until the Whitney stress diagram was reached.

4.3. Summary of Test Data

The maximum moment and shear values for each test are presented in Table 4.# for an overall look at how each test compared to the others.

Table 4.3 Summary of Test Data

Test	Moment kN-m (kip-ft.)	Shear kN (kip)
G3-1d(a)	1620 (1190)	1769 (398)
G3-1d(b)	1526(1126)	1670 (375)
Average 1d	**1573 (1158)**	**1720 (386)**
G6-2d(a)	1805 (1331)	987 (222)

G4-2d(b)	1673 (1233)	915 (206)
Average 2d	**1739 (1282)**	**951 (214)**
G4-4d(a)	1731 (1276)	505 (113)
G6-4d(b)	1849 (1363)	472 (106)
Average 4d	**1790 (1320)**	**489 (110)**
Mid-Span	1596 (1174)	296 (66)
Total Average	**1675 (1234)**	**864 (194)**

The following tables are a plot of measured moment and shear down the length of the girder for each test. It is interesting to note that the moment doesn't change much depending on the test. This is confirmed by a visual inspection of the failures as mentioned in the previous sections that discuss each test. The shear values decrease as the load is moved towards the center of the girder, which is expected due to the fact that the moment can become large from small applied forces that it usually governs the further from the supports the load is applied.

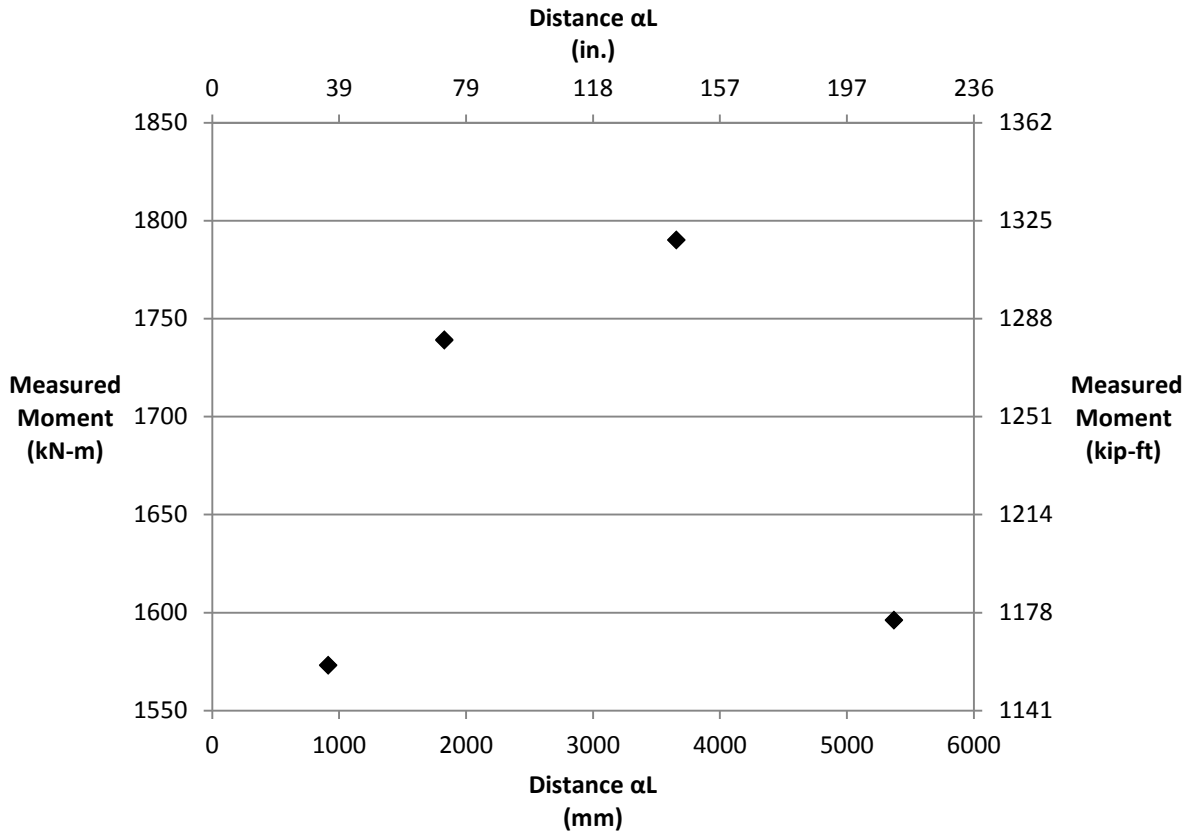

Fig. 4.32 Moment capacity at each test location

Figure 4.28 is the maximum measured moment for each test vs. the distance from the closest reaction. The measured maximum moment has an average value of 1675 kN-m (1234 kip-ft.) with a standard deviation of 106 kN-m (78.2 kip-ft.). Below in Figure 4.29 is the plot of Measured Shear vs. Distance from support. As seen in Figure 4.29 the measured shear decreases the further form the reaction the load is placed and therefore no overall average value was necessary. However the average value for each test was calculated and is in Table 4.3 above. The distance αL is seen in Figures 4.28 and 4.29, which is the distance that defines which test was done such as a 1d, 2d, 4d or mid-span test.

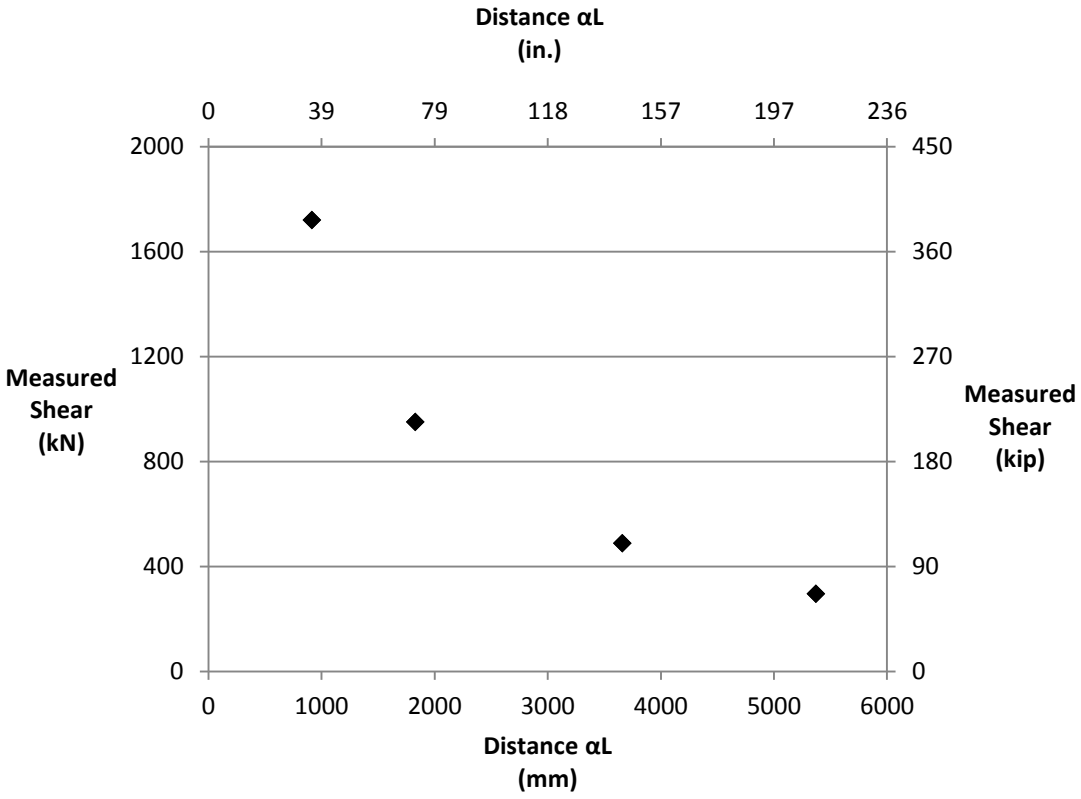

Fig. 4.33 Shear capacity at each test location

The strain gauges on the girders for the 2d, 4d, and mid-span tests showed the neutral axis in approximately the same starting location and it continued to rise with increased applied moments. This proves that the cross section of a prestressed concrete girder remains plane prior to significant cracking. After cracks have propagated up the bottom flange of the girder plane sections are no longer plane and a Whitney stress block analysis is required.

5. Comparison of Testing Results to AASHTO LRFD Design and ANSYS

The measured girder results from Chapter 4 were compared with those calculated in accordance to the AASHTO LRFD Specifications (2012). The AASHTO Specifications provides methodologies for calculating prestressing losses and nominal moment and shear capacities. Chapter five presents the comparisons between the measured and predicted values. Section 5.4 presents the finite-element modeling program ANSYS, which modeled the tests performed on the girders.

5.1. Prestressing Losses

Section 9.5 of chapter 5 of the AASHTO manual presents the methodologies for determining prestress loss due to short term and time-dependent losses. The two recommended methods for calculating prestress losses are the general method and the refined method. The two methods are applied for this research and compared to the measured prestress losses for each girder obtained during the cracking moment test in Section 4.1.

5.1.1. General Prestress Losses AASHTO 5.9.5.1

For this method, the total prestress losses (Δf_{pT}) are defined in Equation 5.1 (AASHTO, 2012) which is the sum of elastic shortening or elongation (Δf_{pEs}) and long-term losses (Δf_{pLT}) caused by shrinkage, creep of concrete and the relaxation of the prestressing steel. The elastic shortening loss is considered the short-term losses at the time of transfer and the long-term losses are all losses that occur after transfer.

$$\Delta f_{pT} = \Delta f_{Es} + \Delta f_{pLT}$$

Eq. 5.1

Both AASHTO methods for calculating prestress losses use the same elastic loss equation which is defined in Equation 5.2. This method of calculating the elastic shortening losses of a prestressed concrete member is typically based on transformed properties not gross properties are recommended in AASHTO for simplification. The other method uses the ratio of modulus of elasticity of steel to concrete and the concrete stress at the centroid of the prestressed strands immediately after transfer. The issue with the second method is calculating what the stress is after the transfer which typically requires iterations to converge on a solution.

$$\Delta f_{pES} = \frac{A_{ps} f_{pbt}\left(I_g + e_m^2 A_g\right) - e_m M_g A_g}{A_{ps}\left(I_g + e_m^2 A_g\right) + \frac{A_g I_g E_{ci}}{E_p}}$$

Eq. 5.2

Where: A_{ps} = Cross sectional area of the prestressing steel (1.95 in.^{2})

I_g = Moment of inertia of the girder (22750 in.^{4})

A_g = Cross sectional area of the girder (276 in.^{2})

E_p = Modulus of Elasticity of the Prestressing tendons (28500 ksi)

E_{ci} = Modulus of Elasticity of the concrete at transfer or at time of load application (3640 ksi)

f_{pbt} = The stress in the prestressed steel before transfer (202.5 ksi)

e_m = The average mild steel eccentricity at the mid span of the girder (5.465 in.)

The long-term losses (f_{pLT}) and correction factors for humidity (γ_h) and concrete strength (γ_{st}) are given in Equations 4.#, 4.# and 4.# respectively.

$$f_{pLT} = 10\frac{f_{pi} A_{ps}}{A_g}\gamma_h \gamma_{st} + 12.0\gamma_h \gamma_{st} + \Delta f_{pR}$$

Eq. 5.3

$$\gamma_h = 1.7 - 0.01H$$

Eq. 5.4

$$\gamma_{st} = \frac{5}{1 + f'_{ci}}$$

Eq. 5.5

Where: f_{pi} = Stress in prestressing steel prior to transfer (202.5 ksi)

γ_h = Correction factor for humidity

γ_{st} = Correction factor for concrete strength

f_{pR} = Estimation of relaxation losses in prestressed steel tendons for low relaxation strands (2.4 ksi)

H = Average annual ambient relative humidity (55 % Based on Figure 5.4.2.3.3-1 (AASHTO, 2012))

f'_{ci} = Concrete strength at transfer (4 ksi)

The plans of the girders list a total prestress force of 1422.1 kN (320.3 kips) after all losses, which when divided by the total area of prestress steel yields a stress per strand of 1132.4 MPa (164.26 ksi). The Table 4.# shows the loss calculation values if the strands were initially stressed to 0.75 of the ultimate stress (f_{pu}) of the strands, which is from Table 5.9.3-1 (AASHTO, 2012).

Table 5.1 General Prestress losses

General Prestress Losses	
Δf_{pEs}	92.4 MPa (13.4 ksi)
Δf_{pLT}	241.7 MPa (35.1 ksi)
Δf_{pT}	334.4 MPa (48.5 ksi)
f_{pe}	1062 MPa (154.0 ksi)

Table 5.2 shows the calculated losses from elastic and long-term losses and the combination for the total losses. The total losses were subtracted from the initial jacking stress of $0.75f_{pu}$ [1396.19 MPa (202.50 ksi)] for a calculated residual prestressing stress (f_{pe}) of 1080 MPa (157 ksi). A comparison of this data is represented in the end of section 5.2 on Table 5.4.

5.1.2. Refined Time Dependent Prestress Losses

The method for calculating the initial elastic shortening losses for the refined method is defined in the previous section; however, the long-term losses for this method are more complicated. This section provides the equations to predict time-dependent losses for the prestress force. The refined method has two different time periods in which long-term prestressing losses are calculated, before deck placement ($_{id}$) and after deck placement ($_{df}$) shown in Equation 5.6 below.

$$\Delta f_{pLT} = \left(\Delta f_{pSR} + \Delta f_{pCR} + \Delta f_{pR1}\right)_{id} + \left(\Delta f_{pSD} + \Delta f_{pCD} + \Delta f_{pR2} + \Delta f_{pss}\right)_{df} \quad \text{Eq. 5.6}$$

Where: Δf_{pSR} = Prestress losses due to the shrinkage of the girder between transfer and deck placement

Δf_{pCR} = Prestress losses due to creep of girder concrete between transfer and deck placement

Δf_{pR1} = Prestress losses due to relaxation of prestress tendons between transfer and deck placement (1.2 ksi for low relaxation strands)

Δf_{pSD} = Prestress losses due to shrinkage of the girder after deck placement

Δf_{pCD} = Prestress losses due to creep of girder after deck placement

Δf_{pR2} = Prestress losses due to relaxation of prestress tendons after deck placement (1.2 ksi for low relaxation strands)

Δf_{pss} = Prestress gain due to shrinkage of deck

Equations 5.7 through 5.9 are used to calculate the time-dependent losses before deck placement and Equations 5.10 through 5.13 are used to calculate the time-dependent losses after deck placement.

$$\Delta f_{pSR} = \varepsilon_{bid} E_p k_{id}$$

Eq. 5.7

$$\Delta f_{pCR} = \left(\frac{E_p}{E_{ci}}\right) f_{cgp} \psi_b(t_d, t_i) k_{id}$$

Eq. 5.8

$$\Delta f_{pR1} = \frac{f_{pt}}{k_L}\left(\frac{f_{pt}}{f_{py}} - 0.55\right)$$

Eq. 5.9

$$\Delta f_{pSD} = \varepsilon_{bdf} E_p k_{df}$$

Eq. 5.10

$$\Delta f_{pCD} = \frac{E_p}{E_{ci}} f_{cgp} \psi_b\left[(t_f, t_i) - \psi_b(t_d, t_i)\right] k_{df} + \frac{E_p}{E_c} \Delta f_{cd} \psi_b(t_d, t_i) k_{df}$$

Eq. 5.11

$$\Delta f_{pR2} = \Delta f_{pR1}$$

Eq. 5.12

$$\Delta f_{pss} = \frac{E_p}{E_c} \Delta f_{cdf} k_{df}\left[1 + 0.7\psi_b\left(t_f, t_d\right)\right]$$

Eq. 5.13

Which:

$$k_{id} = \frac{1}{1 + \frac{E_p}{E_{ci}}\frac{A_{ps}}{A_g}\left(1 + \frac{A_g e_{pg}^2}{I_g}\right)\left[1 + 0.7\psi_b\left(t_f, t_i\right)\right]}$$

Eq. 5.14

$$\varepsilon_{bdf} = k_s k_{hs} k_f k_{td} 0.48 \times 10^{-3}$$

Eq. 5.15

$$\Delta f_{cd} = \frac{\Delta P}{A_g} + \frac{\Delta P e_{pg}^2}{I_g} + \frac{M_g e_{pg}}{I_g}$$

Eq. 5.16

$$\Delta P = \left(\Delta f_{pES} + \Delta f_{pSR} + \Delta f_{pCR} + \Delta f_{pR1}\right) A_{ps}$$

Eq. 5.17

$$k_{df} = \frac{1}{1 + \frac{E_p}{E_{ci}}\frac{A_{ps}}{A_g}\left(1 + \frac{A_g e_{pc}^2}{I_g}\right)\left[1 + 0.7\psi_b\left(t_f, t_i\right)\right]}$$

Eq. 5.18

$$\Delta f_{cdf} = \frac{\varepsilon_{ddf} A_d E_{ed}}{\left[1 - 0.7\psi_b\left(t_f, t_d\right)\right]}\left(\frac{1}{A_c} - \frac{e_{pc} e_d}{I_c}\right)$$

Eq. 5.19

$$\psi_b(t, t_i) = 1.9 k_s k_{hc} k_f k_{td} t_i^{-0.118}$$

Eq. 5.20

$$k_s = 1.45 - 0.13\left({}^{V}/_{S}\right) \geq 1.0$$

Eq. 5.21

$$k_{hc} = 1.56 - 0.008H$$

Eq. 5.22

$$k_f = \frac{5}{1 + f'_{ci}}$$

Eq. 5.23

$$k_{td} = \frac{t}{61 - 4f'_{ci} + t}$$

Eq. 5.24

Where: ε_{bid} = Concrete shrinkage strain before deck placement (0.0003)

k_{id} = Transformed section coefficient that accounts for time dependent interaction between the concrete and the steel tendons prior to deck placement (0.88)

f_{cgp} = Concrete stress at prestressing centroid after transfer and elastic losses (1.73 ksi)

e_{pg} = Eccentricity of the prestressing force from the centroid of the girder (5.465 in.)

$\psi_b(t, t_i)$ = Girder creep coefficient, value depends on *t* values used

t_f = Final time (2920 days)

t_i = Transfer time (0.75 days)

t_d = Age to deck placement (56 days)

Δf_{pt} = Stress in prestressing strands immediately after transfer, taken not less than $0.55 f_{py}$

k_l = 30 for low relaxation strands and 7 for all other strands

ε_{bdf} = Shrinkage strain of girder after deck placement (0.00026)

ε_{ddf} = Shrinkage strain of deck after deck placement (0.00061)

k_{df} = Transformed section coefficient that accounts for time dependent interaction between the concrete and steel tendons after deck placement. (0.838)

E_c = Modulus of elasticity of concrete at 28 day strength (4070 ksi)

ΔP = The change in prestressing force prior to deck placement (75.7 kip)

Δf_{cd} = Stress of concrete at prestressing centroid after deck placement (0.4 ksi)

Δf_{cdf} = Change in concrete stress at centroid of prestressing steel due to deck shrinkage (-0.6 ksi)

H = Relative humidity (55 %). In the absence of better information, H may be taken from Figure 5.4.2.3.3-1 (AASHTO, 2012) or from a reliable accurate source

A_d = Cross sectional area of deck concrete (504 in.^{2})

V = Volume of girder (120060 in.^{3})

S = Surface area of girder (39420 in.^{2})

k_s = Factor for the effect of the volume-to-surface ratio of the component (1.05)

k_{hc} = Humidity factor for creep (1.13)

k_f = Factor for the effect of the concrete strength (1.0)

k_{td} = Time development factor, value depends on time used

t = Maturity of concrete, t = 0 days at time of casting, t_f = 2920 days at time of demolition, t_d = 56 days at time of deck placement and t_i = 0.75 days at time of transfer.

Table 5.3 lists the calculated values for all of the components that add to the total losses. The elastic losses need to be added to the total long term losses to get a total loss. The elastic prestress losses are the same as the general losses calculated in the previous section.

Table 5.2 Refined Prestress Losses

Long-Term Loss Components	
Δf_{pES}	+92.4 MPa (+13.4 ksi)
Δf_{pSR}	+60.0 MPa (+8.7 ksi)
Δf_{pCR}	+106.8 MPa (+15.4 ksi)
Δf_{pR1}	+8.27 MPa (+1.20 ksi)
Δf_{pSD}	+42.7 MPa (+6.2 ksi)
Δf_{pCD}	+13.1 MPa (+1.9 ksi)
Δf_{pR2}	+8.27 MPa (+1.20ksi)
Δf_{pss}	-38.7 MPa (-5.6 ksi)
Total Long-Term Losses from Refined Method	
Δf_{pLT}	200.0 MPa (29.0 ksi)
Total Prestressing Losses from Refined Method	
Δf_{pT}	292.3 MPa (42.4 ksi)

The total loss (Δf_{pT}) is subtracted from $0.75f_{pu}$, which is the jacking stress prior to transfer, yields a final effective stress (f_{ps}) for the prestressing steel of 1103 MPa (160 ksi) that is 2.1% less than the jacking stress. This final stress correlates to a total prestressing force (P_e) at the time of testing of 1388 kN (312 kips).

5.1.3. Comparison of AASHTO and Cracking Tests for Effective Prestress

The average effective prestressing stress from the cracking moment tests is 1010 MPa (147 ksi) with a standard deviation of 19.68 MPa (2.69 ksi). This average is compared to the two different methods of prestress losses in Table 5.4 below.

Table 5.3, Comparison of Calculated Prestressing to Measured

Method	Calculated Effective Prestress	% from Test Average
Cracking Moment	1010 MPa (147 ksi)	NA
General Prestress Loss	1062 MPa (154.0 ksi)	4.8%
Refined Long-Term loss	1103 MPa (160 ksi)	8.8%

The general method predicted a prestress loss 4.8% higher than the value from the moment cracking tests. The general method is considered the more conservative method as was expected to be lower than tested results. The refined method was higher than the general method as expected. The refined method is meant to be more accurate and therefore less conservative or should calculate less prestress losses. It was no surprise that this method predicted a higher prestress value than tested values and the general method. Even though both methods over predicted the prestressing value, they were both under the value on the bridge plans of 1131MPa (164 ksi). The bridge plans did not indicate how the prestess losses were calculated.

5.2. Moment Design

The moment capacity was predicted using two methods for this research, the equations from AASHTO LRFD Specifications (2012) and the finite element computer software ANSYS. The capacity of both methods is used and compared to the testing results at the end of this section.

5.2.1. AASHTO LRFD Moment Design

The nominal moment capacity (M_n) of a concrete member according to AASHTO LRFD Specifications (2012) is provide as equation 5.25. The strength reduction factor was neglected for this calculation so a direct comparison with the measured results could be obtained.

$$M_n = A_{ps}f_{ps}\left(d_p - {}^{a}/_{2}\right) + A_s f_s\left(d_s - {}^{a}/_{2}\right) - A'_s f'_s\left(d'_s - {}^{a}/_{2}\right) + 0.85 f'_c (b - b_w) h_f \left({}^{a}/_{2} - {}^{h_f}/_{2}\right)$$

Eq. 5.25

Where:

A_{ps}= the total area of prestressing steel (1.95 in.^{2})

f_{ps}= Specified tensile strength of prestressing steel (270 ksi)

A_s= Total area of tensile mild steel reinforcement (0.62 in.^{2})

f_s= Stress in tensile mild steel (60 ksi)

A'_s= Total area of compression mild steel (1.24 in.^{2})

f'_s= Stress in compression mild steel (60 ksi)

f'_c= Compressive stress of the concrete (8.5 ksi)

d_p= Distance from top of compression block to centroid of the prestressing (28.9 in.)

d_s= Distance from top of compression block to centroid of mild tensile steel (26.0 in.)

d'_s= Distance from top of compression block to centroid of mild compression steel (11.0 in.)

b= Compression flange width (12.0 in.)

b_w= Width of girder web (6.0 in.)

h_f = Depth of compression flange (8.0 in.)

a= Depth of effective concrete compressive stress from top of compression block (5.12 in.)

Many of the variables have to be solved for with the following equations. The effective depth of concrete compressive stress (a) is solved for with Equation 5.26 and the stress block factor (β_1) and the depth to the neutral axis (c) are found in Equations 5.27 and 5.28 respectively.

$$a = \beta_1 c$$

Eq. 5.26

$$\beta_1 = 0.85 - 0.05(f_c' - 4) \geq 0.65, for\ all\ f_c' > 4ksi$$

Eq. 5.27

$$c = \frac{A_{ps} f_{pu} + A_s f_s - A_s' f_s'}{0.85 f_c' \beta_1 b + k A_{ps} {}^{f_{pu}}\!/_{d_p}}$$

Eq. 5.28

The variables in Equations 5.27 and 5.28 are the same as for Equation 5.25 above with the exception of k which is defined in Equation 5.29 or Table 5.5. The constant k is dependent on the prestressing steel yield stress (f_{py}) and the ultimate prestressing steel stress (f_{pu}), which both have units of ksi. The prestressing strands were specified as low relaxation strands, therefore, a value of 0.28 was used for k in this research.

$$k = 2\left(1.04 - {}^{f_{py}}\!/_{f_{pu}}\right)$$

Eq. 5.29

Table 5.4 k values based on strand type

Type of Tendon	f_{py}/f_{pu}	k
Low relaxation strand	0.90	0.28
Stress-relieved Strand & Type I High-Strength Bar	0.85	0.38
Type II High-Strength Bar	0.80	0.48

The specified tensile stress of the prestressing steel (f_{ps}) is defined by Equation 5.30.

$$f_{ps} = f_{pu}\left(1 - k\, {}^{c}\!/_{f_{pu}}\right)$$

Eq. 5.30

The comparison of the recorded data from each girder and AASHTO LRFD Flexure Design are compared below in Table 5.6. The AASHTO design is conservative by approximately 10% on the average of all girder results.

Table 5.5 Moment comparison of Girders to AASHTO

	Moment kN-m (kip-ft.)	% Difference from AASHTO
AASHTO LRFD Design	1536 (1133)	NA
Girder # 3	1572 (1160)	2.4%
Girder # 4	1700 (1255)	10.8%
Girder # 5	1592 (1174)	3.6%
Girder # 6	1826 (1347)	18.9%
Average of all Girders	1684 (1242)	9.6%

5.3. Shear Design

Section 5.3 provides comparison of the AASTHO LRFD method for calculating shear capacity with the ANSYS finite-element model. There are two AASHTO methods for shear resistance capacity used in this research which are the simplified procedure for a prestressed girder and a strut-and-tie model.

5.3.1. AASHTO LRFD Simplified Shear Design for Prestressed Girders

Section 5.8.3.3 of the AASHTO LRFD Design Manual was the method used to calculate the nominal shear resistance (V_n) of the prestressed girders. There are three values of shear resistance that are used to calculate V_n which are the stirrup resistance (V_s) and the shear resistance provided by the concrete for the two conditions of cracking, combined flexure and shear cracks (V_{ci}) and excessive tensile forces in the web (V_{cw}). As seen in Equation 5.35 the prestressing resistance (V_p) is accounted for in V_{cw} term. The V_p is the shear resistance from a component of the prestressing force usually due to harped strands where the prestressing force at the end of the girder has a vertical component. For this research the girders had only straight

strands and therefore V_p is zero. The following equations are how to calculate the previously mentioned values.

$$V_n = (V_{cw} or\ V_{ci}) + V_s$$

Eq. 5.31

$$V_s = \frac{A_v f_y d_v (cot\theta + cot\alpha) sin\alpha}{s}$$

Eq. 5.32

$$V_{ci} = 0.02\sqrt{f'_{cg}} b_v d_v + V_d + \frac{V_i M_{cr}}{M_{max}}$$

Eq. 5.33

$$V_{cw} = \left(0.06\sqrt{f'_{cg}} + 0.3 f_{pc}\right) b_v d_v + V_p$$

Eq. 5.34

Which:

$$d_v = the\ least\ of \begin{cases} d_e - {}^{a}/_{2} \\ 0.9 d_e \\ 0.72H \end{cases}$$

Eq. 5.35

$$M_{cr} = S_c \left(f_r + f_{cpe} - \frac{M_{dnc}}{S_{nc}}\right)$$

Eq. 5.36

$$S_c = \frac{I_c}{c_c}$$

Eq. 5.37

$$f_r = 0.2\sqrt{f'_c}$$

Eq. 5.38

$$f_{cpe} = \frac{P_e}{A_g} + \frac{P_e c_2 c_g}{I_g}$$

Eq. 5.39

$$M_{dnc} = \frac{W_d x}{2}(l - x)$$

Eq. 5.40

$$V_d = \frac{W_d}{2}(l - x)$$

Eq. 5.41

$$S_{nc} = \frac{I_g}{c_g}$$

Eq. 5.42

$$f_{pc} = \frac{P_e}{A_g} - \frac{P_e e(c_c - c_g)}{I_g} + \frac{M_d(c_c - c_g)}{I_g}$$

Eq. 5.43

$$\cot(\theta) = \begin{cases} if\ V_{ci} > V_{cw}; 1.0 + 3\left(\frac{f_{pc}}{\sqrt{f'_{cg}}}\right) \leq 1.8 \\ otherwise, 1.0 \end{cases}$$

Eq. 5.44

Where: V_{ci} = Shear resistance provided by concrete when inclined cracking occurs from combined shear and moment forces (kip)

V_{cw} = Shear resistance provided by concrete when inclined cracking occurs from excessive principal tension forces in the web (kip)

V_s = Shear resistance due to the mild steel reinforcing (kip)

V_p = Shear resistance due to the component of prestressing in the direction of applied shear (0 kip)

f_{cg}' = Girder concrete compressive strength (11.2 ksi)

b_v = Minimum web width within the depth d_v (6.0 in.)

d_v = Effective shear depth (25.9 in.)

a = Depth of Whitney stress block from flexure analysis (5.9 in.)

d_e = Distance from top of compression block to centroid of prestressing steel (28.9 in.)

H = Height of girder (36 in.)

M_{cr} = Cracking moment (kip-in.)

S_c = Composite section modulus (2753 in.^{3})

I_c = Moment of inertia of composite section (46806 in.^{4})

c_c = Distance from bottom of girder to composite neutral axis (17.0 in.)

S_{nc} = Non-composite or girder section modulus (1807 in.^{3})

I_g = Moment of inertia of non-composite section or girder (22750 in.^{4})

C_c = Distance from bottom of girder to non-composite or girder neutral axis (12.6 in.)

f_r = Modulus of rupture of concrete (0.67 ksi)

f_{cpe} = Compressive stress in concrete due to effective prestress forces after all losses at extreme fiber of section where tensile stress is caused by externally applied loads (2.07 ksi)

c_2 = Distance between centroid of prestressing steel and girder neutral axis (5.5 in.)

M_{dnc} = Moment at distance x along the girder due to dead load (kip-in.)

V_d = Shear at distance x along the girder due to dead load (kip)

W_d = Uniform distributed load due to dead weight of the girder (0.032 kip/in.)

x = Distance from center of support to center of applied load (in.)

l = Distance between the reactions (423 in.)

f_{pc} = The resultant compressive stress after all prestress losses have occurred at the centroid of composite section (0.84 ksi)

A_v = Area of shear reinforcement within a distance s (0.62 in.^{2})

s = Spacing of mild shear reinforcing at a distance x along the girder (in.)

α = Angle of inclination of transverse reinforcement to longitudinal axis (90^o)

θ = Angle of inclination of diagonal compressive force (deg)

Not all of the above defined variables had consistent values for each test and therefore a value was not given in the definition. All of the variables without given values can be calculated with the given equations; however, only the three values of V_{ci}, V_{cw} and V_s for each location x of applied load are in Table 5.7 below.

Table 5.6 Values of V_{ci}, V_{cw} and V_s for each test

Test	x mm (in.)	V_{ci} kN (kip)	V_{cw} kN (kip)	V_s kN (kip)
1d	914 (36)	961 (216)	316 (70.6)	1254 (282)
2d	1829 (72)	494 (111)	320 (72.0)	636 (143)
4d	3658 (144)	249 (56)	329 (74)	236 (53)
Mid-span	5372 (212)	187 (42)	334 (75)	236 (53)

As seen on Table 5.7 the V_{cw} value governs for the 1d and 2d tests and therefore the $cot(\theta)$ was calculated using Equation 5.45, where for the other two tests a value of 1.0 was used. The values of V_n are presented below in Table 5.8 and are compared to the average measured shear values for each test from Table 4.3.

Table 5.7 Comparison of theoretical shear resistance to measured shear

Test	V_n kN (kip)	V_i kN (kip)	% Diff.
1d	1570 (353)	1717 (386)	-8.5%
2d	961 (216)	952 (214)	0.9%
4d	490 (110)	489 (110)	0.1%
Mid-span	429 (96)	294 (66)	46%

This calculation for shear resistance was 1.0% more or not conservative of the measured values for the 2d and 4d test indicating that those locations are within an area where the combined forces of shear and flexure govern the failure mode. The 1d test is 8.5% conservative of the measured values. Though this is sufficiently accurate for predicting shear capacities at the end of the girder near the support a strut and tie model was calculated for this location in section

5.4.2 for a more accurate representation of how the girder failed. The mid-span predicted shear value is almost 50% more than measured, which indicates that the mid-span is in a location where flexure governs the failure mode.

5.3.2. AASHTO LRFD Strut and Tie Model

Strut and tie models are applicable when a point load is within a distance 2*d*, where *d* is the depth form the top of the compression block to the centroid of the prestressing steel, from a support or discontinuity, which will cause a nonlinear strain distribution (AASHTO, 2012). This type of nodal analysis is shown in Fig. **5.1**, which shows the supports, nodes A and C, and the bearing plate, node B, where the load was applied. The tie AC was at the centroid of the prestressing steel. Each node for this analysis is assigned a region type to determine the limits for the concrete compressive stress in each region. The two types of nodal regions used in this research which were nodes surrounded by compressive struts and a compressive bearing area (c-c-c) and nodes with one direction tension tie anchored in (c-c-t). Node B was a c-c-c and nodes A and C were c-c-t.

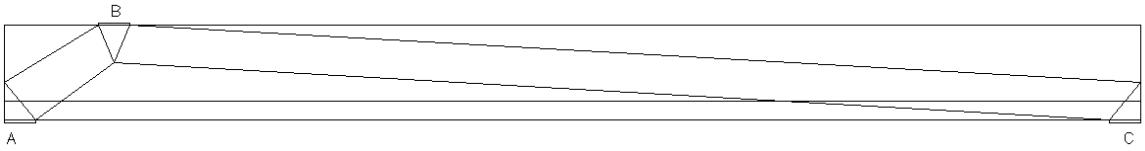

Fig. 5.1 Strut and Tie model of the girder with compressive struts AB and BC and tie AC

Any truss may be used for a strut and tie analysis and is therefore an iterative process to find the most accurate model. The simple truss ABC in Fig. **5.1** was used for this research to calculate the shear strength for the 1*d* test because the forces of interest were in between nodes A and B due to the failure cracking. The opposite side could have been modeled differently with a more complex truss; however this would have had no effect on the forces in strut AB and

therefore was not considered. It should also be noted that to remain consistent with this research no strength reduction factors were used. The following equations were used to calculate the shear resistance of the girder.

$$M_B = f_{ce} h_b t\left(H - c_p - h_b\right) \quad \text{Eq. 5.45}$$

$$f_{ce} = \begin{cases} (c - c - t), 0.75 f_c' \\ (c - c - c), 0.85 f_c' \end{cases} \quad \text{Eq. 5.46}$$

$$\alpha = \tan^{-1}\left(\frac{H - \frac{h_b}{2} - c_p}{x}\right) \quad \text{Eq. 5.47}$$

$$F_{AB} = \frac{R_A}{\sin(\alpha)} \quad \text{Eq. 5.48}$$

$$\varepsilon_1 = \varepsilon_s + (\varepsilon_s + 0.002)\cot(\alpha)^2 \quad \text{Eq. 5.49}$$

$$f_{cu} = \frac{f_c'}{0.8 + 170\varepsilon_s} \quad \text{Eq. 5.50}$$

$$P_n = f_{cu} A_{cs} \quad \text{Eq. 5.51}$$

$$A_{cs} = (l_b \sin(\alpha) + h_a \cos(\alpha))t \quad \text{Eq. 5.52}$$

$$V = P_n \sin(\alpha) \quad \text{Eq. 5.53}$$

Where: f_{ce} = Limiting concrete compressive stress for each nodal region type (ksi)

f_c' = Concrete compressive stress at each node (ksi), deck strength at node B and girder strength at nodes A and C

M = Moment due to applied point load (13896 kip-in.)

H = Height of the girder (36 in.)

c_p = Distance from bottom of girder to centroid of prestressing steel (7.125 in.)

h_b = Solved for in Eq. **5.45** as the depth of nodal influence (6.67 in.)

α = Angle between the tie AC and strut AB (35.4^0)

F_{ab} = Compressive force in strut AB (667 kip)

R_1 = Reaction force from applied point load at node B (386 kip)

ε_1 = Principle tensile strain in cracked concrete due to applied loads (0.00658)

ε_s = Tensile strain due to the tension force in tie AC minus the prestressing strain (0.00087)

f_{cu} = Limiting concrete compressive stress (5.84 ksi)

P_n = Limiting compressive force in strut AB (650 kip)

A_{cs} = Cross sectional area of strut AB perpendicular to the strut (111 $in.^2$)

V = Shear capacity or vertical component of P_n (376 kip)

The calculated shear resistance from the strut and tie model was 1673 kN (376 kip) which is 2.6% less than the measured value of 1717 kN (386 kip). The strut and tie model is a conservative method of calculating shear resistance of a concrete member with a concentrated load near a reaction. The AASHTO LRFD Simplified method was extremely accurate in determining shear resistance at a distance of more than 2*d* from a reaction, but was 8.5% less than the measured value for the 1d test. These results prove that near the reaction shear forces represented by a strut and tie model govern the failure mechanism.

5.4. ANSYS Finite Element Modeling

The girder testing was modeled using the finite-element software ANSYS. This software was selected to model the girders due to its nonlinear modeling capabilities. The same girder model was used to replicate each test, that is to say that the only difference in the individual tests

is that the application of the load was positioned in different locations, mid-point, 1-d, 2-d and 4-d, on the girder model.

For this research the ANSYS model was created using a text file (see Appendix #) with the program commands written in it which were inserted into ANSYS that read the commands and created a model based on what was in the text file. Volumes for a model are the different parts of the prototype, for example volumes for this research are the concrete girder and deck and the steel bearing pads. Creating a volume involved defining key points as corners of a volume. Eight key points must be defined for each volume (adjacent volumes can shear key points if desired). Volumes are defined by selecting eight key points that make up an acceptable shape, which is defined for each element (ANSYS, Inc., 2009).

5.4.1. Materials

Each volume was then assigned a material type, real constant and element type. Material types have assigned properties and a material number for individual application. For this research the material numbers and equivalent use is listed in Table 5.1.

Table 5.8 ANSYS Material numbers and assigned materials

Material Number	Material
1	Mild Reinforcing
2	Girder Concrete
3	Prestressed Strands
4	Deck Concrete
5	Steel Plates

All materials and their respective properties were based on the measured properties and are defined in the model code in Appendix A3. For the purpose of creating an accurate model, the material properties were adjusted, increased or decreased, depending on the behavior of the

model until the output was similar to the measured values. In the code all the material properties are defined in tables or real constants.

5.4.2. Tables

The tables are predefined in the software and are used for specific materials. Tables are used to make sure materials act how they are supposed to. For this research two different types of tables were used, a concrete table and a biso table. The concrete table has user defined material properties, such as compressive and tensile strength, and the table makes sure it behaves like concrete. The biso table is used for materials have two separate slopes on the stress strain diagram, such as steel. Steel has the linear elastic region prior to yielding and the elastic region after yielding. The biso table enables a material to yield and continue to the ultimate strength.

5.4.3. Real Constants

Real constants are properties ANSYS uses for defining properties that are not material properties. These constraints are specific to individual element types, such as the real constants for reinforcing was used to specify the area of steel and any prestressing present, which is defined by an initial strain. Concrete also required real constants to define the percentage of smeared bars and the orientation with respect to the girder longitudinal axis. Every volume must be assigned a real constant although not all volumes have the need for these extra properties defined. The steel plates in this research have a real constant but do not have or use any information defined in the real constant.

The initial strain for the prestressing strands had six real constants used for different sections of the strands. The strands were modeled to have a low initial strain near the ends of the girders to replicate the gradual increase in stress over the transfer length. To accomplish this

behavior the strain was linearly increased over five spaces of 152 mm (6 in.) until it reached the maximum value. This was also modeled to keep the strands from pulling out of the girder concrete at the ends.

5.4.4. Element Types

There are multiple element types that are available to model any application. There were three types of elements used to model the girder for this research. The Solid 65 (ANSYS, Inc., 2009) element was used for the concrete because of its ability to replicate cracking in tension, crushing in compression and the nonlinear behavior through failure. The Solid 65 element has the option modeling discrete pieces of rebar as a smeared mesh. Together these types of attributes make the Solid 65 ideal for modeling nonlinear, reinforced concrete.

The Solid 45 (ANSYS, Inc., 2009) Element was used to model the steel plates. The Solid 45 Element is capable of modeling plastic behavior, stress stiffening and large strains. The plastic behavior is defined by the slope of the modulus of elasticity (E_s) and a second slope after yield stress is exceeded. The Solid 45 Element was used to model the base plates and the bearing plate under the external load. Both the Solid 65 and the Solid 45 volumes are defined by using eight keypoints for the corners of the solid. Figure 5.1 below shows how the keypoints are used to define volumes. The same shapes are available for the Solid 65 Element.

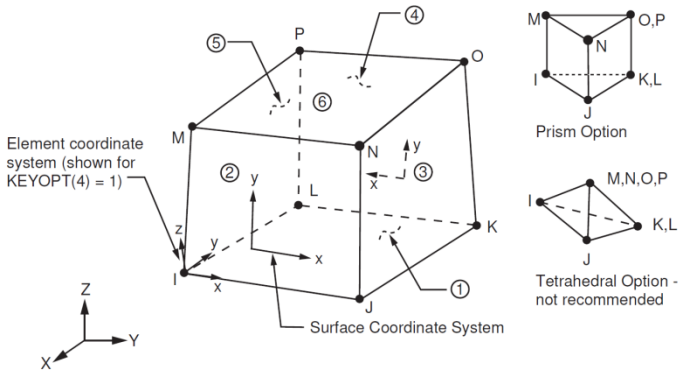

Fig. 5.2, The Solid 45 geometric shapes, (ANSYS, Inc., 2009)

Multiple volumes make up a model. The volumes in this research were all modeled as connected to the one next to it. The volumes are connected to one another with a process known as gluing.

The element selected to model the mild reinforcing and the prestressed strands was the Link 8 Element, (ANSYS, Inc., 2009). Link 8 Element is capable of modeling tension and compression forces. This element is defined by a straight line between two keypoints or the edge of a solid. The Link 8 Element is can be assigned an initial strain that can be used to replicate the prestressing force and a cross sectional area to represent the reinforcing dimensions.

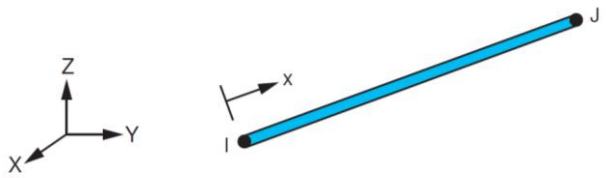

Fig. 5.3, The Link 8 Element geometry, (ANSYS, Inc., 2009)

The Link 8 Element is depicted in Figure 5.2 above that shows the two key points at the ends of the element. For this research the keypoints defined for the solid elements were used for the link elements. Using the same keypoints ensures the link elements to connect to the solid elements, much like rebar or prestressing strands are bonded to the concrete surrounding them.

5.4.5. Running a Model

Once all volumes have been created and assigned a material, real constant and an element type the model is then meshed. Meshing is the process by which ANSYS makes finite elements out of the previously defined volumes. A defined finite element size is one number that defines all three dimensions of a cube. The element size is an approximation of what is produced by the ANSYS. Due to the fact that irregular shapes occur during meshing not all finite elements will have the exact same size. However, if there are element sizes too large or small then errors will occur during meshing. Therefore there is an optimum element size range for each model. For this research a finite element size of 51 mm (2 in.) was used because it produced no errors when meshing and would therefore be an accurate model. The corners of these elements are nodes, similar to the keypoints used for the volumes. Once the whole model is defined by elements and nodes the boundary conditions can be defined. Boundary conditions are used to define the support conditions and the area of the applied load. Individual nodes were assigned the specific boundary conditions. For this research, the supports were modeled as a pin and a roller. The bearing plate of steel on top of the girder used to distribute the load from the ram to the girder.

After the elements are discretized and boundary conditions applied the model can be analyzed. The load is applied in incremental time steps defined by either a user defined function or the program default values. The time steps range from one to one hundred, or basically the time step is a percent of the predefined load. ANSYS increases the load based on the convergence of the previous time step. For this research the predefined load was set to be higher than was recorded during the experiment to ensure girder failure prior to the termination of the program at time 100. The program will also stop prior to time step 100 if the structure fails or exceeds the strength of the members. The predefined load was set at a value 1.5% higher than

the recorded experimental data. This ensured that the load increments per time step were as small as possible for a more refined analysis.

5.5. ANSYS Models

The following sections describe the model for each test preformed for this research. The model for each test was the same with the only difference being the magnitude and location of the load and some reaction conditions, which varied depending on the test and are described below in each individual model. All the codes for the models are found in Appendix A3.

Each deflection plot was compared with an R^2 value as determined by Equation 5.54 below and the ultimate capacity of the model as compared to the experiment.

$$R^2 = \frac{cov\left(M_{Model,}M_{Experimental}\right)}{\sigma(M_{Model})\sigma\left(M_{Experiemtal}\right)} \quad \text{Eq. 5.54}$$

Where: *cov* = Covariance of two lists of data (632)

M_{Model} = Moment values from the finite element model

$M_{Experimental}$ = Moment values from experimental data

σ = Standard deviation of selected data (24.14 and 26.51 for the Model and Experimental data respectively)

5.5.1. 1d ANSYS Model

An image of the test set up for the 1*d* test is seen in Figure 5.4 which shows the load at a distance 1*d* from the center of the support, which was the experimental set up. The original bearing pads were replaced with steel plates to keep the end of the girder from excessive deflection that was expected to occur with the bearing pads. This changed the boundary conditions for the model by moving the pin-roller conditions from the middle of the support to

the inside edge. This was done due to the fact that during testing the rotation at the supports was about the inner edge of the reaction steel and not the middle of the support.

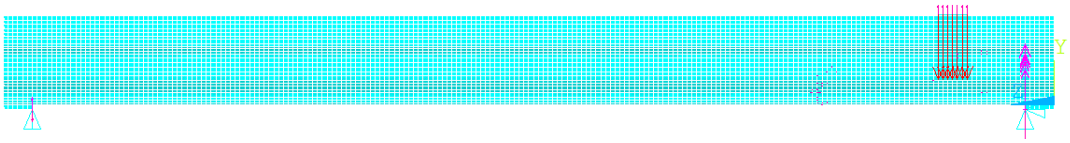

Fig. 5.4 1d ANSYS test set up

Once the model had converged on a solution there were three of checks done to confirm that the model performed like the experiment. First, the cracking scheme had to be similar, the mode of failure had to be the same and the deflection plots had to match up. Figure 5.# is a comparison of the cracking prior to failure.

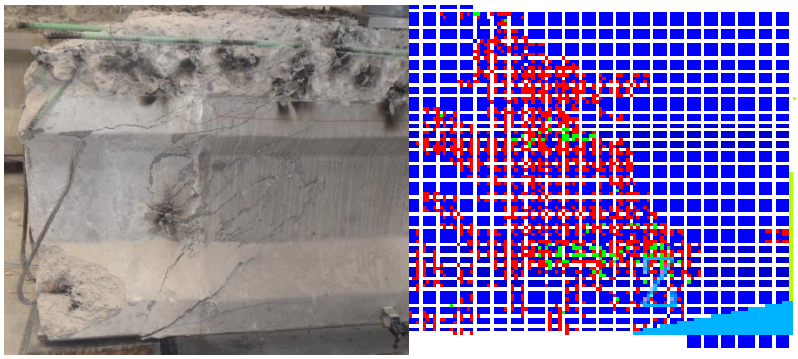

Fig. 5.5 G3-1d(a) (left) and ANSYS 1d (right) failure cracking comparison

Lastly the deflection under the load of the experiment is compared to the deflection of the exact same location from the ANSYS model. Figure 5.# is the comparison the 1*d* model and the deflection data from G3-1*d*(a) because the effective length of the two are the same and therefore the stiffness is comparable.

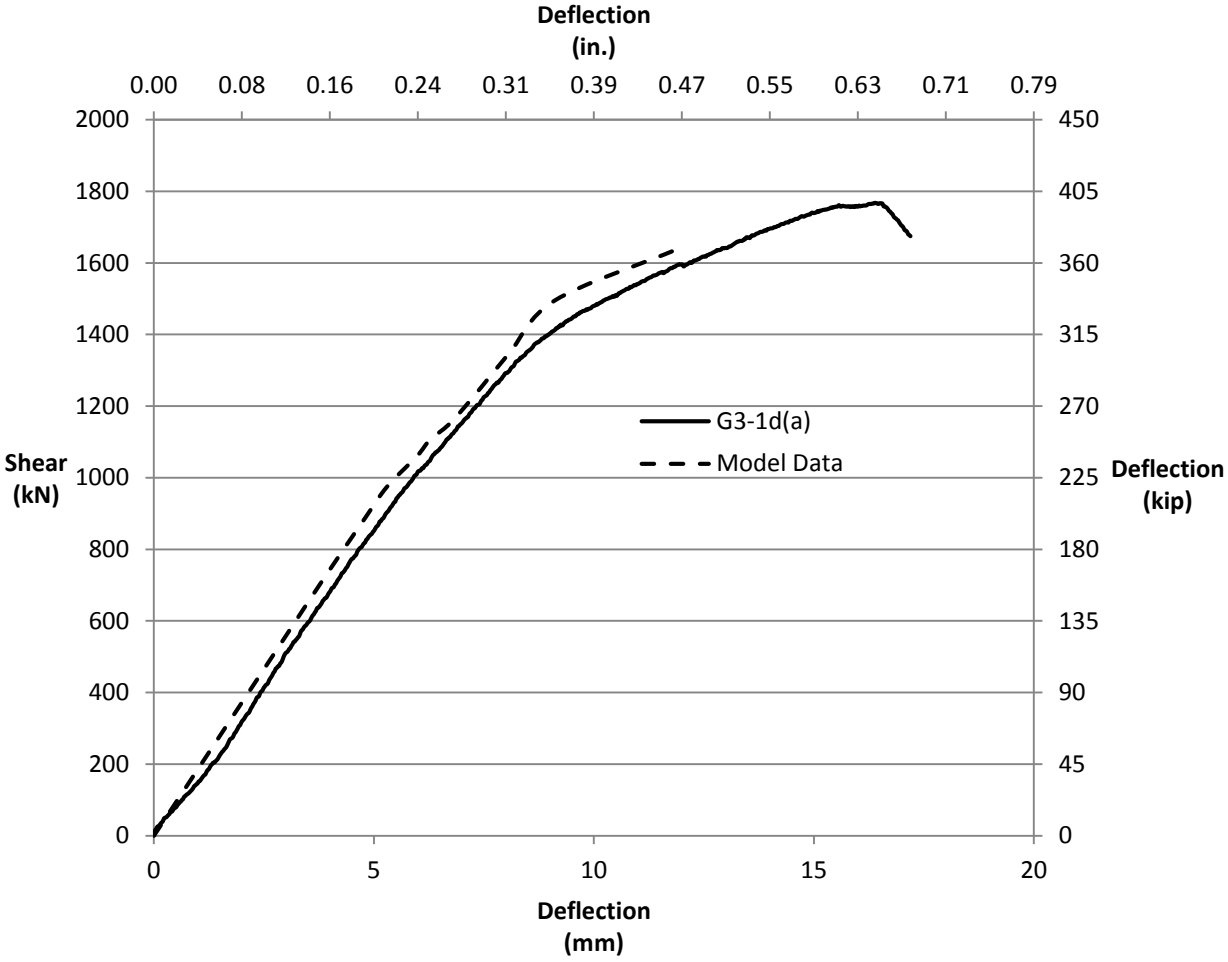

Fig. 5.6 Shear vs. Deflection comparison of the Model and the Girder

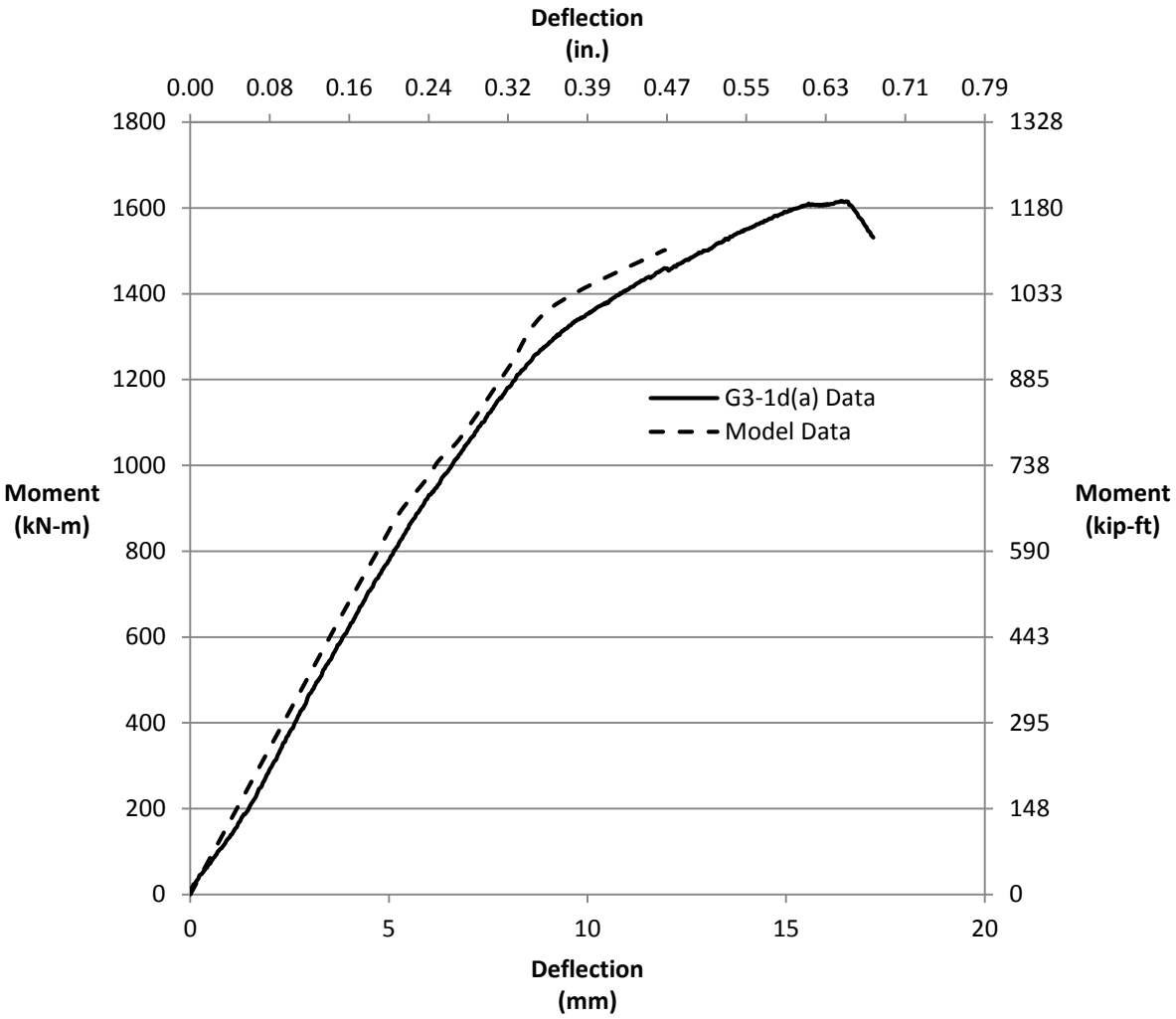

Fig. 5.7 Moment vs. Deflection comparison of the Model and Girder Data

The R^2 value for the above plot is # and the ultimate capacity of the model is # which is #% below the actual data.

5.5.2. 2d and 4d ANSYS Model

The 2*d* and 4*d* models were set up to mimic the experiment as shown in Figure 5.# below. The support conditions were kept at the inner edge of the bearing plates for these models as well as the 1*d* model because the model performance was similar to the experimental data.

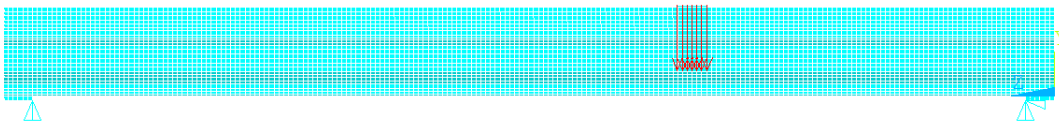

Fig. 5.8 4d ANSYS test set up

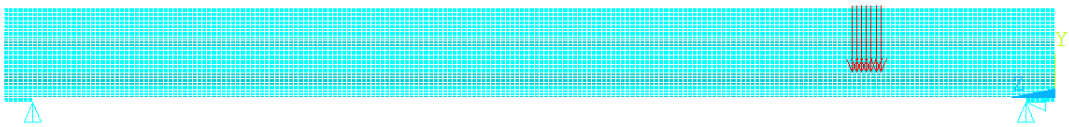

Fig. 5.9 2d ANSYS test set up

The supports are consistent with the other test in ANSYS with the supports on the inner edge of the bearing plates. As the load moves into the middle of the girder the placement of the supports has less of an influence on the performance of the model, however this was done to be consistent with other tests.

Figure 5.10 below is the comparison of the girder failure cracking to the model cracking for the 4d test. The similarities can be noticed between the two in that the left side of the load on the model has more of a flexural cracking pattern and the right side has a combination of flexure and shear cracking. This is consistent with the calculated failure mode in section 5.3.1 for both the 4d and 2d tests and is more easily seen in Figure 5.11 for the 2d comparison.

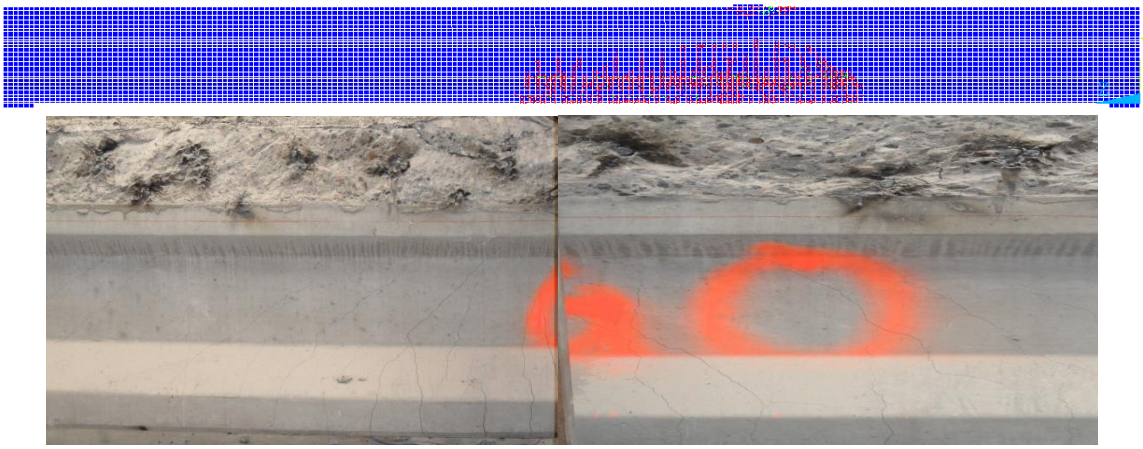

Fig. 5.10 ANSYS 4d test (top), both sides of the G6-4d(b) (bottom) failure cracking

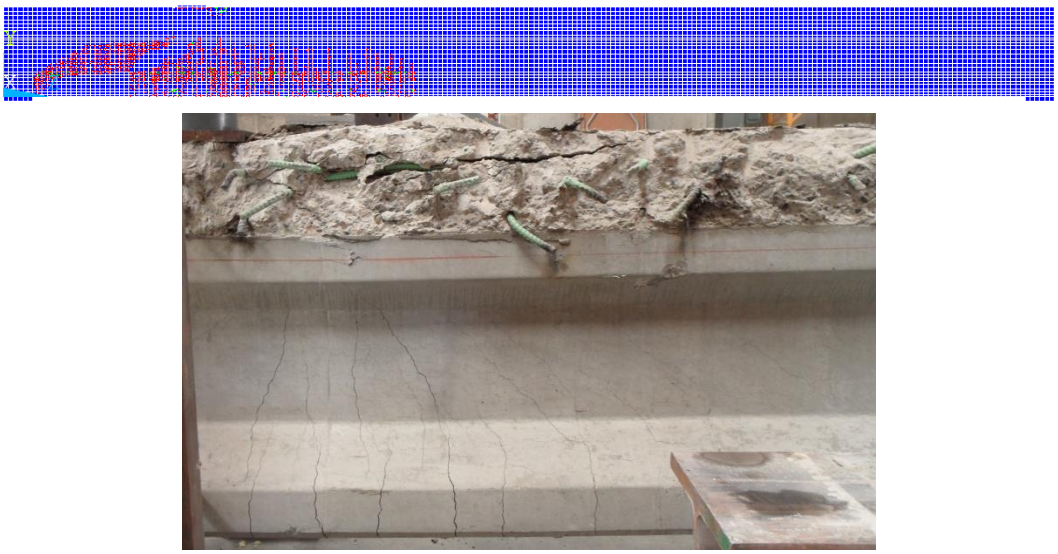

Fig. 5.11 G4-2d(b) (bottom) and ANSYS 2d test (top) failure cracking

The model for Figure 5.11 was turned around to match the same side as the girder picture. The combination of flexure shear failure is readily seen in the model but the major similarity is that the cracking by the load is the same. The deck concrete is crushing right next to the load and the cracking is extending up from the bottom of the girder in the same pattern.

The final comparisons for the tests were the deflection values of the string pots to the model deflection values. Figures 5.12 and 5.13 are the comparison of the 2*d* experimental data to the model data for moment and shear respectively, and Figures 5.14 and 5.15 are the 4d comparisons to the moment and shear respectively.

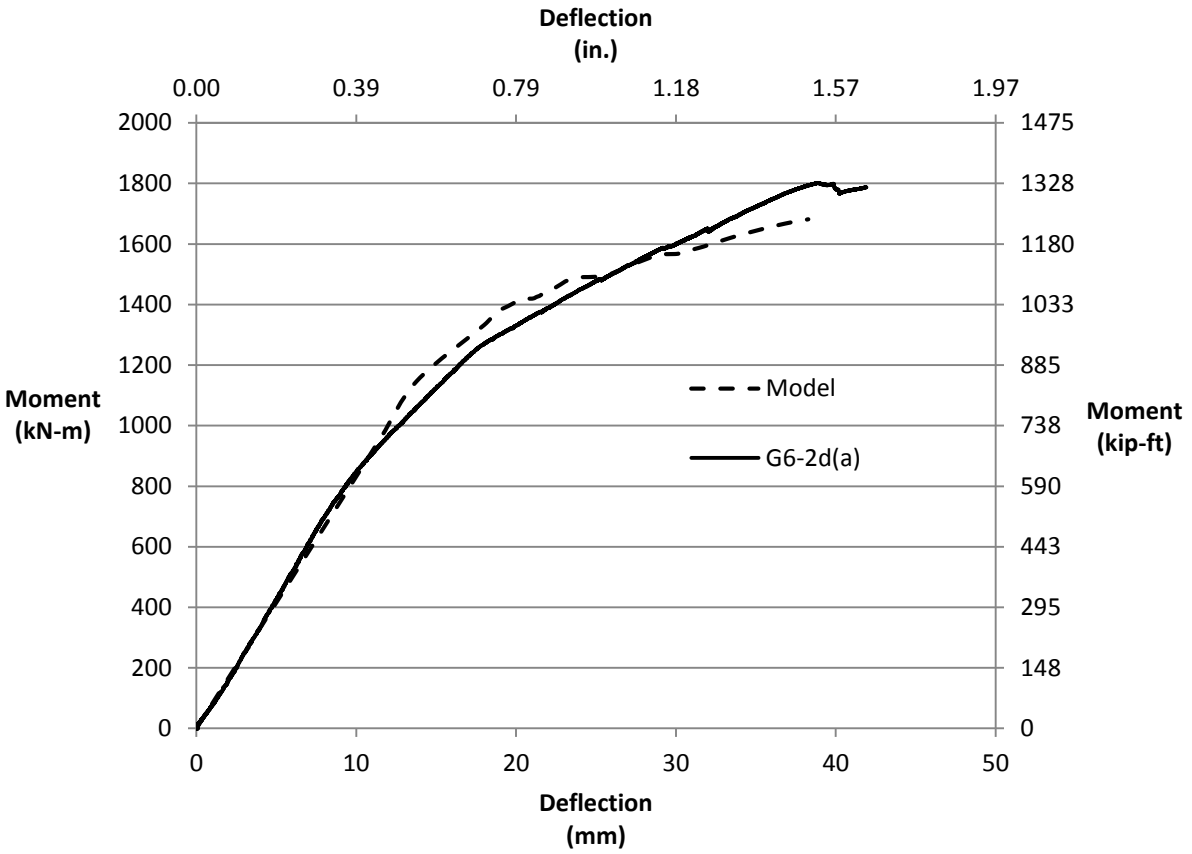

Fig. 5.12 Moment vs. Deflection comparison of model and test data

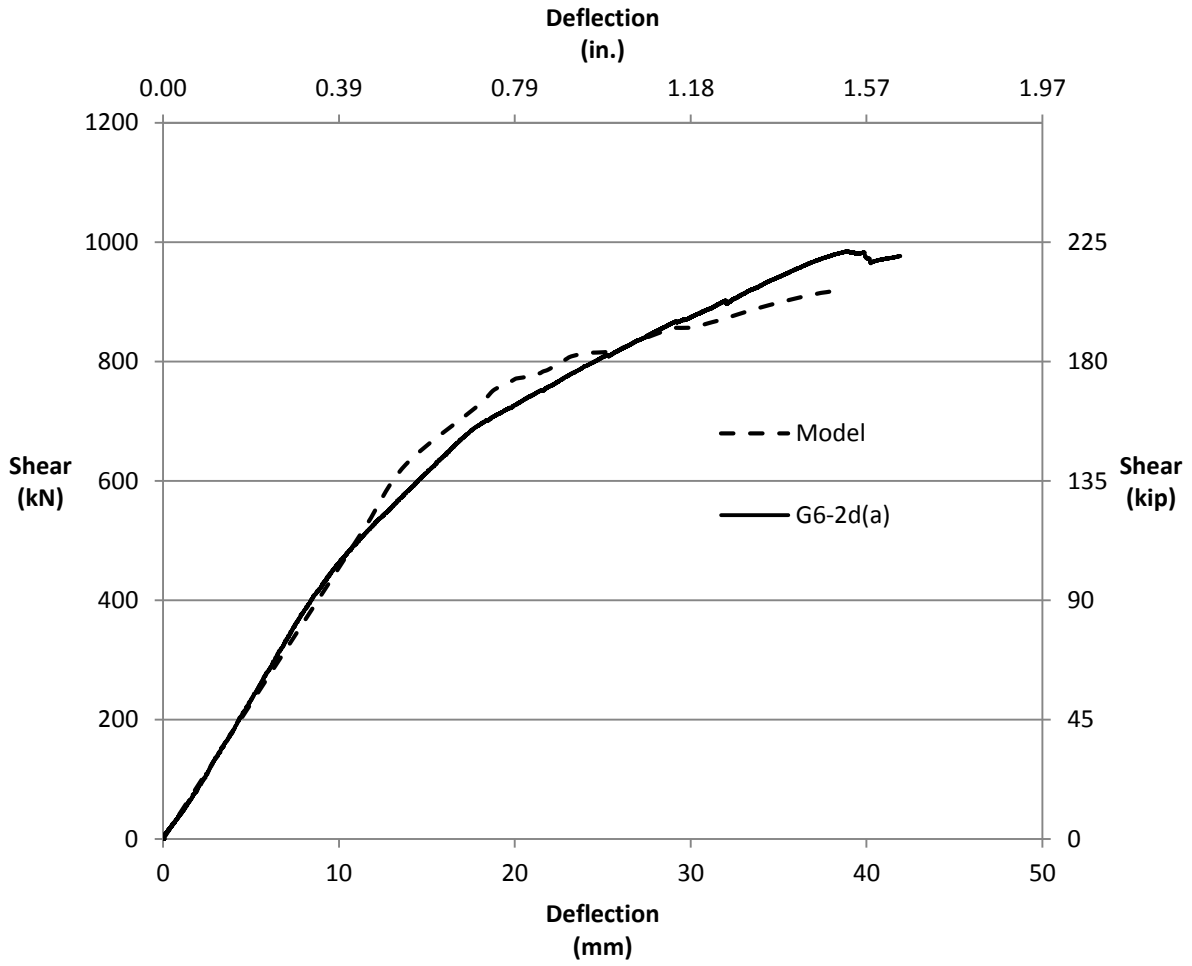

Fig. 5.13 Shear vs. Deflection comparison of G6-2d(a) and ANSYS

The model has a R^2 value equal to 0.937 for the 2d model, indicating that the model is an accurate representation of the experiment. The stiffness of the model is about the same as the experimental data for the 2d test. The modulus of elasticity (E) was the same in the model for each test and the model was too stiff on some and less stiff on others, however the general shape is the same for each comparison.

Figure 5.14 and 5.15 are the moment and shear, respectively, vs. deflection comparisons of the girder and ANSYS.

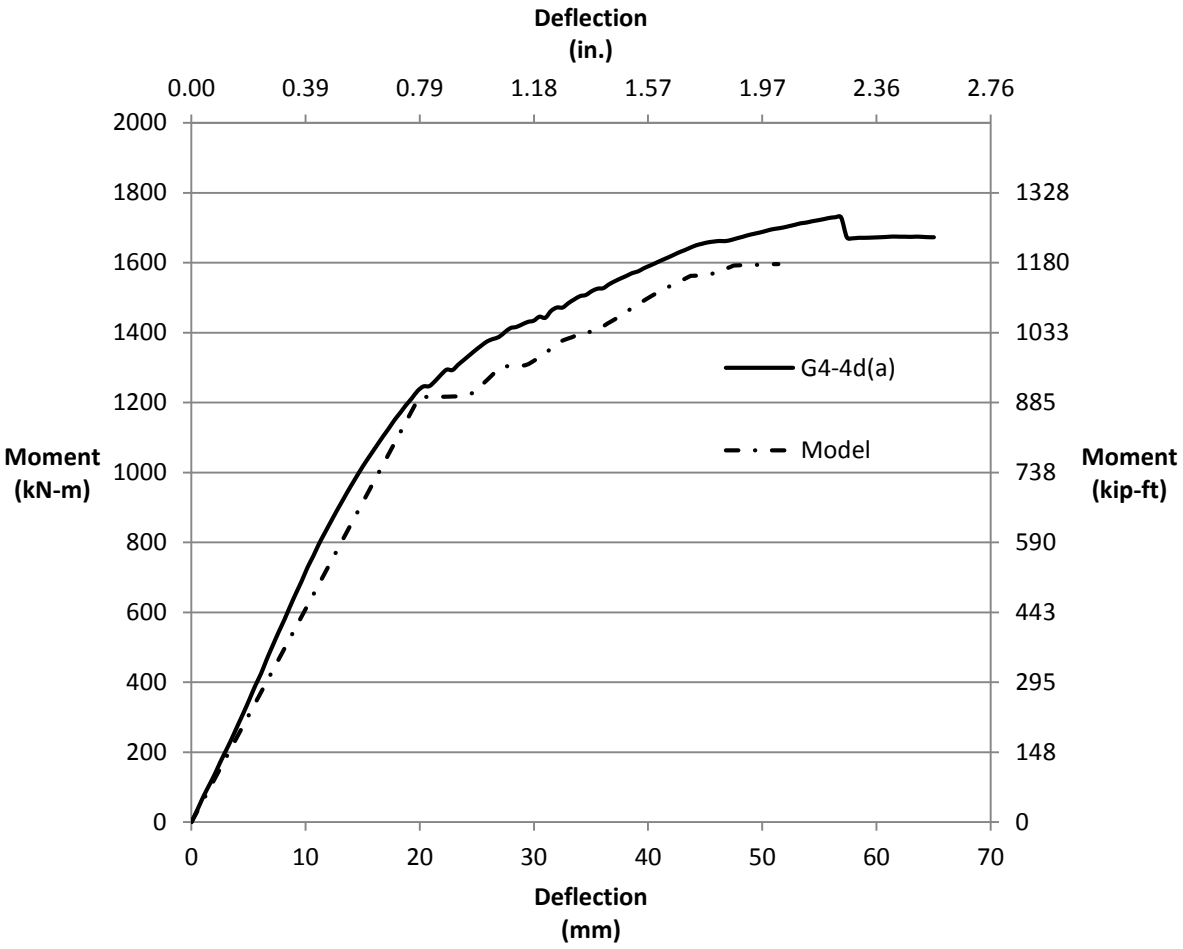

Fig. 5.14 Moment vs. Deflection comparison of Girder to ANSYS

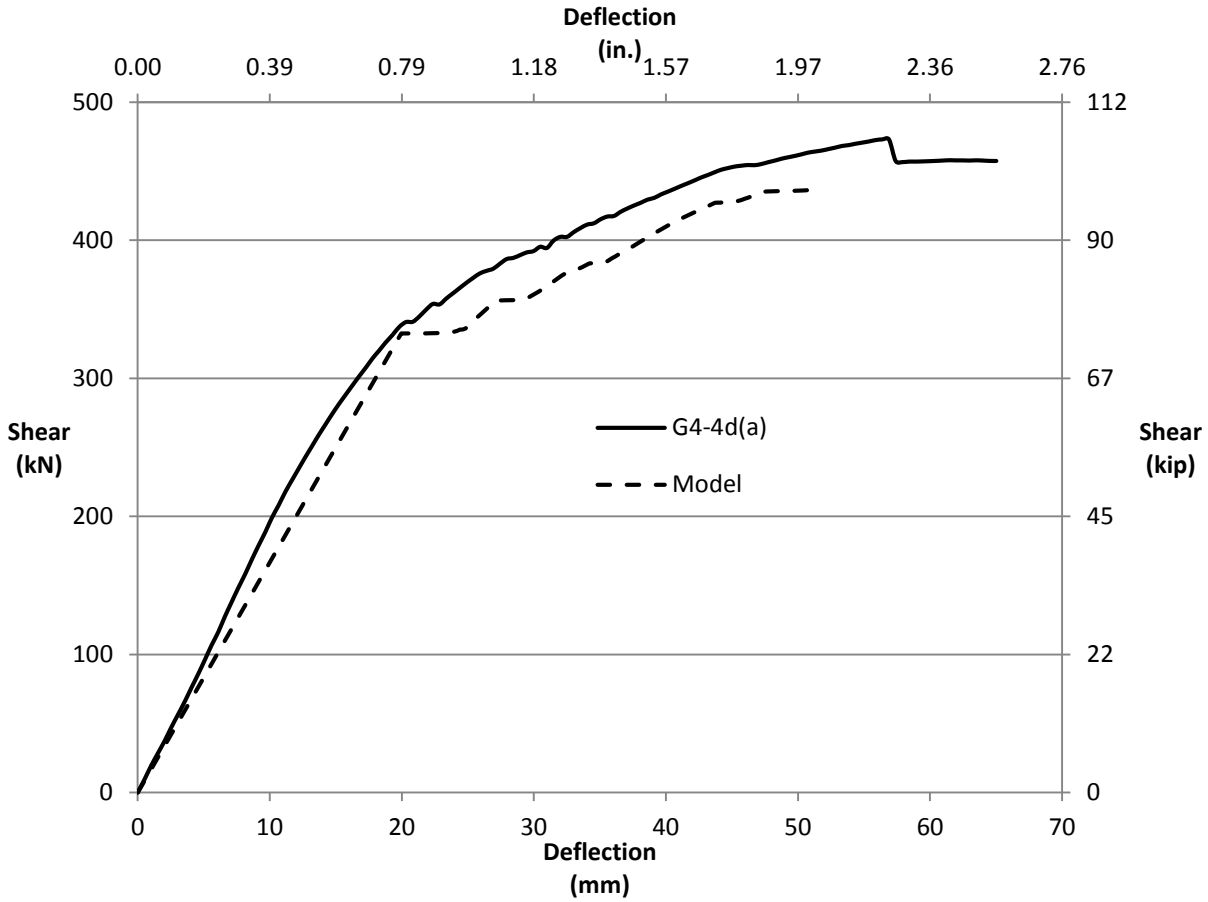

Fig. 5.15 Shear vs. Deflection comparison of Girder and ANSYS

The stiffness of the model has now switched to being less stiff than the girder was. The R^2 value was 0.980 showing that the model is acting like the girder had. As seen for each the 2d and 4d comparison graphs the model losses the stiffness at the same time as the girder shows that the prestressing used in the model was accurate. When the prestressing was increased the model would keep the original stiffness for a higher capacity and would not match the girder.

5.5.3. Mid-Span ANSYS Model

The finite element modeling program ANSYS was used to simulate the same flexural tests that were performed in the SMASH Lab. The results from ANSYS were compared to the

measured moment deflection graph of the respective tests that were being replicated on ANSYS. The following sections describe the finite element model and the loading conditions.

A graphical elevation view of the ANSYS model is shown in Figure 5.3 below, with the load in the middle and the supports on the ends. The pin-roller supports shown in the model were used to replicate the actual test conditions. Steel bearing plates were used at the supports and under the applied mid-span load.

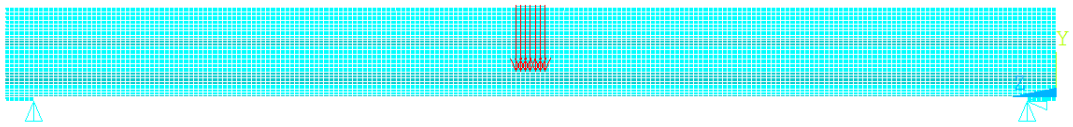

Fig. 5.16 Mid-span ANSYS test set up

The model above was discretized into approximately 51mm (2 in.) cube elements which are shown with the small turquoise squares. The blue triangles at the support plates are the pin support on the left and the roller support on the right. The red arrows pointing down at the mid span is the applied load and its direction.

Figure 5.# shows a comparison of the finite element predicted behavior with the test data from Figure 4.8. The model was slightly stiffer than the actual girder in the linearly elastic region; however, after cracking the model performs similar to the girder. The overall results of the model are an accurate representation of the test.

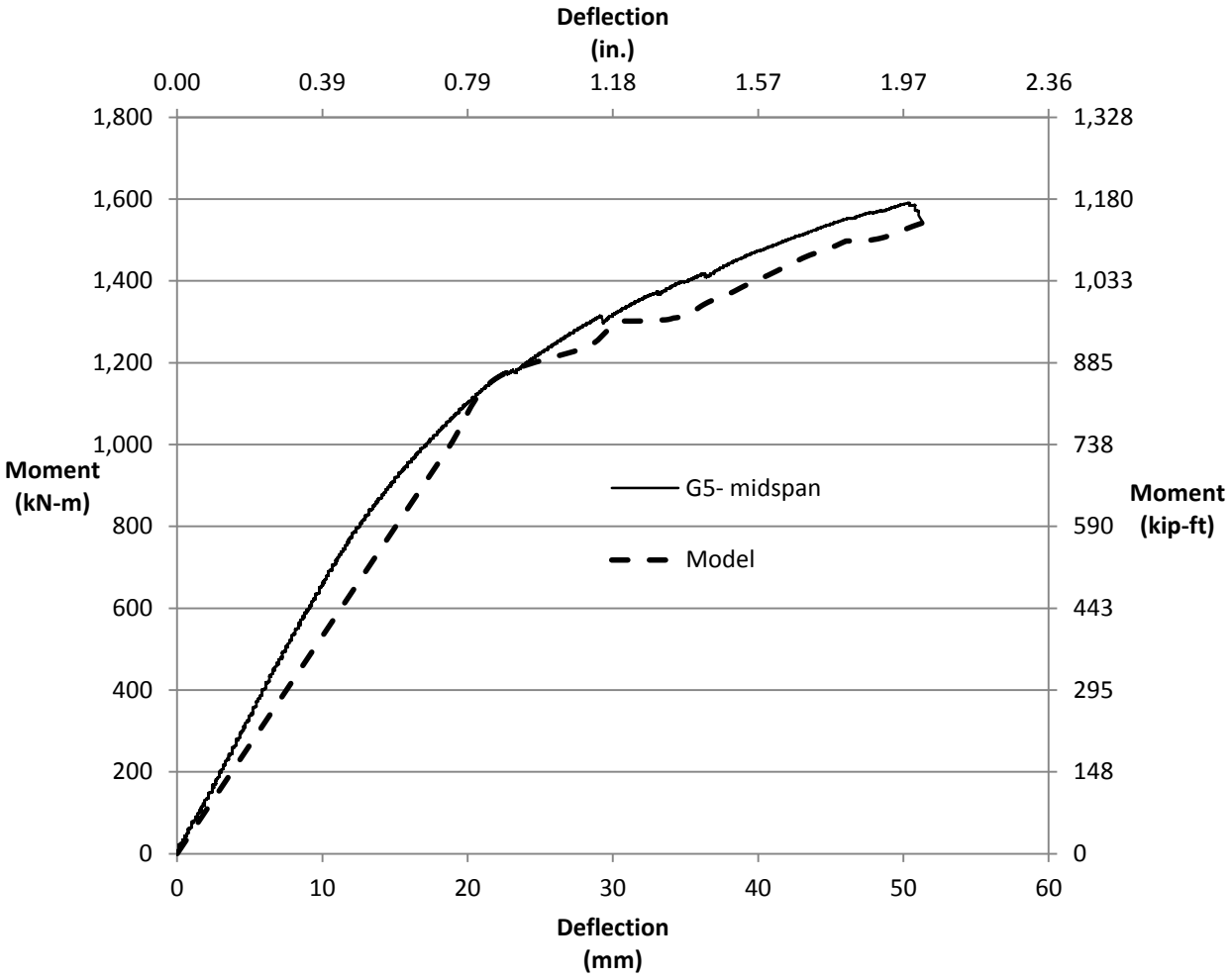

Fig. 5.17 Moment vs. Deflection comparison of the Girder and ANSYS

The maximum calculated moment the finite element model was 1555 kN-m (1147 kip-ft.) with a deflection at the mid-span of the girder of 52 mm (2.06 in.). The test data for girder #5 showed a maximum moment of 1590 kN-m (1173 kip-ft.) with a mid-span deflection of 50.29 mm (1.98 in.). The model and the test data had equivalent maximum shear values of 288 kN (65 kip) and 296 kN (67 kip), respectively. The difference in moment between the finite element model and experimental data was 2.94%, and using Equation 5.31 the R^2 value is 0.988.

The model and girder failure cracking patterns are shown in Figure 5.18. The Girder 5 is just the right side of the load and shows the cracks that propagated on the tensile side of the girder. Only one side was needed due to the symmetry of the loading.

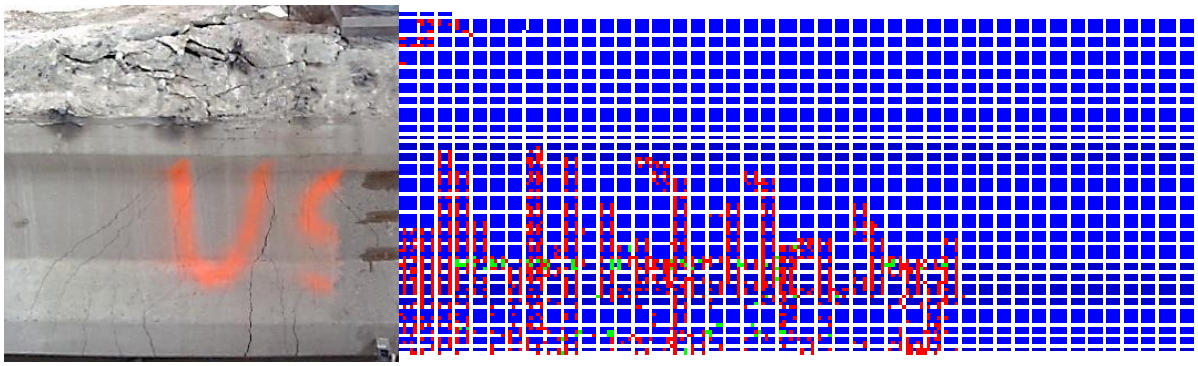

Fig. 5.18, Shows the cracking scheme of the actual girder (left) to the ANSYS model (right)

The cracking patterns are the same in each the model and the girder in Figure 5.18, which is an indication that they failed in the same manner. The cracking scheme of this test also shows that the tensile capacity of the model concrete was an accurate representation of actual conditions. The tensile capacity of the girder concrete was never tested and therefore had to be assumed for the model. Different tensile capacities were used during the modeling; however the determining factor was if the cracking scheme of the model was similar to the test.

5.5.4. Summary of ANSYS Models

The ANSYS model of the girder was accurate from up to 10% of the maximum load and had adequate R^2 values of no less than 0.90 showing that the model was performing like the girder. The program had issues with the strength and modulus of elasticity of the concrete material. The concrete for both the deck and the girder had to be increased by 25% and 56% respectively. This was attributed to the fact that high strength concrete is not common and reacts differently than normal strength concrete. This action was seen during the cylinder compression tests in which the lower strength concrete cylinders would produce a crack during failure and the

high strength concrete from the girders would not have any cracking prior to a total crushing failure.

The same model was used for each test, meaning that the same material properties and prestressing value was for each test. The only difference in the models was the location of the load. ANSYS provided an accurate model of the girders as a whole and it performed as the girders did during experimentation.

6. Summary and Conclusions

Four prestressed concrete girders built in 2004 were tested to failure in moment and shear. The test results were compared to AASHTO LRFD Design Manual and an ANSYS finite element model.

In conclusion:

- The tested moment capacity of the girders was 9.6% higher than that of the AASTHO LRFD Design Manual specifications for the nominal moment capacity.
- The AASHTO LRFD Specifications for flexure-shear capacity of the girders was 1.0% more conservative than the tested results and therefore the AASHTO LRFD Design Manual is accurate for high strength prestressed concrete girders.
- The Refined Time depended prestress loss calculations from AASHTO LRFD was 8.8% not conservative as compared to the average residual prestressing that was calculated from the cracking tests.
- The General prestress loss method was 4.8% not conservative as compared to the average residual prestressing from the cracking tests. This shows that more losses have occurred than either method predicted.
- The ANSYS model was within 10% of the failure moment or shear values and had an R^2 value greater than 0.90 and was therefore an accurate representation of the girders.
- The ANSYS Finite Element program had difficulties modeling the actual concrete material properties. The model was not strong enough and was much too stiff than the girders performed. An increases in compressive strength and a decrease

to the modulus of elasticity was necessary in order for the model to match actual data.

A. Appendix

A.1. Cracking Moment Test Data

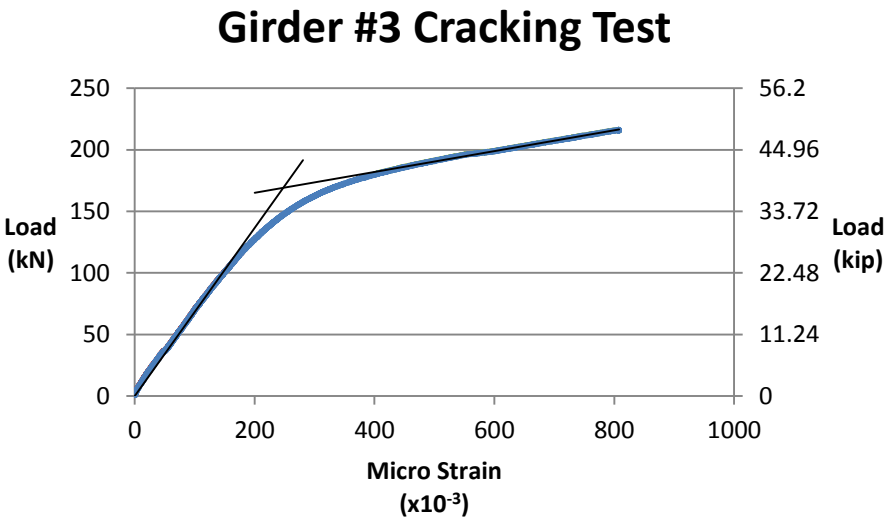

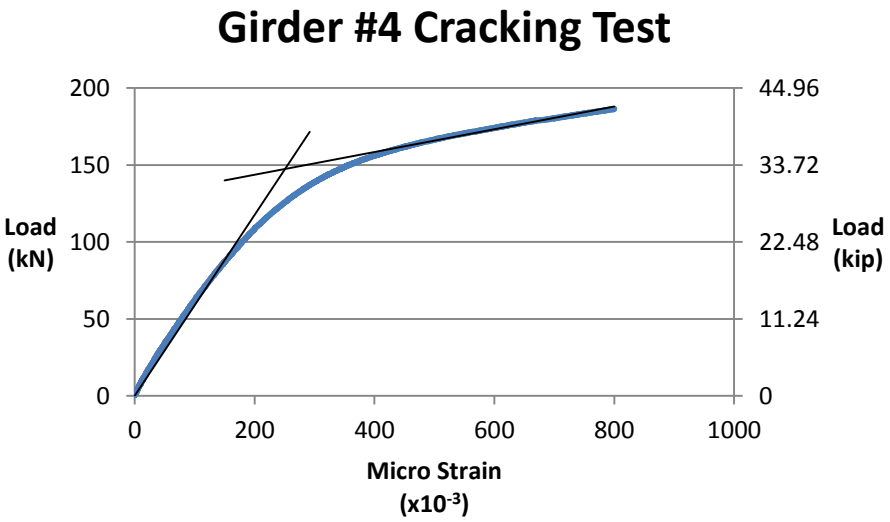

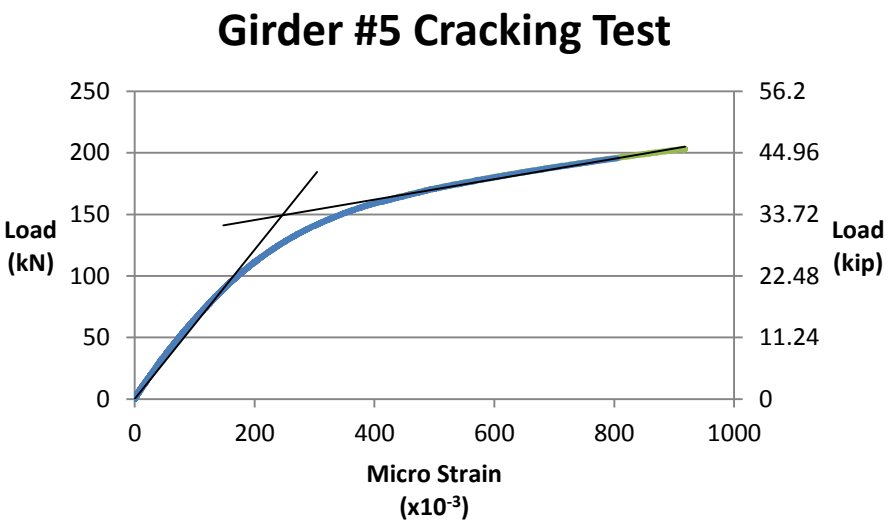
Girder #5 Cracking Test
250
200
150
100
50
0
Load (kN)
56.2
44.96
33.72
22.48
11.24
0
Load (kip)
0
200
400
600
800
1000
Micro Strain (x10-3)

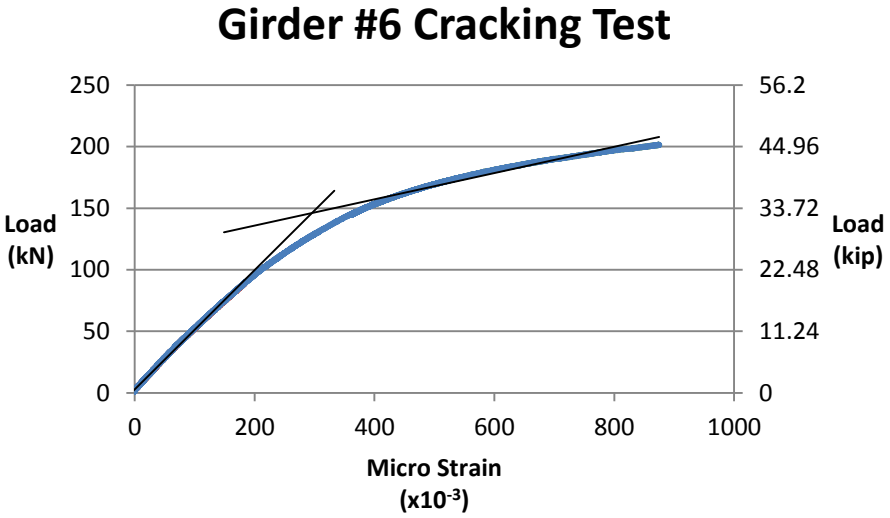
Girder #6 Cracking Test
250
200
150
100
50
0
Load (kN)
56.2
44.96
33.72
22.48
11.24
0
Load (kip)
0
200
400
600
800
1000
Micro Strain (x10-3)

A.2. Failure Data

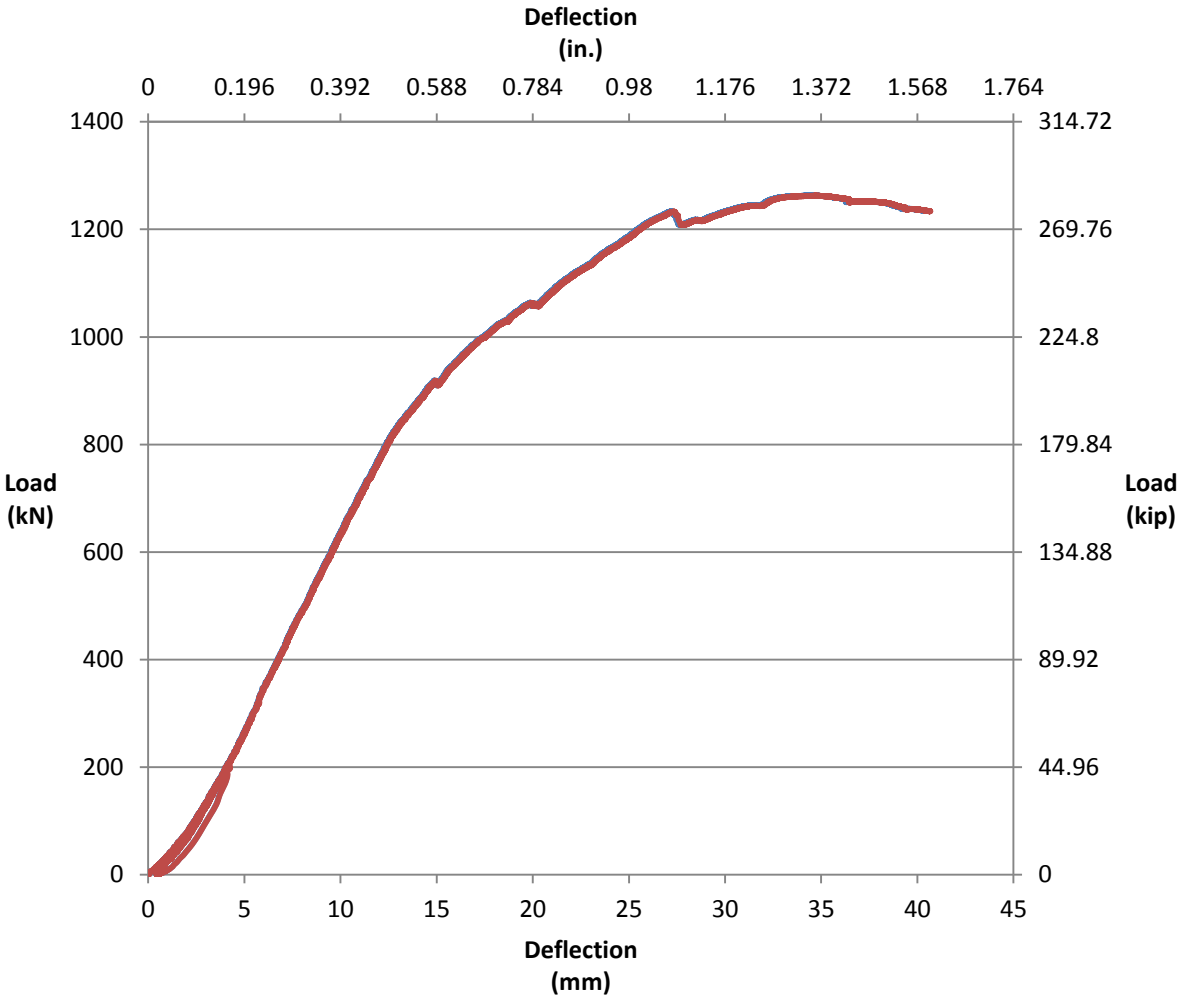

Fig. #, girder #4-4d test data

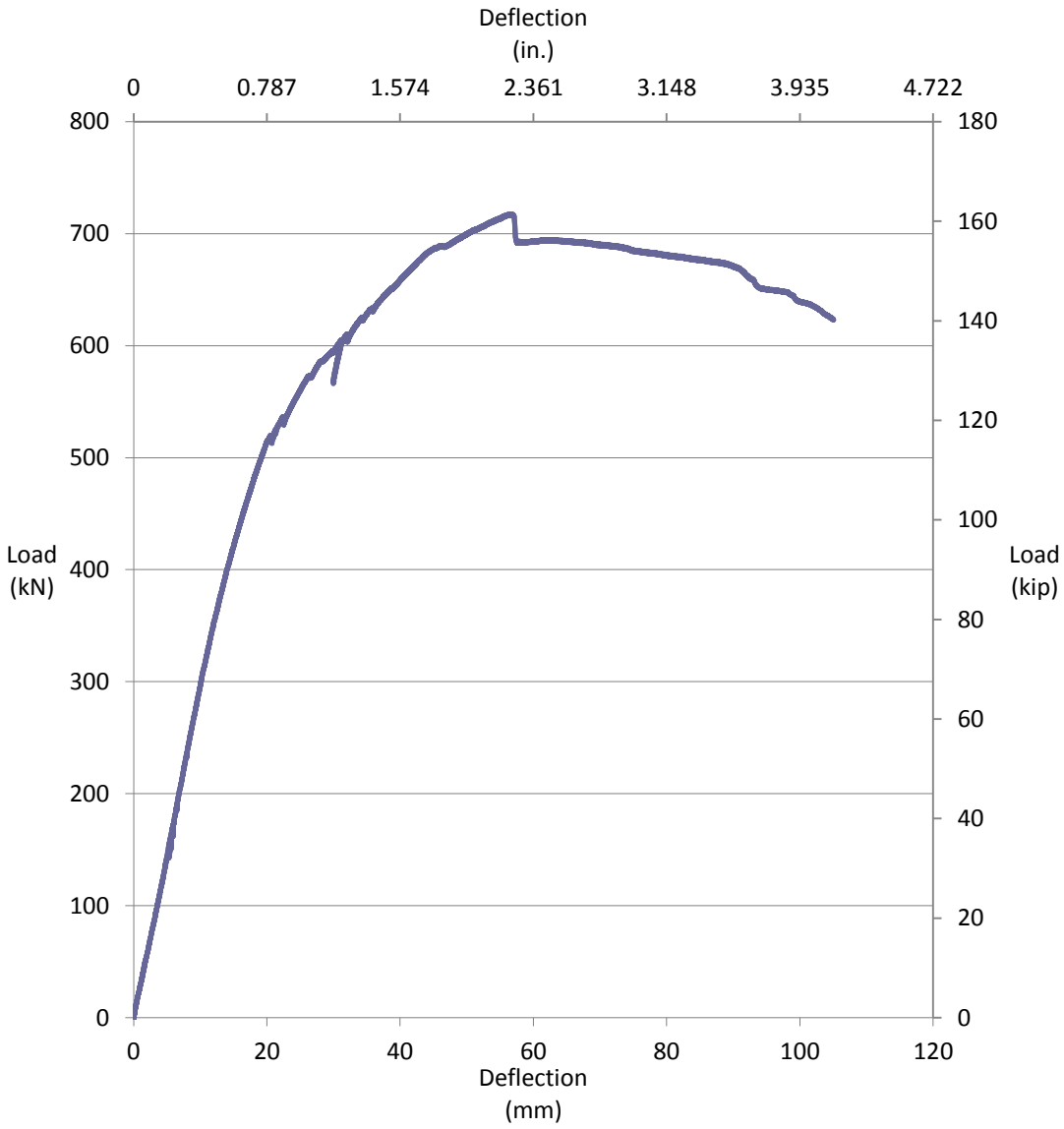

Fig. #, Girder #4-2d test data

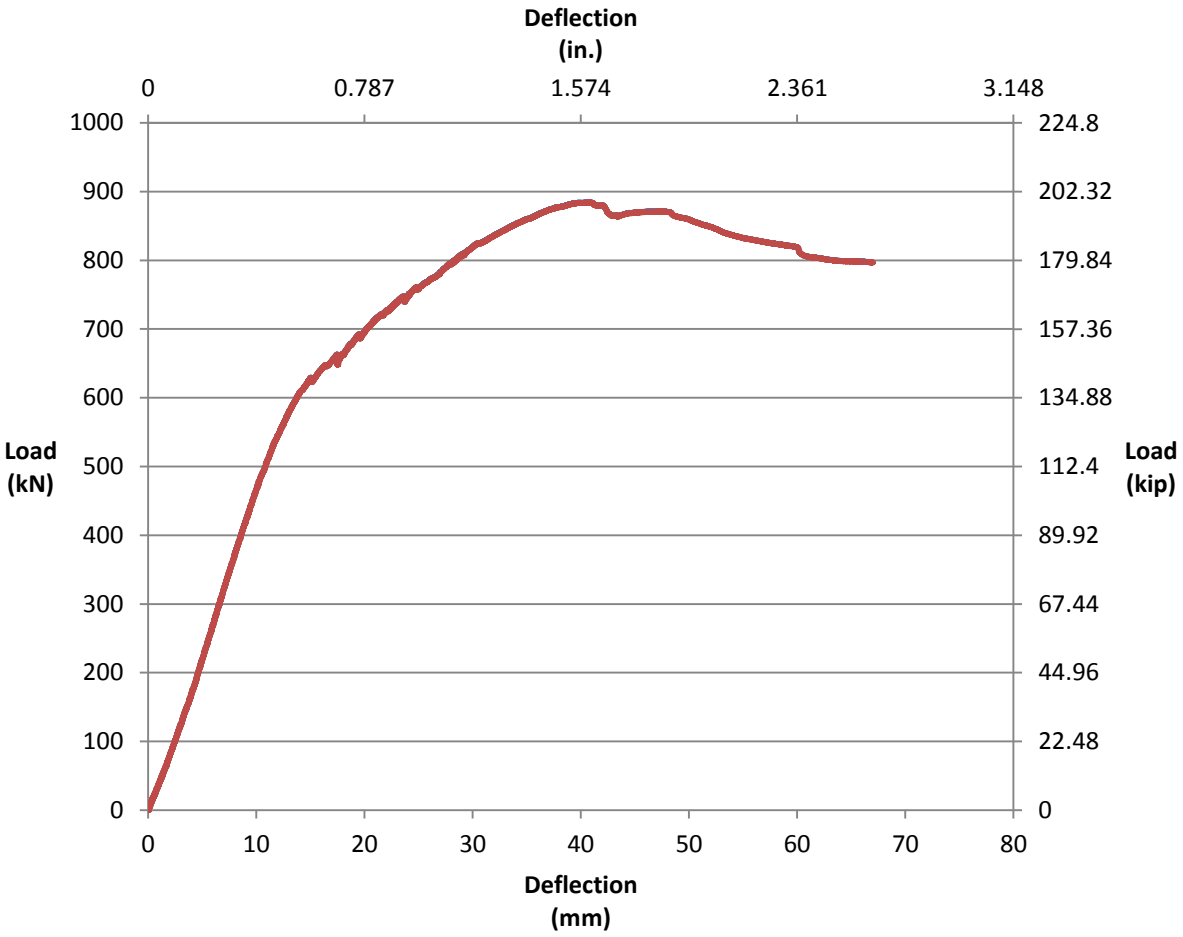

Girder #6-4d test data

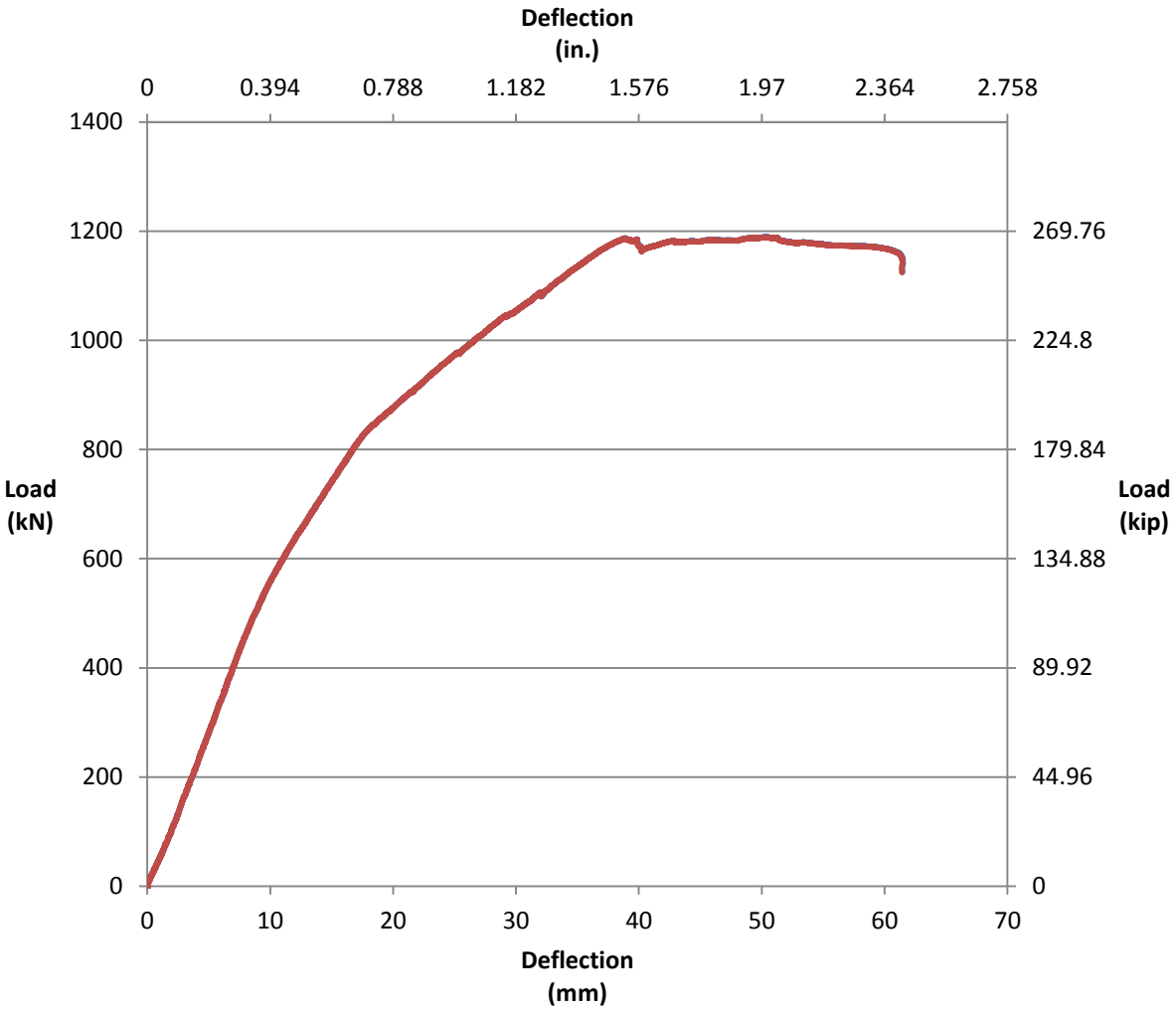

Girder #6-2d test data

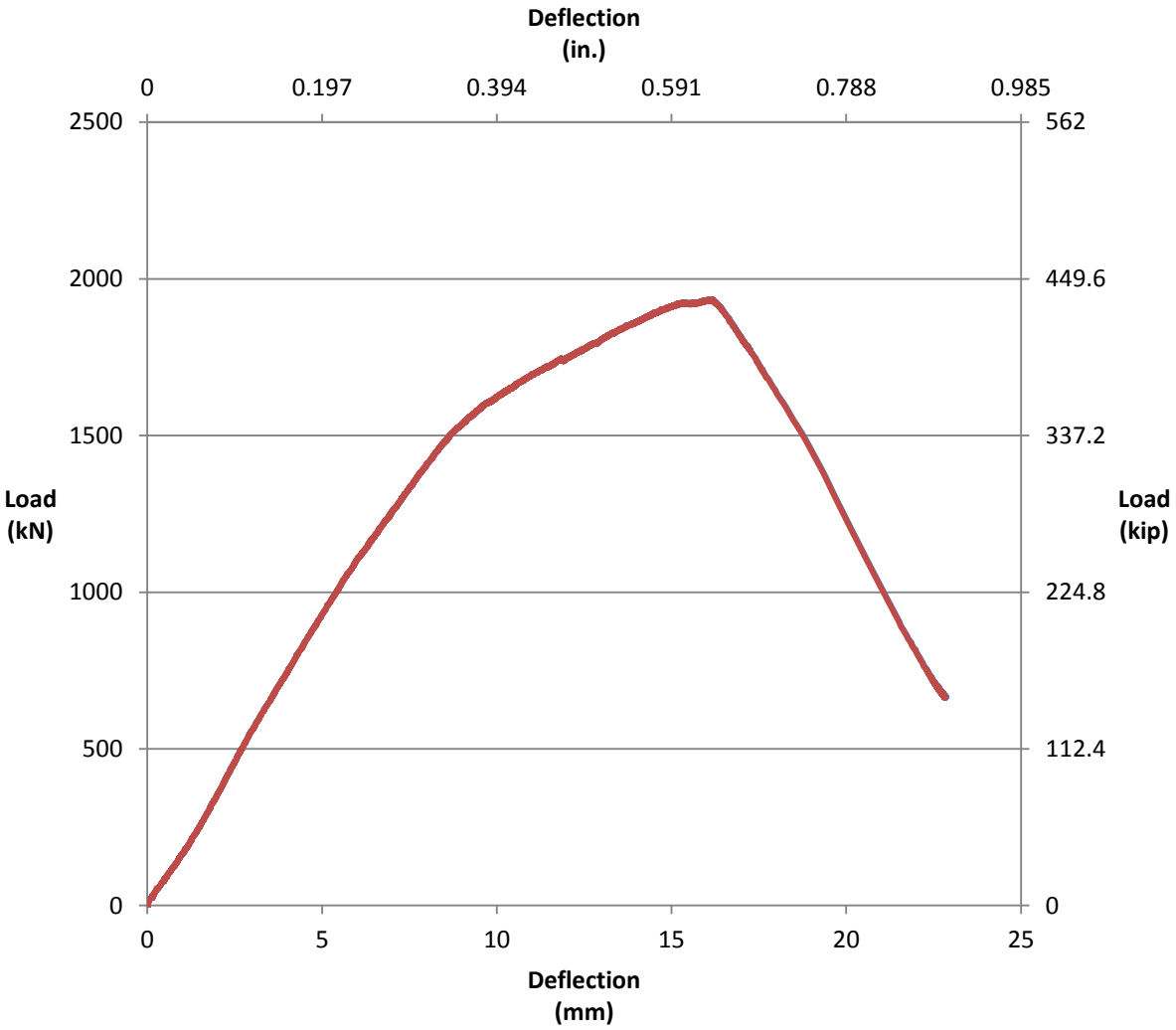

Girder #3-1d test

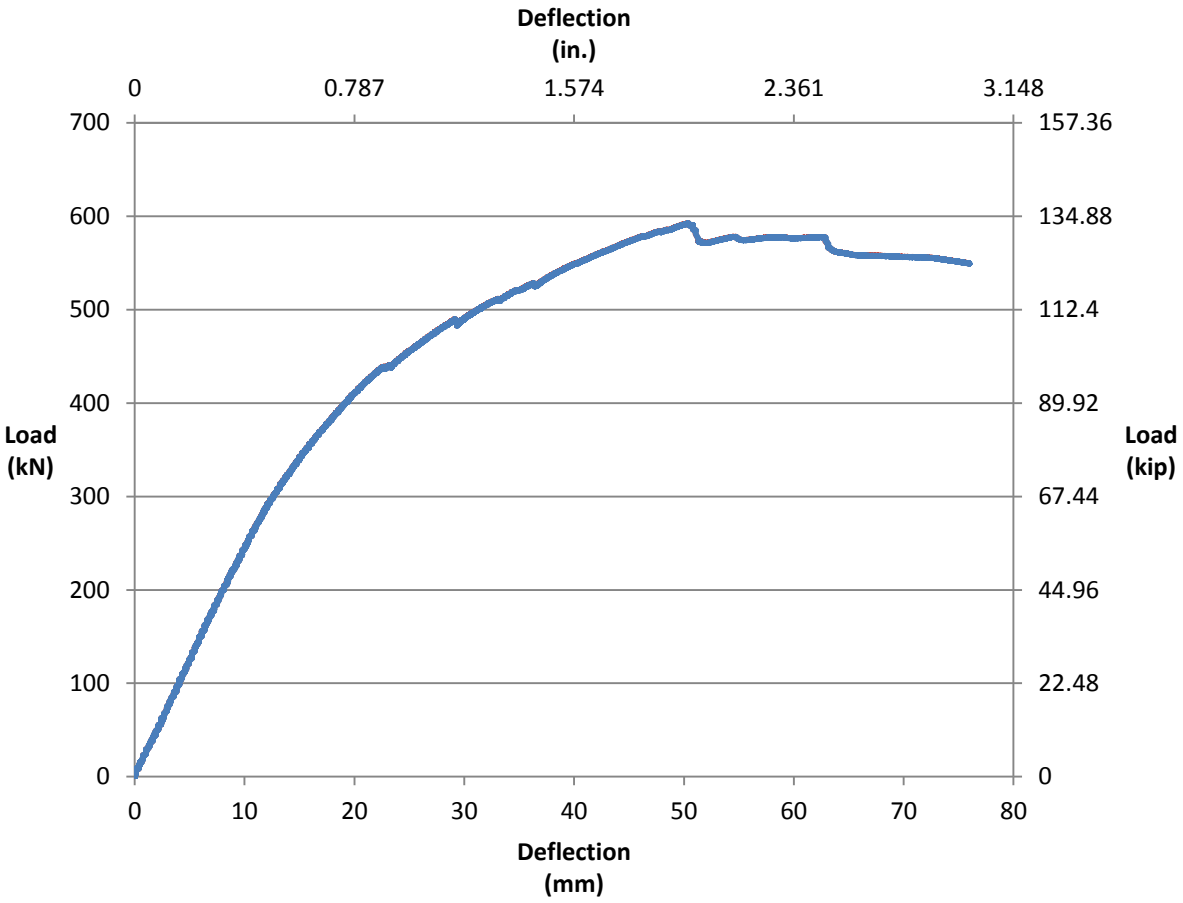

Girder #5-midspan test data

A.3. ANSYS Model Code

```
finish
/clear
/title,new beams

/prep7

!Units in Kips and inches

!Material Variables
Es=29000
Eps=28500
E=500000000
Emus=0.3
fys=240
fy=75
fyu=1000

Ec=3500
!use test info, beam prop
Emuc=0.18
fc=17.5
ft.=1.5

Ecd=2000
!use test info, deck prop
Emucd=0.2
```

```
fcd=10.0
ftd=.9

Eg=3122
fg=3
!Reduced from 7
fgt=0.411
!Reduced from 0.575

MP,EX,1,Es
MP,PRXY,1,Emus
TB,BISO,1
TBDATA,,fy,2.9

MP,EX,3,Eps
MP,PRXY,3,Emus
!MP,DENS,3,0.7331E-6
TB,BISO,3,,2
TBData,,fys,1000

MP,EX,2,Ec
MP,PRXY,2,Emuc
MP,DENS,2,1.188E-4

TB,CONCR,2
TBDATA,,.2,.8,ft,fc,  !see element types

MP,EX,4,Ecd
MP,PRXY,4,Emucd
MP,DENS,4,1.188E-4

TB,CONCR,4
TBDATA,,.2,.6,ftd,fcd,

MP,EX,5,E
MP,PRXY,5,Emus
TB,BISO,5
TBDATA,,fyu,2.9

!REAL CONSTANS FOR STEEL
R,1,,
!BEARING PLATES
R,2,.31,
!REBAR
R,3,.15,0.0057
!PRESTRESSED STRANDS

R,4,1,0.018,90,90      !CONCRETE SMEARED
R,5,.62,,
!SHEAR BARS
R,6,1,0.026,90         !CONCRETE SMEARING
R,7
!CONCRETE
R,8,.15,0.0048
R,9,.15,0.0038
R,10,.15,0.0029
R,11,.15,0.0019
R,12,.15,0.00094
R,13,1,0.013,90
R,14,1,0.009,90

!TYPES FOR EACH MATERIAL
!LOOK UP ELEMENTS IN CATALOG
ET,1,SOLID45
      !BEARING PLATES
ET,2,LINK8
      !BAR OR STRANDS
ET,4,SOLID65
      !CONCRETE

K,1,.75,,
K,2,15.25,,
K,3,,.75,
K,4,16,.75,
K,5,,5,
K,6,16,5,
K,7,5,10,
K,8,11,10,
K,9,5,21,
K,10,11,21,
K,11,2,24,
K,12,14,24,
K,13,2,28,
K,14,14,28,
KGEN,2,ALL,,,,,435,
```

```
!TOP PAD
BLOCK,2,14,28,36.5,0,435

!VOLUMES
V,1,2,4,3,15,16,18,17
V,11,12,14,13,25,26,28,27
V,3,4,6,5,17,18,20,19

WPROTA,,,-90
WPOFF,,,-3
VSBW,ALL
WPOFF,,,-2
VSBW,ALL
WPOFF,,,-2
VSBW,ALL
WPOFF,,,-1
VSBW,ALL
WPOFF,,,-1
VSBW,ALL
WPOFF,,,-2
VSBW,ALL
WPOFF,,,-2
VSBW,ALL
WPSTYL,DEFA

V,5,6,8,7,19,20,22,21
V,7,8,10,9,21,22,24,23
V,9,10,12,11,23,24,26,25

WPROTA,,,-90
WPOFF,,,-6
VSBW,ALL
WPOFF,,,-4
VSBW,ALL
WPSTYL,DEFA

WPROTA,,90,
WPOFF,,,-3
VSBW,ALL
WPOFF,,,-6
VSBW,ALL
WPOFF,,,-13
VSBW,ALL
WPOFF,,,-3
VSBW,ALL
WPOFF,,,-2
VSBW,ALL
WPSTYL,DEFA

WPOFF,,,2
VSBW,ALL
WPOFF,,,4
VSBW,ALL
WPOFF,,,6
VSBW,ALL
WPOFF,,,6
VSBW,ALL
WPOFF,,,6
VSBW,ALL
WPOFF,,,6
VSBW,ALL
WPOFF,,,6
VSBW,ALL
WPOFF,,,6
VSBW,ALL
WPOFF,,,6
VSBW,ALL
WPOFF,,,84
VSBW,ALL
WPOFF,,,159
VSBW,ALL
WPOFF,,,84
VSBW,ALL
WPOFF,,,6
VSBW,ALL
WPOFF,,,6
VSBW,ALL
WPOFF,,,6
VSBW,ALL
WPOFF,,,6
VSBW,ALL
WPOFF,,,6
VSBW,ALL
WPOFF,,,6
```

```
VSBW,ALL
WPOFF,,,4
VSBW,ALL
WPSTYL,DEFA

!BEARING PLATES
BLOCK,.75,15.25,0,-2,0,12

BLOCK,.75,15.25,0,-2,423,435
BLOCK,2,14,36.5,37.5,72,84
!MOVE THIS BLOCK TO MOVE LOAD

VSEL,ALL
VGLUE,ALL

!CREATING PRESTRESSED STRANDS
LSEL,S,LOC,Y,25
LSEL,R,LOC,X,7,9
LSEL,U,LOC,X,7.5,8.5
LSEL,U,LOC,Z,0,30
LSEL,U,LOC,Z,405,435
LATT,3,3,2
ESIZE,2
LMESH,ALL
LSEL,S,LOC,Y,25
LSEL,R,LOC,X,7,9
LSEL,U,LOC,X,7.5,8.5
LSEL,U,LOC,Z,0,24
LSEL,U,LOC,Z,30,405
LSEL,U,LOC,Z,411,435
LATT,3,8,2
ESIZE,2
LMESH,ALL
LSEL,S,LOC,Y,25
LSEL,R,LOC,X,7,9
LSEL,U,LOC,X,7.5,8.5
LSEL,U,LOC,Z,0,18
LSEL,U,LOC,Z,24,411
LSEL,U,LOC,Z,417,435
LATT,3,9,2
ESIZE,2
LMESH,ALL
LSEL,S,LOC,Y,25
LSEL,R,LOC,X,7,9
LSEL,U,LOC,X,7.5,8.5
LSEL,U,LOC,Z,0,12
LSEL,U,LOC,Z,18,417
LSEL,U,LOC,Z,423,435
LATT,3,10,2
ESIZE,2
LMESH,ALL
LSEL,S,LOC,Y,25
LSEL,R,LOC,X,7,9
LSEL,U,LOC,X,7.5,8.5
LSEL,U,LOC,Z,0,6
LSEL,U,LOC,Z,12,423
LSEL,U,LOC,Z,429,435
LATT,3,11,2
ESIZE,2
LMESH,ALL
LSEL,S,LOC,Y,25
LSEL,R,LOC,X,7,9
LSEL,U,LOC,X,7.5,8.5
LSEL,U,LOC,Z,6,429
LATT,3,12,2
ESIZE,2
LMESH,ALL

LSEL,S,LOC,X,3
LSEL,A,LOC,X,5
LSEL,A,LOC,X,8
LSEL,A,LOC,X,11
LSEL,A,LOC,X,13
LSEL,R,LOC,Y,5
LSEL,U,TAN1,X,1
LSEL,U,TAN2,X,1
LSEL,U,LOC,Z,0,30
LSEL,U,LOC,Z,405,435
LATT,3,3,2
ESIZE,2
LMESH,ALL
LSEL,S,LOC,X,3
LSEL,A,LOC,X,5
LSEL,A,LOC,X,8
LSEL,A,LOC,X,11
LSEL,A,LOC,X,13
LSEL,R,LOC,Y,5
LSEL,U,TAN1,X,1
```

```
LSEL,U,TAN2,X,1
LSEL,U,LOC,Z,0,24
LSEL,U,LOC,Z,30,405
LSEL,U,LOC,Z,411,435
LATT,3,8,2
ESIZE,2
LMESH,ALL
LSEL,S,LOC,X,3
LSEL,A,LOC,X,5
LSEL,A,LOC,X,8
LSEL,A,LOC,X,11
LSEL,A,LOC,X,13
LSEL,R,LOC,Y,5
LSEL,U,TAN1,X,1
LSEL,U,TAN2,X,1
LSEL,U,LOC,Z,0,18
LSEL,U,LOC,Z,24,411
LSEL,U,LOC,Z,417,435
LATT,3,9,2
ESIZE,2
LMESH,ALL
LSEL,S,LOC,X,3
LSEL,A,LOC,X,5
LSEL,A,LOC,X,8
LSEL,A,LOC,X,11
LSEL,A,LOC,X,13
LSEL,R,LOC,Y,5
LSEL,U,TAN1,X,1
LSEL,U,TAN2,X,1
LSEL,U,LOC,Z,0,12
LSEL,U,LOC,Z,18,417
LSEL,U,LOC,Z,423,435
LATT,3,10,2
ESIZE,2
LMESH,ALL
LSEL,S,LOC,X,3
LSEL,A,LOC,X,5
LSEL,A,LOC,X,8
LSEL,A,LOC,X,11
LSEL,A,LOC,X,13
LSEL,R,LOC,Y,5
LSEL,U,TAN1,X,1
LSEL,U,TAN2,X,1
LSEL,U,LOC,Z,0,6
LSEL,U,LOC,Z,12,423
LSEL,U,LOC,Z,429,435
LATT,3,11,2
ESIZE,2
LMESH,ALL
LSEL,S,LOC,X,3
LSEL,A,LOC,X,5
LSEL,A,LOC,X,8
LSEL,A,LOC,X,11
LSEL,A,LOC,X,13
LSEL,R,LOC,Y,5
LSEL,U,TAN1,X,1
LSEL,U,TAN2,X,1
LSEL,U,LOC,Z,6,429
LATT,3,12,2
ESIZE,2
LMESH,ALL

LSEL,S,LOC,X,3
LSEL,A,LOC,X,5
LSEL,A,LOC,X,7
LSEL,A,LOC,X,9
LSEL,A,LOC,X,11
LSEL,A,LOC,X,13
LSEL,R,LOC,Y,3
LSEL,U,TAN1,X,1
LSEL,U,TAN2,X,1
LSEL,U,LOC,Z,0,30
LSEL,U,LOC,Z,405,435
LATT,3,3,2
ESIZE,2
LMESH,ALL
LSEL,S,LOC,X,3
LSEL,A,LOC,X,5
LSEL,A,LOC,X,7
LSEL,A,LOC,X,9
LSEL,A,LOC,X,11
LSEL,A,LOC,X,13
LSEL,R,LOC,Y,3
LSEL,U,TAN1,X,1
LSEL,U,TAN2,X,1
LSEL,U,LOC,Z,0,24
LSEL,U,LOC,Z,30,405
LSEL,U,LOC,Z,411,435
LATT,3,8,2
ESIZE,2
```

```
LMESH,ALL
LSEL,S,LOC,X,3
LSEL,A,LOC,X,5
LSEL,A,LOC,X,7
LSEL,A,LOC,X,9
LSEL,A,LOC,X,11
LSEL,A,LOC,X,13
LSEL,R,LOC,Y,3
LSEL,U,TAN1,X,1
LSEL,U,TAN2,X,1
LSEL,U,LOC,Z,0,18
LSEL,U,LOC,Z,24,411
LSEL,U,LOC,Z,417,435
LATT,3,9,2
ESIZE,2
LMESH,ALL
LSEL,S,LOC,X,3
LSEL,A,LOC,X,5
LSEL,A,LOC,X,7
LSEL,A,LOC,X,9
LSEL,A,LOC,X,11
LSEL,A,LOC,X,13
LSEL,R,LOC,Y,3
LSEL,U,TAN1,X,1
LSEL,U,TAN2,X,1
LSEL,U,LOC,Z,0,12
LSEL,U,LOC,Z,18,417
LSEL,U,LOC,Z,423,435
LATT,3,10,2
ESIZE,2
LMESH,ALL
LSEL,S,LOC,X,3
LSEL,A,LOC,X,5
LSEL,A,LOC,X,7
LSEL,A,LOC,X,9
LSEL,A,LOC,X,11
LSEL,A,LOC,X,13
LSEL,R,LOC,Y,3
LSEL,U,TAN1,X,1
LSEL,U,TAN2,X,1
LSEL,U,LOC,Z,0,6
LSEL,U,LOC,Z,12,423
LSEL,U,LOC,Z,429,435
LATT,3,11,2
ESIZE,2
LMESH,ALL
LSEL,S,LOC,X,3
LSEL,A,LOC,X,5
LSEL,A,LOC,X,7
LSEL,A,LOC,X,9
LSEL,A,LOC,X,11
LSEL,A,LOC,X,13
LSEL,R,LOC,Y,3
LSEL,U,TAN1,X,1
LSEL,U,TAN2,X,1
LSEL,U,LOC,Z,6,429
LATT,3,12,2
ESIZE,2
LMESH,ALL

!LONGITUDINAL LINES FOR BAR
LSEL,S,LOC,Y,9
LSEL,R,LOC,X,6
LATT,1,2,2
ESIZE,2
LMESH,ALL
LSEL,S,LOC,Y,9
LSEL,R,LOC,X,10
LATT,1,2,2
ESIZE,2
LMESH,ALL
LSEL,S,LOC,Y,22
LSEL,R,LOC,X,6
LATT,1,2,2
ESIZE,2
LMESH,ALL
LSEL,S,LOC,Y,22
LSEL,R,LOC,X,10
LATT,1,2,2
ESIZE,2
LMESH,ALL
LSEL,S,LOC,Y,27
LSEL,R,LOC,X,3
LATT,1,2,2
ESIZE,2
LMESH,ALL
LSEL,S,LOC,Y,27
LSEL,R,LOC,X,13
LATT,1,2,2
```

```
ESIZE,2
LMESH,ALL

!SOME OF THE VOLUMES HAVE ISSUES WITH SWEEPING
ALLSEL,ALL
VGLUE,ALL

VSEL,S,LOC,X,6,10
!FIRST SECTIONS OF SHEAR BARS
VSEL,R,LOC,Y,5,28
VSEL,U,LOC,Z,54,381
VATT,2,6,4

VSEL,S,LOC,X,6,10
!SECOND SECTIONS OF SHEAR BARS
VSEL,R,LOC,Y,5,28
VSEL,U,LOC,Z,0,54
VSEL,U,LOC,Z,138,297
VSEL,U,LOC,Z,381,435
VATT,2,13,4

VSEL,S,LOC,X,6,10
!MIDDLE SECTION OF SHEAR BARS
VSEL,R,LOC,Y,5,28
VSEL,U,LOC,Z,0,138
VSEL,U,LOC,Z,297,435
VATT,2,14,4

VSEL,S,LOC,Y,36.5,37.5
VSEL,A,LOC,Y,0,-2
VATT,5,1,1

VSEL,S,LOC,Y,28,36.5
VATT,4,4,4

VSEL,S,LOC,Y,0,28
VSEL,U,LOC,X,6,10
VSEL,A,LOC,Y,0,5
VATT,2,7,4

VSEL,ALL
ESIZE,2
!CHOSE WHICHEVER GIVES LESS ERRORS
VSWEEP,ALL
ALLSEL,ALL

finish
/solu
Allsel,all
wpstyl,defa
!TAKES CORD SYSTEM BACK TO DEFAULT POSSITION
Nsel,s,node,,51925,51933
!NSEL,S,LOC,Y,-2
!NSEL,R,LOC,Z,423

d,all,uy
!Nsel,s,node,,51812,51852,5
NSEL,S,LOC,Y,-2
NSEL,R,LOC,Z,12
d,all,uz
d,all,uy

Nsel,s,loc,y,37.5
*Get,Ncount,node,0,count
F=275
F,all,Fy,-F/Ncount


allsel,all
cnvtol,f,,0.05,2,0.01
nsubst,100
outres,all,all
autots,1
ncnv,2
neqit,200
pred,on
time,100
solve
```

A.4. Bridge Plans

Appendix A.4 are the relevant pages from the original bridge plans for the addition.

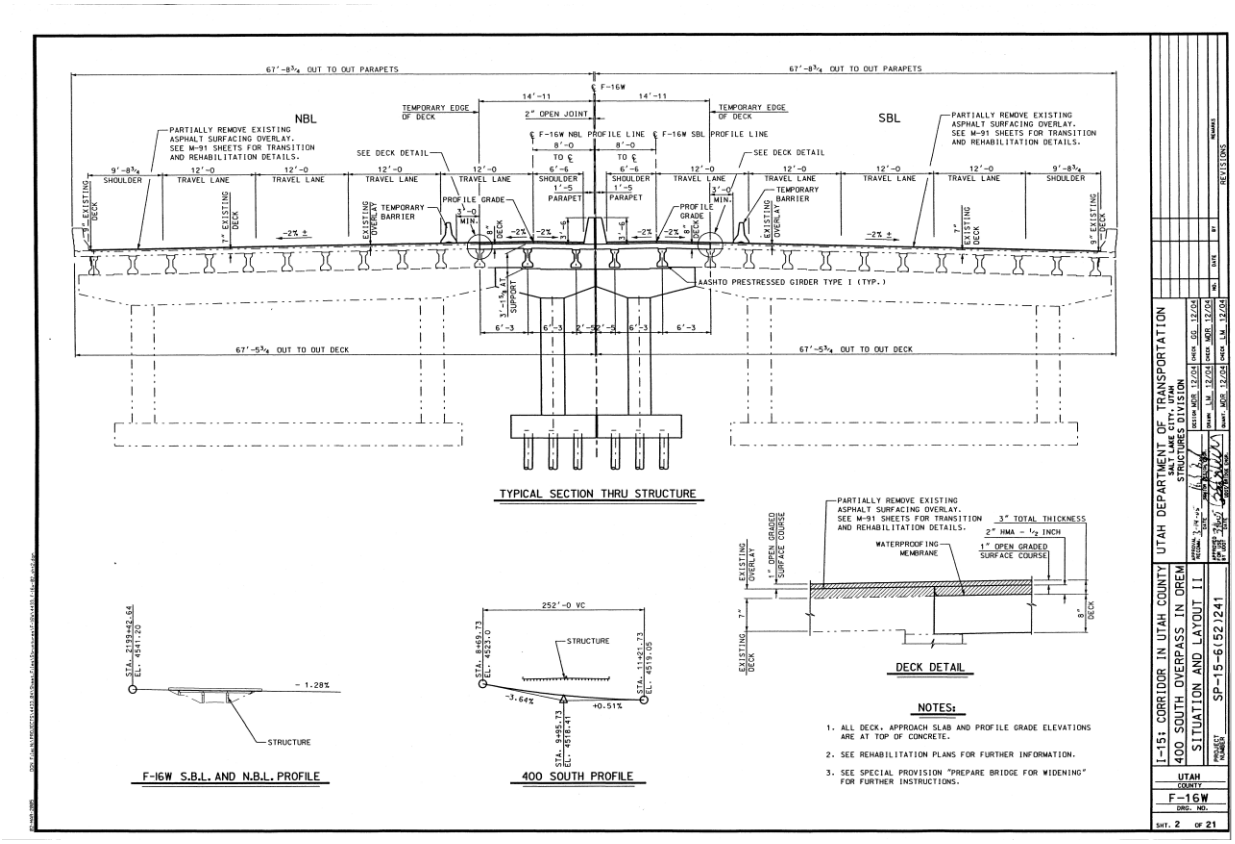

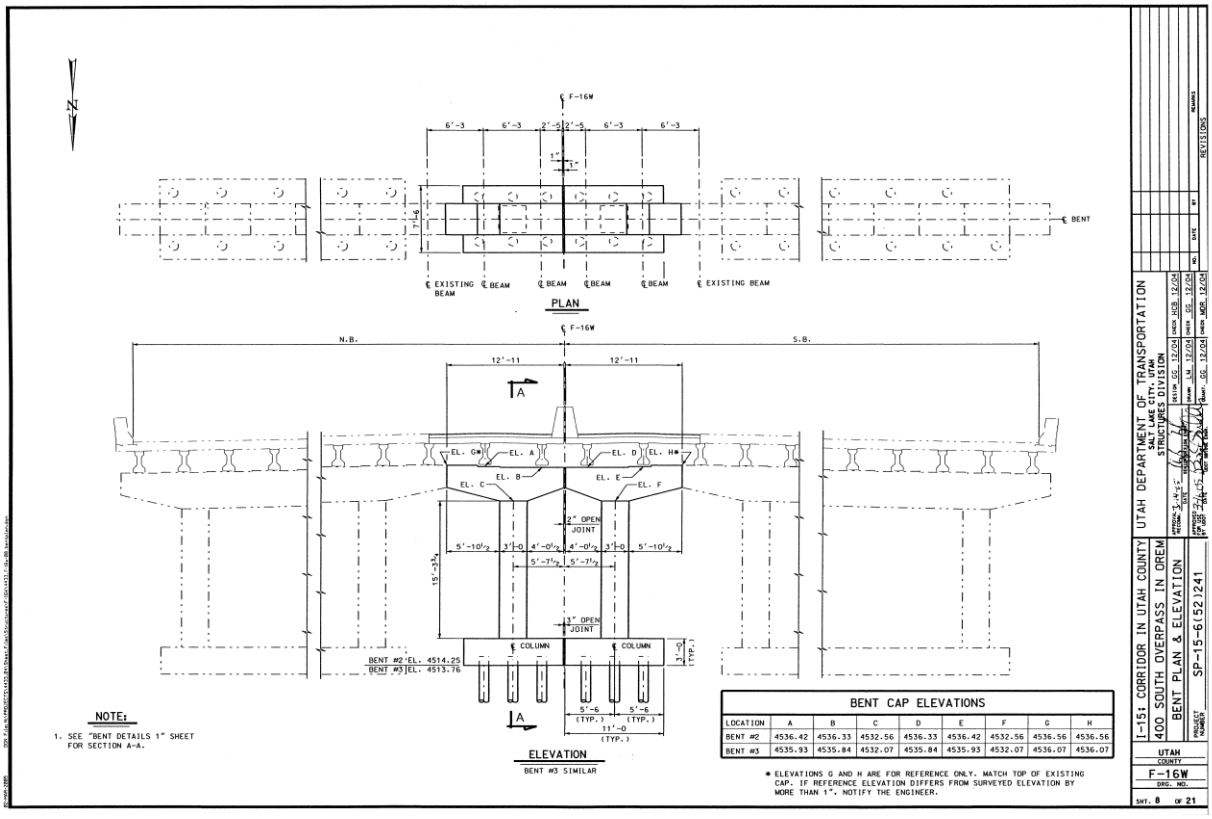

LOCATION	A	B	C	D	E	F	G	H
BENT #2	4536.42	4536.33	4532.56	4536.33	4536.42	4532.56	4536.56	4536.56
BENT #3	4535.93	4535.84	4532.07	4535.84	4535.93	4532.07	4536.07	4536.07

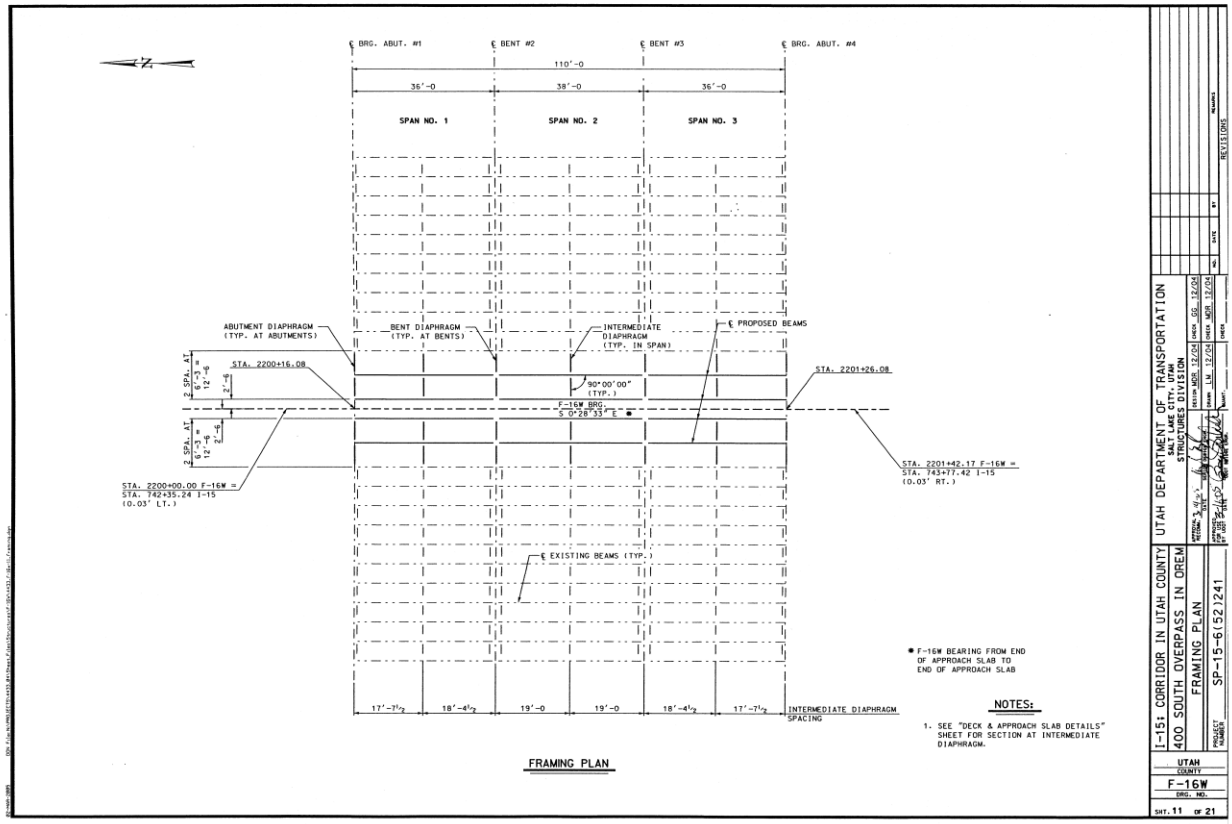
℄ BRG. ABUT. #1
℄ BENT #2
℄ BENT #3
℄ BRG. ABUT. #4
110'-0
36'-0
38'-0
36'-0
SPAN NO. 1
SPAN NO. 2
SPAN NO. 3
ABUTMENT DIAPHRAGM (TYP. AT ABUTMENTS)
BENT DIAPHRAGM (TYP. AT BENTS)
INTERMEDIATE DIAPHRAGM (TYP. IN SPAN)
℄ PROPOSED BEAMS
2 SPA. AT 6'-3" = 12'-6"
2'-6"
STA. 2200+16.08
90°00'00" (TYP.)
STA. 2201+26.08
F-16W BRG. S 0°28'33" E ●
2 SPA. AT 6'-3" = 12'-6"
2'-6"
STA. 2200+00.00 F-16W = STA. 742+35.24 I-15 (0.03' LT.)
STA. 2201+42.17 F-16W = STA. 743+17.42 I-15 (0.03' RT.)
℄ EXISTING BEAMS (TYP.)
17'-7½
18'-4½
19'-0
19'-0
18'-4½
17'-7½
INTERMEDIATE DIAPHRAGM SPACING
● F-16W BEARING FROM END OF APPROACH SLAB TO END OF APPROACH SLAB
NOTES:
1. SEE "DECK & APPROACH SLAB DETAILS" SHEET FOR SECTION AT INTERMEDIATE DIAPHRAGM.
FRAMING PLAN
I-15: CORRIDOR IN UTAH COUNTY
400 SOUTH OVERPASS IN OREM
FRAMING PLAN
SP-15-61(52)241
UTAH DEPARTMENT OF TRANSPORTATION
SALT LAKE CITY, UTAH
STRUCTURES DIVISION
DESIGN MDR 12/04
DRAWN LM 12/04
CHECK SG 12/04
CHECK MDR 12/04
UTAH
COUNTY
F-16W
DRG. NO.
SHT. 11 OF 21

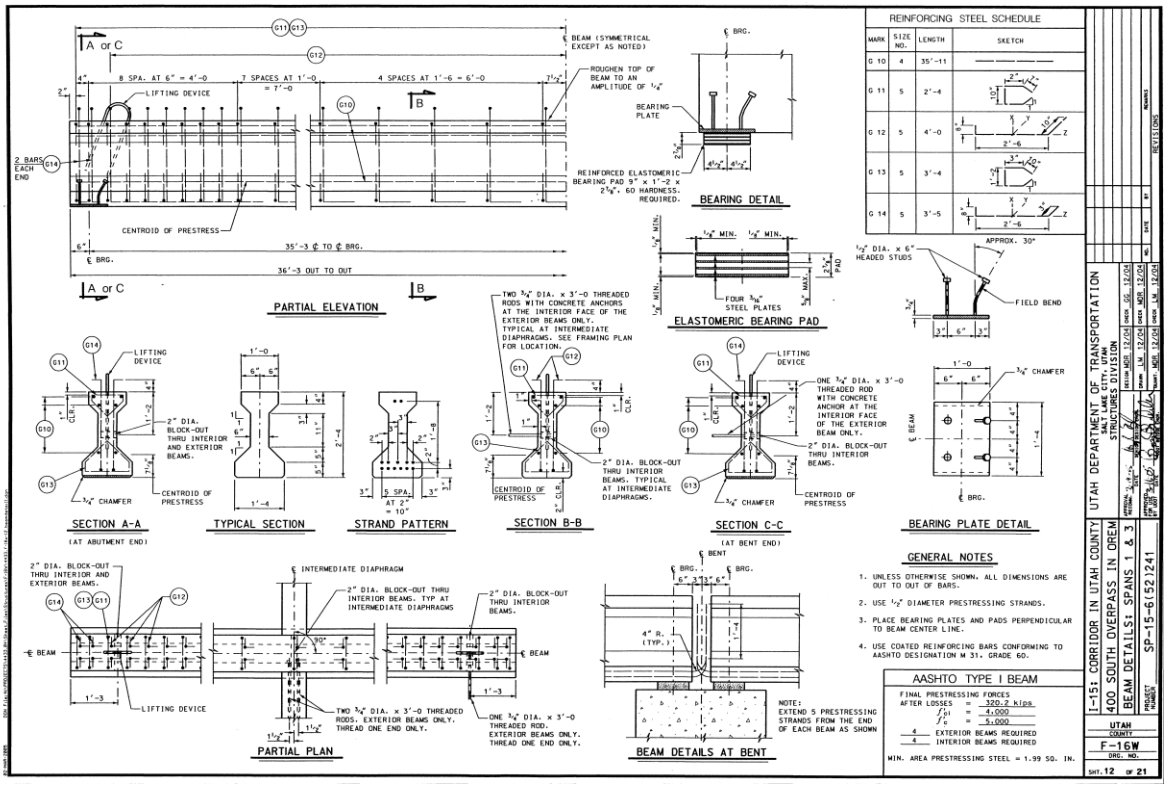
REINFORCING STEEL SCHEDULE
MARK
SIZE NO.
LENGTH
SKETCH
G 10
4
35'-11
G 11
5
2'-4
G 12
5
4'-0
G 13
5
3'-4
G 14
5
3'-5
PARTIAL ELEVATION
BEARING DETAIL
ELASTOMERIC BEARING PAD
SECTION A-A
(AT ABUTMENT END)
TYPICAL SECTION
STRAND PATTERN
SECTION B-B
SECTION C-C
(AT BENT END)
BEARING PLATE DETAIL
PARTIAL PLAN
BEAM DETAILS AT BENT
GENERAL NOTES
1. UNLESS OTHERWISE SHOWN, ALL DIMENSIONS ARE OUT TO OUT OF BARS.
2. USE ½" DIAMETER PRESTRESSING STRANDS.
3. PLACE BEARING PLATES AND PADS PERPENDICULAR TO BEAM CENTER LINE.
4. USE COATED REINFORCING BARS CONFORMING TO AASHTO DESIGNATION M 31, GRADE 60.
AASHTO TYPE I BEAM
FINAL PRESTRESSING FORCES AFTER LOSSES = 320.2 kips
f'ci = 4,000
f'c = 5,000
4 EXTERIOR BEAMS REQUIRED
4 INTERIOR BEAMS REQUIRED
MIN. AREA PRESTRESSING STEEL = 1.99 SQ. IN.
UTAH DEPARTMENT OF TRANSPORTATION
SALT LAKE CITY, UTAH
STRUCTURES DIVISION
I-15: CORRIDOR IN UTAH COUNTY
400 SOUTH OVERPASS IN OREM
BEAM DETAILS: SPANS 1 & 3
PROJECT NUMBER
SP-15-6(52)241
UTAH
COUNTY
F-16W
DRG. NO.
SHT. 12 OF 21

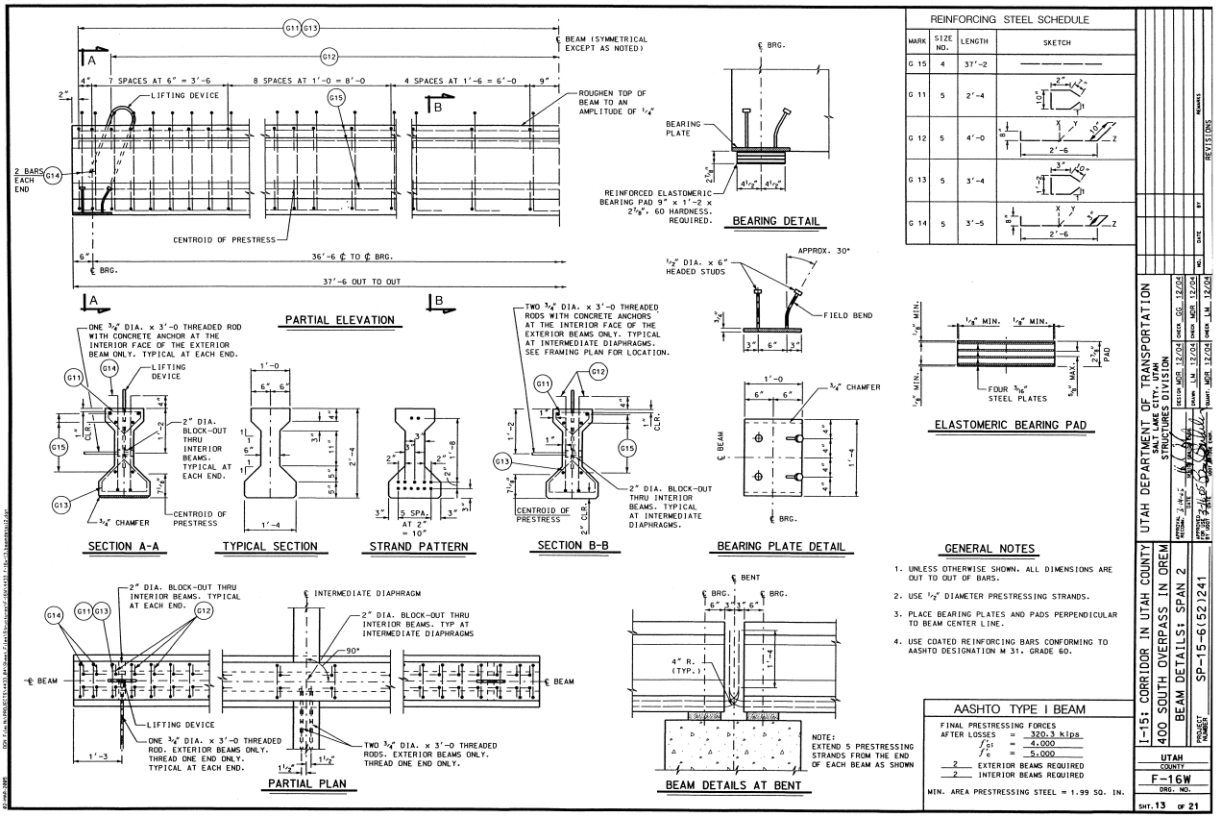
PARTIAL ELEVATION
BEARING DETAIL
REINFORCING STEEL SCHEDULE
SECTION A-A
TYPICAL SECTION
STRAND PATTERN
SECTION B-B
BEARING PLATE DETAIL
ELASTOMERIC BEARING PAD
GENERAL NOTES
1. UNLESS OTHERWISE SHOWN, ALL DIMENSIONS ARE OUT TO OUT OF BARS.
2. USE 1/2" DIAMETER PRESTRESSING STRANDS.
3. PLACE BEARING PLATES AND PADS PERPENDICULAR TO BEAM CENTER LINE.
4. USE COATED REINFORCING BARS CONFORMING TO AASHTO DESIGNATION M 31, GRADE 60.
PARTIAL PLAN
BEAM DETAILS AT BENT
AASHTO TYPE I BEAM
FINAL PRESTRESSING FORCES AFTER LOSSES = 320.3 kips
f'c = 4,000
f'ci = 5,000
2 EXTERIOR BEAMS REQUIRED
2 INTERIOR BEAMS REQUIRED
MIN. AREA PRESTRESSING STEEL = 1.99 SQ. IN.
UTAH DEPARTMENT OF TRANSPORTATION
I-15; CORRIDOR IN UTAH COUNTY
400 SOUTH OVERPASS IN OREM
BEAM DETAILS: SPAN 2
PROJECT NUMBER SP-15-6(152)241
UTAH
COUNTY
F-16W
DRG. NO.
SHT. 13 OF 21

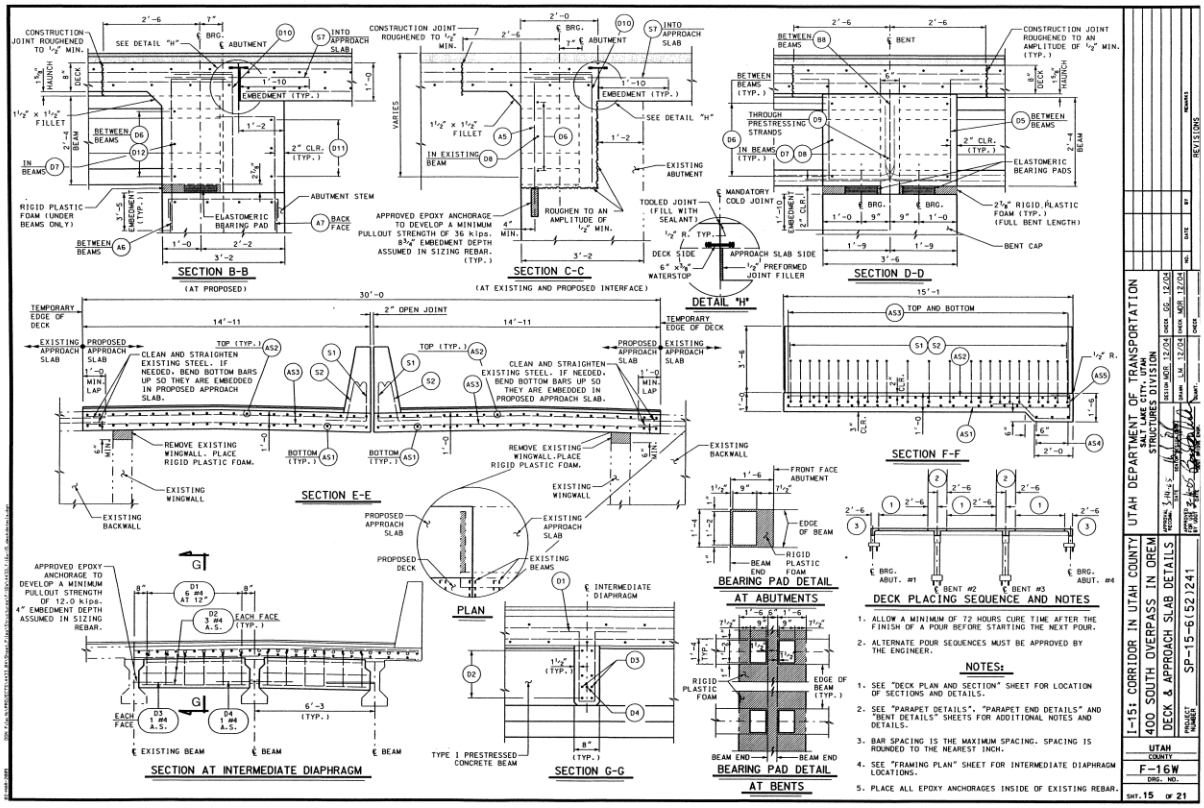
SECTION B-B
(AT PROPOSED)
SECTION C-C
(AT EXISTING AND PROPOSED INTERFACE)
SECTION D-D
DETAIL "H"
SECTION E-E
SECTION F-F
SECTION AT INTERMEDIATE DIAPHRAGM
PLAN
SECTION G-G
BEARING PAD DETAIL
AT ABUTMENTS
BEARING PAD DETAIL
AT BENTS
DECK PLACING SEQUENCE AND NOTES
NOTES:
1. SEE "DECK PLAN AND SECTION" SHEET FOR LOCATION OF SECTIONS AND DETAILS.
2. SEE "PARAPET DETAILS", "PARAPET END DETAILS" AND "BENT DETAILS" SHEETS FOR ADDITIONAL NOTES AND DETAILS.
3. BAR SPACING IS THE MAXIMUM SPACING. SPACING IS ROUNDED TO THE NEAREST INCH.
4. SEE "FRAMING PLAN" SHEET FOR INTERMEDIATE DIAPHRAGM LOCATIONS.
5. PLACE ALL EPOXY ANCHORAGES INSIDE OF EXISTING REBAR.
1. ALLOW A MINIMUM OF 72 HOURS CURE TIME AFTER THE FINISH OF A POUR BEFORE STARTING THE NEXT POUR.
2. ALTERNATE POUR SEQUENCES MUST BE APPROVED BY THE ENGINEER.
UTAH DEPARTMENT OF TRANSPORTATION
SALT LAKE CITY, UTAH
STRUCTURES DIVISION
I-15: CORRIDOR IN UTAH COUNTY
400 SOUTH OVERPASS IN OREM
DECK & APPROACH SLAB DETAILS
PROJECT NUMBER SP-15-6(52)241
UTAH COUNTY
F-16W
DRG. NO.
SHT. 15 OF 21